8-2008

Collision-Induced Dissociation of Multiply-Charged Anions

Nasrin Mirsaleh Kohan
University of Tennessee - Knoxville

To the Graduate Council:

I am submitting herewith a dissertation written by Nasrin Mirsaleh Kohan entitled "Collision-Induced Dissociation of Multiply-Charged Anions." I have examined the final electronic copy of this dissertation for form and content and recommend that it be accepted in partial fulfillment of the requirements for the degree of Doctor of Philosophy, with a major in Physics.

Robert N. Compton, Major Professor

We have read this dissertation and recommend its acceptance:

Elbio Dagotto, Michael W. Guidry, Joseph H. Macek, Charles Feigerle

Accepted for the Council:

Carolyn R. Hodges

Vice Provost and Dean of the Graduate School

(Original signatures are on file with official student records.)

To the Graduate Council

I am submitting herewith a dissertation written by Nasrin Mirsaleh Kohan entitled "Collision-Induced Dissociation of Multiply-Charged Anions." I have examined the final copy of this dissertation for form and content and recommend that it be accepted in partial fulfillment of the requirements for the degree of Doctor of Philosophy with a major in Physics.

Robert N. Compton, Major Professor

We have read this dissertation
And recommend its acceptance:

Elbio Dagotto

Michael W. Guidry

Joseph H. Macek

Charles Feigerle

Accepted for the Council:

Carolyn R. Hodges

Vice Provost and Dean of the Graduate School

(Original signatures are on file with official student records)

Collision-Induced Dissociation of Multiply-Charged Anions

A Dissertation
Presented for the
Doctor of Philosophy
Degree
The University of Tennessee, Knoxville

Nasrin Mirsaleh Kohan
August 2008

DEDICATION

This dissertation is dedicated in loving memory of my father, Asghar Mirsaleh Kohan, who sadly passed away during preparation of this thesis. To my mother and sisters for their unconditional love and patience. I also would like to dedicate this thesis to my wonderful husband, David K. Sauerteig for all of his love, emotional support, and understanding. Last but not least I dedicate this work to my father-in-law, Robert H. Sauerteig and my mother-in-law Linda L. Sauerteig for their love and encouraging words.

ACKNOWLEDGEMENTS

I sincerely thank my advisor Dr. Robert N. Compton for his guidance, support and encouragement during this study. I could not imagine having a better advisor. His passion and love for science is contagious. He is always accessible for his students. He is not only one of the smartest scientists I have seen; he is also a very good human being. I specifically would like to thank my advisor for teaching me how to write a scientific paper. He will continue to be a role model for me in my scientific and personal life.

My thanks also go to my committee members Dr. Elbio Dagotto, Dr. Charles Feigerle, Dr. Michael W. Guidry and Dr. Joseph H. Macek for their insight and suggestions. I also thank Dr. Feigerle for helping me with the Raman experiment.

I am also very grateful to Dr. Liguo Song, director of the Mass Spectrometry Center in the department of Chemistry for his assistance with the electrospray ionization source.

Grateful acknowledgement is extended to my fellow lab students, Wesley Robertson, Andy Fisher, Jeff Steill, Watheq Al-Basheer, Shaun Ard, Jason Lambert and many others for their support and many helpful discussions.

ABSTRACTS

Electrospray ionization has proven to be a powerful method for the study of multiply-charged-anions (MCA) in the gas-phase. Stability of the MCA toward ionic fragmentation and electron detachment has attracted wide interest. The stability of dianions is due to the "repulsive Coulomb barrier" to the addition or removed of an excess electron to a negative ion. The repulsive Coulomb barrier (RCB) is primarily the result of a long-range Coulomb repulsion and the short-range polarizibility attraction between an electron and a negative ion. The RCB can render unbound MCAs metastable or add stability to bound MCAs. In this dissertation, a collision-induced dissociation (CID) technique has been applied to investigate the stability of dianions produced in the gas-phase.

In this work collision-induced dissociation of salt clusters is investigated in order to examine the role of the repulsive Coulomb barrier in the stability of these dianions against ionic fragmentation and electron detachment. In addition, the CID technique is performed to estimate the heights of inner and outer RCB for a group of dicarboxylate and disulfonic dianions with respect to electron detachment and ionic fragmentation. Furthermore, the decay pathways of these dianions are investigated experimentally and theoretically.

The importance of the collision-induced dissociation method in measuring the bond dissociation energies of singly-charged anions will also be emphasized. In this context, the bond dissociation energy of $NaCl_2^-$ ion into NaCl and Cl^- ion is determined employing the CID technique. Experimental value of the bond dissociation energy is compared with theoretical values.

TABLE OF CONTENTS

LIST OF TABLES

LIST OF FIGURES

ABBREVIATIONS

EA	Electron Affinity
EA_a	Adiabatic Electron Affinity
MCA	Multiply Charged Anion
RCB	Repulsive Coulomb Barrier
EB	Electron Binding
ESI	Electrospray Ionization
CID	Collision-Induced Dissociation
CC	Collision Cell
DFT	Density Functional Theory
BDE	Bond Dissociation Energy
FWHM	Full-Width, Half-Maximum
ELISA	Electrostatic Ion Storage Ring, Aarhus
TDAE	Tetrakis(dimethylamino)ethylene
IP	Ionization Potential
IP_a	Adiabatic Ionization Potential
IP_v	Vertical Ionization Potential
TOFMS	Time-of-Flight Mass Spectrometry
EI	Electron Impact
MALDI	Matrix Assisted Laser Desorption
TEM	Trochoidal Electron Monochromator
IR	Infrared Absorption

CHAPTER I

Introduction

This dissertation examines the properties of multiply-charged anions (MCA), especially stability of MCAs toward electron detachment and ionic fragmentation. An electrospray ionization source is used in order to produce multiply-charged anions. The primary method employed in this work to investigate the stability of MCAs is the collision-induced dissociation technique.

Chapter II provides a basic introduction and historical background on the subject of negative ions. This chapter provides more details on the multiply-charged anions. The repulsive Coulomb barrier characteristic of multiply-charged anions is introduced in this chapter. The goal of Chapter III is to introduce the electrospray ionization mass spectrometry along with the collision-induced dissociation method.

Chapters IV and VI mainly examine the stability of MCAs and the role of the so-called repulsive Coulomb barrier in their stability.

In Chapter IV, a study of the repulsive Coulomb barrier heights for dissociation of a doubly charged $[Na_xCl_{x+2}]^{2-}$ (x =7 & 9) cluster with respect to electron loss or ionic fragmentation will be examined. Furthermore, threshold energies of doubly charged reactant ions will be discussed using the collision-induced dissociation method (CID). Chapter VI aims to investigate stability of a group of dicarboxylate and
disulfonic dianions with respect to electron detachment and ionic fragmentation. The main objective of this chapter is obtaining a correlation between electronic properties of MCAs and their stability. These two groups of dianions were chosen since they have different electronic properties.

Chapter V emphasizes the importance of the collision-induced dissociation method in studying bond dissociation energies of negative species, especially singly-charged anions. In this chapter, the bond dissociation energy of $NaCl_2^-$ produced in the gas-phase will be investigated. The experimental bond dissociation energy will be compared with theoretical results.

Although the subject of Chapter VII differs from the rest of this dissertation, it has a very important relevance to the field of multiply-charged anions. tetrakis(dimethylamino)ethylene ($C_{10}H_{24}N_4$, TDAE) is known to have an adiabatic ionization potential of less than 5.36 eV; however, the exact ionization potential of this molecule has not been measured experimentally prior to our study. One of important properties of TDAE is its readiness to give up an electron in a reaction. This property of TDAE has found an application in the production of multiply-charged anions in the gas phase. In Chapter VII, the adiabatic ionization potential of TDAE will be measured employing two different techniques, the electron impact and photoionization. Further, mass spectra of the TDAE molecule will be presented employing a linear time-of-flight mass spectrometer.

CHAPTER II

Negative Ions

Introduction

Negative ions play a significant role in many areas of Physics and Chemistry involving weakly ionized gases and plasmas. A small concentration of negatively charged atoms and molecules reduces the electrical conductivity in plasma and changes the rate of recombination between positive and negative ions in the plasma.

Importantly, negative ions play a major role in astrophysics. For example, low energy associative detachment between hydrogen negative ions and hydrogen atoms is the primarily mechanism leading to the formation of hydrogen molecules in interstellar gas clouds, $H^- + H \rightarrow H_2 + e^-$. Negative ions such as O^- and O_2^- are important in determining the density of free electrons that are critical in radio communications through their effects on the Heaviside layer.

Negative ions are also used in Tandem accelerators. In a Tandem accelerator, negative ions are introduced in the front end of the accelerator at ground potential. A high positive voltage at the end of the accelerator is used to accelerate these negative ions to the terminal energy. Following acceleration the ions collide with a gas target or thin foil and two (or more) electrons are stripped off from the negative ions leaving the resulting ions positively charged. Upon their creation the positive ions are accelerated back down to ground potential, reaching energies of twice the terminal voltage for singly charged positive ions or higher for multiply-charged positive ions.

In nature, negative ions are produced from the reaction of sunlight, radiation and moving air and water with air molecules. An abundant concentration of negative ions can be found in certain locations such as mountains, waterfalls and beaches. Recently, researchers have focused on the effects of negative ions on human health. Some researchers believe that controlled amount of negative ions in the air can produce biochemical reaction that improves the level of mood and well being. It is often claimed that the reason one feels good while walking on the beach is due to the presence of an excess abundance of negative ions. Despite the wide attention in the non-scientific literature this area of research is a matter of some scientific controversy.

The most important implication of negative ions involves the dielectric strength of gases. Gases such as sulfur hexafluoride are used to increase the dielectric strength of gases for all types of high voltage applications. The SF_6 molecule soaks up slow electrons in a growing discharge converting the electrons into slow heavy ions thereby reducing its ability to liberate further electrons, which feed the discharge.

These small numbers of applications of negative ions demonstrate the importance of negative ions studies.

Singly Charged Negative Ions

When an electron is bound to a neutral atom, molecule or cluster, a singly negative ion is formed. Massey[1] and Smirnov[2] have written monographs on the subject of negative ions. Also Bates summarized the theoretical aspects of negative ions studies in a review article.[3]

It is now known that almost 80% of the elements in the periodic table form stable negative ions, i.e., they possess positive electron affinities.[4] Only helium, nitrogen, beryllium, magnesium, mercury, and zinc are not believed to form stable negative ions. The other rare gases also are incapable of binding an extra electron since their outer shell is closed. However, there are many cases of negative ions in which that electron is bound to an excited state of the neutral atom. The negative excited state anion decays via the process of autodetachment.

The structure of negative ions differs from neutral atoms and positive ions, which are bound by a long-range Coulomb potential. In a negative ion, the outer electron is bound by a short-range induced potential that arises from the polarization of the atomic core. This short-range potential is very shallow and usually supports a finite number of excited states.

The main characterization of a negative ion is its electron affinity. The electron affinity, EA, is the difference between total energy of the ground state of the atoms (E_{tot}), and its negative ion.

$$EA\ (A) = E_{tot}\ (A) - E_{tot}\ (A^-) \tag{2.1}$$

Positive electron affinity means that the neutral atom lies energetically above the negative ion. In other words, the negative ion is stable. Atoms with negative electron affinities do not exist for a long period of time (only a few picoseconds) and decay through autodetachment.

Negative ions of many molecules are known to exist as well.[5] The attachment of an electron to a molecule arises when the electron and the molecule are temporarily associated. The initial step of electron attachment involves the formation of a transient

negative ion. The fate of this transient anion can result in many possibilities including dissociation and autodetachment. Schulz[6] classified three types of conditions that involve the transient capture of an electron by a molecule:

1. Nuclear excited Feshbach Resonance: This process occurs when the interaction potential between the incident electron (called an open channel) and the molecule (called closed channel) is strong enough to support a bound state. In this case the incoming electron energy and the electron affinity energy of the molecule are shared among the available vibrational modes of the molecular anion. As a result, this process violates the Born-Oppenheimer approximation since the interaction between the electronic and molecular motion plays an important role. The electron is held up by the molecule for a characteristic time (lifetime) before autodetachment occurs. The autodetachment lifetime can be expressed through an equation using the principle of detailed balance first introduced by Compton et al.[7]. The equation relates the lifetime against autodetachment (τ) to the attachment cross section (σ):

$$\tau = \frac{m^2 \rho^-}{\pi^2 h^3 \nu \sigma} \tag{2.2}$$

where ρ^- is the density of the states of the negative ion, ν is the incident electron velocity and m is the electron mass. As it is apparent in Equation 2.2, the density of the states of the anion determines the lifetime against autodetachment. The density of states can be conveniently calculated from the prescription by Whitten and Rabinowicz[8]:

$$\rho^- = \frac{(E + aE_z)^N}{\Gamma(N)\Pi(h\upsilon_i)} \tag{2.3}$$

where E is the total energy including the electron affinity and kinetic energy of the electron, E_z is the total zero energy which is one-half the sum of the first vibrational state energy, $\Gamma(N)$ is the gamma function, $\Pi(h\upsilon_i)$ is the multiplication of all of the vibrational frequencies, and a is an empirical factor.

Equation 2.2 provides insight on the lifetime and its dependency upon the density of states for the negative ion. From this simple relationship, it can be concluded that a large density of states leads to a longer lifetime. The anion has a large density of states when it has a large number of vibrational degrees of freedom and possesses a large electron affinity (Equation 2.3). Overall, electron attachment leading to a nuclear excited Feshbach resonance will take place for any molecule with a positive electron affinity. However, in some cases (i.e., small molecular anion) the autodetachment lifetime may not be long enough to be observed in the mass spectrometer. For most mass spectrometers the lifetime is required to be greater than a few microseconds in order for the anion to be observed.

2. Electronically excited Feshbach resonance: This process is associated with an electronically excited state of the molecule. An electronically excited Feshbach resonance occurs when the incoming electron excites one or more electrons in the molecule and occupies an empty orbital (hole). In this procedure, the incident electron energy and the electron affinity energy of the excited state of the molecule is shared between the vibrational and electronic densities of state of the molecular anion.

3. Shape resonance: In this case, the incident electron is trapped in a "shape" potential as a result of a long range repulsive force and the attractive short-range

polarization force. For most molecules, the long-range repulsive force is a centrifugal barrier. The electron can remain temporarily trapped in this resultant potential before tunneling out. For the case of electron attachment to a negative ion, the penetrable potential hill is referred to as a Coulomb barrier. The height and width of this barrier is responsible for the lifetime against autodetachment.

The angular momentum of the electron must be non-zero for shape resonances to occur, i.e., the repulsive centrifugal force is $\frac{l(l+1)h^2}{2mr^2}$ where l is angular momentum of the electron. The lifetimes of shape resonances are typically much shorter than those in Feshbach resonances, however it is conceivable that a shape resonance can be a doorway state to the formation of a nuclear excited Feshbach resonance.

When an electron interacts with a molecule, another process may occur depending on the energy of the electron: dissociative capture with electron energy approximately 0-10 eV, i. e., $AB + e \rightarrow A + B^-$

In the initial step of this process, an electron can attach to the molecule resulting from one of the above resonances. For instance, an electron might be captured by an electronically excited Feshbach resonance and then dissociate into a negative ion fragment and a neutral.

We shall include one more possible case, ion-pair formation, which can occur by the electron impact method as shown below

$$AB + e \rightarrow A^+ + B^- + e$$

Thus ion-pair formation occurs when the incident electron excites an electronically state of the molecule that results in dissociation of the molecule into positive and negative

ions. Because a third body (electron) recedes from the reaction, a resonance does not occur in the ion-pair formation. In this case, the electron is not captured but it acts as source of the necessary energy to produce the electronic transition in the molecule. Photon and other collisions can produce ion-pairs. The threshold energy (electron energy) for this process is the ionization potential of the positive ion plus the bond dissociation energy of the molecule minus the electron affinity of the negative fragment.

Multiply Charged Negative Ions

Although over some three decades singly charged negative atomic and molecular ions have received a wide range of attention, theoretical and experimental information on free multiply charged negative ions is rather scarce. Multiply charged anions (MCA) are generally produced in the condensed or solution phase where solvation and other electrostatic interactions can act to stabilize the MCAs. However producing small MCAs directly in the gas phase has proven challenging since there is no media present to stabilize the charges on small MCAs. For example, although CO_3^{2-}, SO_4^{2-}, SeO_4^{2-}, and PO_4^{3-} are stable ions in the condensed phase, they are electronically unstable in the gas phase.[9,10].

The subject of the existence of the doubly charged atomic ions has been a matter of controversy. In 1966, Stuckey and Kiser[11] reported the observation of doubly-charged negative ions of oxygen, fluorine, chlorine and bromine with the lifetimes on the order of 10^{-4} seconds. However later on Fremlin[12] recognized the possible experimental errors in the method used by Stuckey and Kiser. There have been several experiments[13-16] which claimed the detection of the doubly charged atomic ions, but most of the claims have

been shown to be artifacts and not reproducible. To date there is no conclusive evidence of bound or at least long-lived (> 10^{-6} s) atomic dianions. Theoretically, the large Coulombic repulsion energy between the two excess electrons confined to the small atomic region makes the occurrence of bound states of atomic dianions very unlikely.

In contrast to the atomic dianion case, there is considerable evidence for existence of gas-phase doubly or even higher charged molecular and clusters anions. One can expect that larger molecules where the two excess charges are well separated (reducing the Coulomb repulsion) with significant electron affinities will form stable, doubly charged anions. Indeed, the first doubly charged anions were observed for fairly large organic molecules. In 1969, Dougherty reported the first doubly charged of a large molecule (benzo[cd]-pyrene-6-one).[17] Since observation of Dougherty many more doubly charged of large molecules have been reported.[18-20] The first observation regarding small molecular dianions was made by Leiter and his co-workers.[21] They reported the existence of doubly charged negative ions of oxygen van der Waals as small as $(O_2)_3^{2-}$. This observation was very significant since the molecule does not have the high binding energy required to bind the second electron and also the excess charges on this small cluster are not well separated to reduce the repulsive Coulomb potential. Four years later, observation of long-lived (> 10^{-3} sec) small carbon cluster dianions, C_n^{2-} (n= 7-28) was reported by Schauer, Williams and Compton.[22] The C_n^{2-} (n= 7-28) were produced using a sputtering source. The observations of small molecular dianions stimulated a lot of interests between theoreticians and experimentalists and they sensed the need of conclusive investigation in the area of multiply charge anions and their stability in gas-phase. Over the past few years, many groups have applied primarily ion sputtering and

electrospray ionization techniques to produce doubly charged of carbon clusters, fullerenes, and other organic and inorganic species.

Experimental Techniques to Produce Multiply Charged Anions

Various experimental techniques have been developed to generate gas-phase doubly charged negative ions. One of the experimentalists concern in detection of dianions is differentiating between a doubly charged anion (M^{2-}) and a singly charged ion of half the mass $(M/2)^-$. Several successful methods resulted in production of doubly charge anions (listed in Table 2.1). The methods and some examples of dianions are briefly summarized below:

1. Laser desorption of electrophilic species from a metal surfaces: Two groups[23,24] reported the observation of long-lived C_{60}^{2-} and C_{70}^{2-} employing laser desorption method. The dianions were produced by laser desorption from a stainless steel plate covered by dilute solution of C_{60} and C_{70} molecules. The monoanions and dianions were detected using Fourier Transform Mass Spectrometry (FTMS). The doubly charged dianions, M^{2-}, was distinguished from $(M/2)^-$ by investigating the carbon-13 isotopes.
2. Sputtering: This method was employed by Schauer et al.[22], and resulted in a very important doubly charged anions, C_n^{2-} (n=7-28) as discussed earlier. In this technique C_n^{2-} (n=7-28), and C_m- (m= 1-27) were produced by sputtering a graphite surface with very high-energy Cs^+ ions (in order of 14.5 keV). The intensities of the doubly charged clusters followed an alternative pattern with even-n clusters being more intense than their neighboring odd-n clusters. In this

Table 2.1 Summary of nine mass spectrometry techniques to produce doubly-charged anions.

Experimental Method	Observed Dianions	References
Laser desorption from a metal surface	C_{60}^{2-}, C_{70}^{2-}	23, 24
Sputtering	C_n^{2-}, n =7-28	22
Electron capture by clusters	$(O_2)_x^{2-}$, x =3, 5, 7, 9	21
Electron impact to form an anion followed by an electron capture	$^-O_2NC_6H_4(CH_2)_nCO_2^-$, n =3,4	18
Sequential electron attachment to a molecule	C_{84}^{2-}	25
Electrospray ionization source	$^-O_3SO\text{-}C_nH_m\text{-}OSO_3^-$, n > 7 $S_2O_6^{2-}$, $S_2O_8^{2-}$	19, 28
Electron capture followed by dimerization	$(C_{19}H_{10}O^-)_2$	17
Electron impact followed by collision-induced dissociation of the monoanion	$^-O_2C(CH_2)_nCO_2^-$, n =2-7	20
Charge exchange collision	$C_{60}F_{36}^{2-}$, $TCNQF_4^{2-}$	26, 27

experiment, sputtering the graphite surface by Ar^+ ions also produced singly charged carbon clusters but not doubly charged clusters.

3. Neutral clusters of molecules capturing electrons: Dianions of oxygen clusters were produced applying this method.[21] Neutral clusters of oxygen were formed by expanding the oxygen gas through a 10μm nozzle at 10K temperature into vacuum. Low-energy electron beam was guided by a very weak magnetic field to the beam of oxygen clusters. Dianions of $(O_2)_n^{2-}$, n= 3, 5, 7 were detected using double-focusing sector field mass spectrometer. Several tests were established to rule out the possibility of monoanions of half the mass, i.e., observed signal is in fact $(O_2)_3^{2-}$ not $(O_2)O^-$ (they both have the same m/z=48 amu).
4. Electron impact on a large organic molecule followed by an electron capture: In this mechanism, first a monoanion is formed by electron impact and then it will become a dianion by capturing a second electron. A large organic molecule that has a high intensity monoanion and contains at least two electron- withdrawing substituents to capture a low energy electron would be the good candidate for this method. For example, *p*-$NO_2C_6H_4(CH_2)_nCO_2$ R with R = CH_3 or H. Bowie and Stapleton employed this method to generate doubly charged of $^-O_2NC_6H_4(CH_2)_nCO_2^-$, n =3,4.[18]
5. Sequential electron attachment to a molecule: This method was employed by Compton et al.[25] in production of C_{84}^{2-}. In this experiment sequential attachment of two electrons to C_{84} was reported. They employed a hybrid magnetic-sector/quadrupole mass spectrometer to produce the dianion of C_{84}. They

produced low energy electrons (0. 5 to 10 eV) through collision of the high-energy beam of electrons with nitrogen gas that was present at the source. C_{84} singly and doubly anions were observed in the mass spectrum. The linear relation between the electron beam current and the ratio intensity of the C_{84}^{2-}/C_{84}^{-} indicated sequential electron attachment. The subsequent autodetachment of the dianion also was consistent with a sequential electron attachment. They reported an autodetachment lifetime of 60 μs for C_{84}^{2-}.

6. Electrospray ionization method: Development of the electrospray ionization source by J. B. Fenn and his colleagues made major progress in the production of doubly and multiply charged anions. This method was applied in this thesis in order to produce doubly charged anions and will be discussed in detail later on. Many groups have used electrospray to produce a number of doubly charged anions of organic, inorganic and fullerene molecules.
7. Electron capture by large organic molecules followed by dimerization: In 1969, Dougherty[17] produced singly negative ions of benzo[cd]-pyrene-6-one at relatively high pressure. He also observed another peak with a very low intensity at m/z =254.5 amu next to the parent ion, m/z=254. This lower intensity peak was identified to be dimmer of benzo[cd]-pyrene-6-one negative ion. The peak at m/z=254.5 amu was only appeared at relatively high pressure.
8. Collision-induced dissociation of a singly negative ion: Doubly charged dicarboxylate negative ions were produced by collision-induced ion-pair formation from singly charged carboxylate anions. In this method, a fast beam of singly charged ions was collided with helium as a target gas and dianions of

$^{-}O_2C(CH_2)_nCO_2^{-}$, n =2-7 were observed, i.e. $RO_2C(CH_2)_nCO_2^{-}$ + He → R^{+} + $^{-}O_2C(CH_2)_nCO_2^{-}$.[20]

9. Charge exchange collision: In this technique doubly charged anions are produced through electron transfer from a molecule or gas to a negative ion in a high-energy collision mechanism. For example, Tuinman and Compton[26] produced $C_{60}F_{36}^{2-}$ through collision between $C_{60}F_{36}^{-}$ and CH_4 at about 50 KeV collision energy, i.e., $C_{60}F_{36}^{2-} \rightarrow C_{60}F_{36}^{-} + CH_4^{+}$. In a similar method reported the formation of doubly charged negative ion of $TCNQF_4$ (perfluorinated tetracyanoquinodimethane) via charge exchange between Na and $TCNQF_4$ negative ion, i.e. $TCNQF_4^{2-} \rightarrow TCNQF_4^{-} + Na^{+}$.[27]

Stability of Multiply Charge Anions

Stability of multiply charged anions has attracted considerable interest among theoreticians. A few review articles[29-32] have highlighted the stability and properties of gas-phase multiply charged anions.

In particular, a gas-phase multiply charged anion must be stable toward electron detachment and ionic fragmentation. Ionic fragmentation also termed Coulombic explosion and thermodynamic decay. Some molecules, such as MgF_4^{2-} and TeF_8^{2-}, are electronically stable (very large electron binding energy), but thermodynamically unstable. On the other hand, some other dianions such as SO_4^{2-} and PO_4^{-3} are electronically metastable. Also some species are electronically and thermodynamically stable in the gas-phase (e.g., $^{-}OOC\text{-}(CH_2)_n\text{-}COO^{-}$ for large enough n).

Stability of a gas-phase MCA is primarily determined by the repulsive Coulomb potential between the excess charges. For a multiply charged anion to be stable electronically and thermodynamically, the Coulomb repulsion has to be smaller than the binding energy of the monoanion (electronically stable) and the chemical bond strength against ionic fragmentation (thermodynamically stable). For smaller multiply charged anions it is very difficult to accomplish these conditions. The search for the smallest multiply charged anions is still an ongoing area of research. Sheller and Cederbaum[33] predicted that the small LiF_3^{2-} dianions and other species consisting of alkali metal halides, MX_3^{2-}, M = Li, Na, K ; X= Cl, Br, are electronically stable in the gas-phase. However, there is no evidence of their existence experimentally. In particular, Wang's group performed an extensive study to produce the doubly charged of these small dianions and they were not successful.[34] Somewhat later calculations performed by Sommerfeld and Child[35] predicted that these species are very short-lived due to their instability toward ionic fragmentations. Multiply charged anions of the MX_4^{2-} form also were predicted to be electronically stable[36] but thermodynamically unstable.[30,36] BeF_4^{2-} and MgF_4^{2-} were observed experimentally to posses a finite lifetime by Middleton and Klein.[37] They showed that these dianions are metastable with respect to fragmentation into two singly charged anions ($MX_4^{2-} \rightarrow MX_3^- + X^-$) as predicted by the theory.

In order to better understand the electronic and thermodynamic stability of multiply charged anions, a primary focus must be on an investigation the nature of the potential that holds the excess electrons together. This potential for the first time was referred to as a repulsive Coulomb barrier in study of multiply charged clusters and fullerene anions.[25, 29, 38-40]

The stability of dianions is due in part to the so-called "Repulsive Coulomb Barrier" (RCB), which has been compared to that of α-particles in heavy atomic nuclei. For nuclei the Coulomb barrier results from the combined long-range Coulomb repulsion and short range nuclear force. For multiply charged negative ions, the repulsive Coulomb barrier is primarily the result of a long-range coulomb repulsion and the short-range polarizibility attraction between an electron and a negative ion. The RCB can render unbound MCAs metastable or add stability to bound MCAs. In addition, many dianions are known to be stable (negative energy level) and the RCB adds additional stability to the ion. Therefore, an extensive study of the RCB is crucial to the understanding of the properties of multiply charged anions.

For a gas-phase MCA, the RCB is also expected to exist against the ionic fragmentation as a result of the long-range Coulomb repulsion between two charged fragments ($AB^{2-} \rightarrow A^- + B^-$). In general, for a MCA, there are two different repulsive Coulomb barriers to decay. The RCB against electron detachment that usually is being referred to as RCB_{ed}, and the RCB against ionic fragmentation that is noted as RCB_{if}.

To demonstrate the repulsive Coulomb barrier, let us consider the potential energy of interaction between an electron and a singly charged dielectric sphere of radius R, and dielectric constant k. This problem has been referred to in many advanced electromagnetism books (e.g. reference 41). The potential for such interaction can be written as:[38]

$$V(r) = -\frac{e^2(k-1)R^3}{2(k+2)r^2(r^2-R^2)} + \frac{e^2}{r} + \frac{l(l+1)}{2mr^2} \qquad (2.4)$$

The first term in the Equation 2.4 represents an attractive polarization potential due to polarization of the anion, the second term corresponds to the electrostatic repulsion from a charge e at the center, and the last term is a repulsive centrifugal potential for an electron with angular momentum of l. The interaction potential, V(r), between an electron and singly charged C_{60} (R = 3.5 Å, k = 4.4) is illustrated in Figure 2.1 for three different values of incident electron's angular momentum, l=0, 1, and 2. As one would expect, the height of the repulsive Coulomb barrier increases as the angular momentum of the electron increases. It can also be demonstrated how the height of the repulsive Coulomb barrier dramatically increases when two charges are placed on a singly charged anion (see Figure 2.2). This repulsive Coulomb potential, as illustrated in Figure 2.2, exhibits a general property that explains why an excess charge on a singly charged anion does not leave immediately because of repulsion between the charges.

The repulsive Coulomb barrier, RCB, has a crucial affect in determining the stability of an MCA, since it can make an MCA metastable even if the system is unstable toward electron detachment or ionic fragmentation. For a hypothetical multiply charged anion, schematic potential curves are shown in Figure 2.3, for two difference cases of electron detachment where the MCA is electronically stable or unstable. RCB (inner) and RCB (outer) are used to differentiate the inner and outer part of the repulsive Coulomb barrier. The inner part, RCB (inner) refers to the height of the barrier from the minimum energy structure of the MCA and the outer part refers to the height of the barrier from the dissociative asymptote. Figure 2.3 (b) shows the case when the long-range Coulomb repulsion is stronger than the short-range electron binding (EB), resulting in a metastable

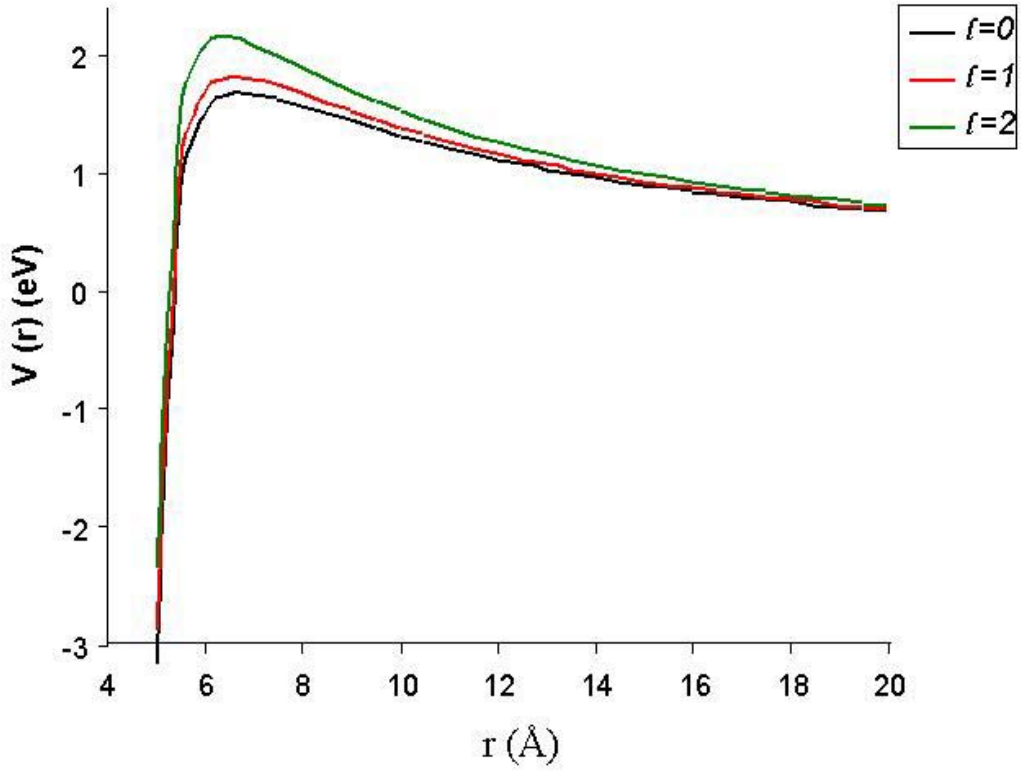

Figure 2.1 Effective interaction potential between an electron with angular momentum of l and a singly charged C_{60} (R = 3.5 Å, k = 4.4). The potential has been graphed for three different values of electron angular momentum, $l = 0$, 1, and 2.

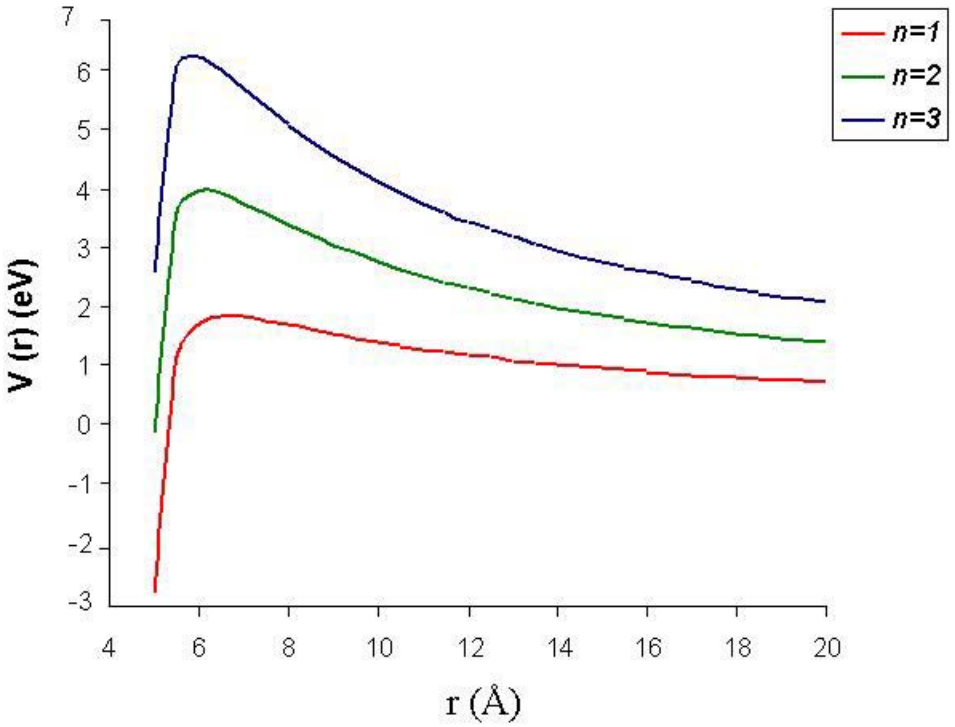

Figure 2.2 Effective interaction potential between an electron with angular momentum of l=1 and a singly charged C_{60} (R = 3.5 Å, k = 4.4). The potential has been graphed for when one charge (n=1), two charges (n=2), and when three charges (n=3) are placed on the C_{60} anion.

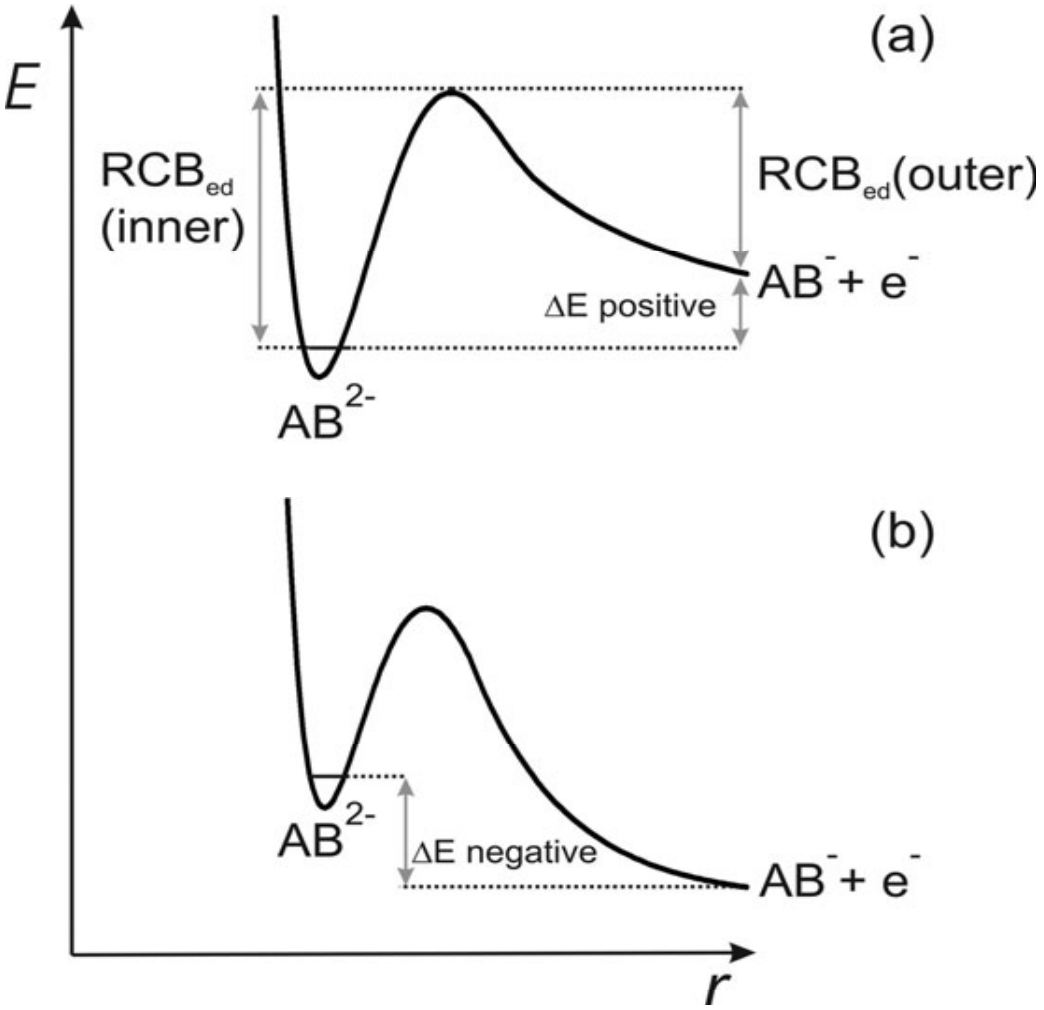

Figure 2.3 Schematic potential curves for an MCA that is (a) electronically stable with a positive electron binding energy and (b) electronically metastable with negative electron binding energy. The inner part, RCB (inner) refers to the height of the barrier from the minimum energy structure of MCA and the outer part refers to the height of the barrier from the dissociative asymptote.[54]

MCA. Metastable MCA can exist because of the repulsive Coulomb barrier, which provides substantial lifetime for the metastable MCA. The height and width of the RCB determine the lifetime of the metastable MCA since the lifetime is a result of tunneling through the Coulomb barrier.

As stated above, an MCA can decay by either electron detachment or ionic fragmentation resulting in two negatively charged particles. There is another possible channel for MCA decay that is decay through loss of a neutral particle (Fig. 2.4 (c)). This decay only occurs for a small number of MCAs. For example, dicarboxylate dianions decay with loss of a neutral molecule.[42,43] Figure 2.4 displays potential energy curves illustrating possible decay pathways of multiply charged anions.

Experimental Evidence of the Repulsive Coulomb Barrier

A number of studies by Compton and others have investigated existence of the repulsive Coulomb barrier, but for the first time Lai-Sheng Wang and co-worker[44] were able to observe the RCB experimentally for citric acid dianions using and ESI source coupled with a magnetic-bottle time-of-flight photoelectron analyzer. In their study, they noted that with photons of 4.66 eV (266 nm), the photoelectron spectra consisted of two spectra bands, which was assigned to be X and A electronic states of monoanion citric acid. At the lower photon energy, 3.49 eV (355 nm), only one single band was observed. Figure 2.5 shows the photoelectron spectra of the citrate dianion at two different photon energies. They also attempted to record a photoelectron spectrum at the lowest photon energy of 2.33 eV (532 nm), but no photoelectron signal was observed, despite the fact that the photon energy was higher than the electron binding energy of X and A states

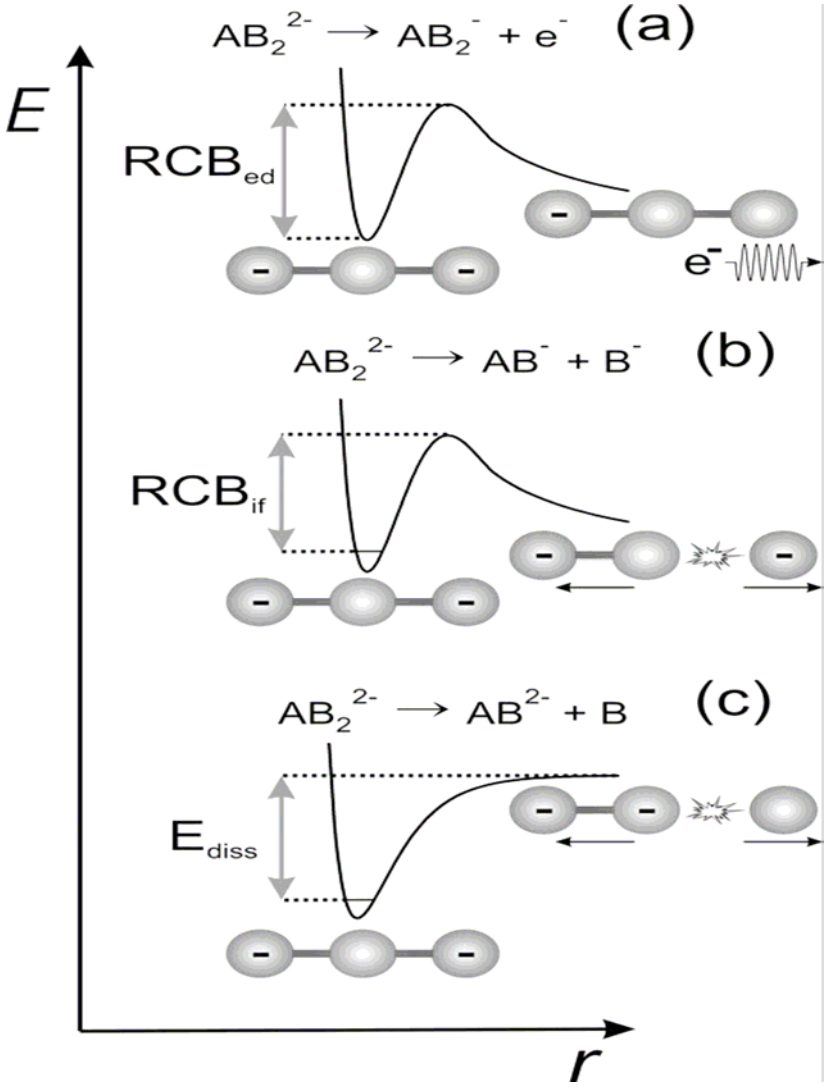

Figure 2.4 Schematic potential energy surfaces for decay pathway of a dianion (a) via electron detachment (b) ionic fragmentation, and (c) loss of a neutral molecule. RCB_{if} represents the repulsive Coulomb barrier for ionic fragmentation, RCB_{ed} represents the repulsive Coulomb barrier for electron detachment, and E_{diss} is the threshold for dissociation energy.[54]

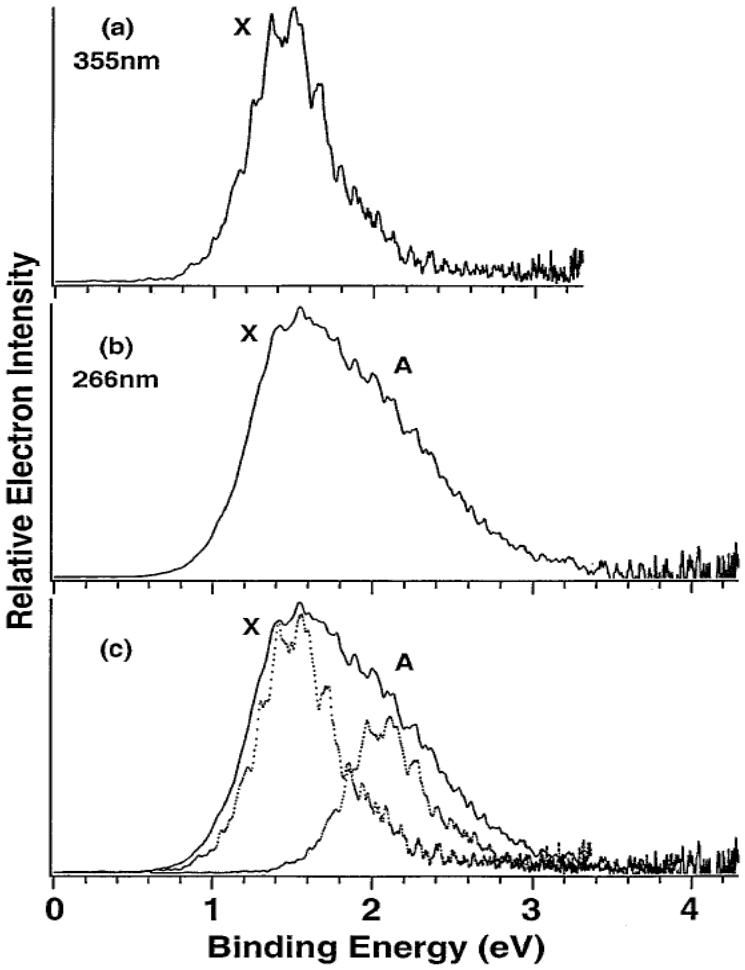

Figure 2.5 Photoelectron spectra of citrate dianion (CA^{2-}) at (a) 355 nm, (b) at 266 nm, and (c) at 266 nm consisted of two spectra bands, X and A electronic states of CA^{-}. [44]

(having binding energy of 1.0 eV and 1.6 eV, respectively). This observation, i.e., that no electron detachment was occurred at 2.33 eV, provided the first evidence of the existence of the repulsive Coulomb barrier. From the photoelectron spectra, they estimated the height of RCB (outer) for electron detachment of the citrate dianions to be about ~ 1.9-2.5 eV (Figure 2.6). Another notable result derived from the Wang el al.[44] experiment was an estimate of the Coulomb repulsion between two excess charges. If one assumes that the electrons are localized on the CO_2 ligands of citric acid (Figure 2.6), the equilibrium distance between two charges would be about 6.14 Å. The Coulomb repulsion energy corresponding to 6.14 Å charge separation [e^2/ (6.14 Å)] would give a value of about 2.31 eV. This value suggested that the obtained RCB (outer) (1.9-2.5 eV) is equal to the Coulomb repulsion energy between two charges. This relation was further examined in study of dicarboxylic dianions that will be discussed in Chapter VI. This result also suggests that the magnitude of the RCB (inner) is related to the binding energy of the excess electron to the singly charged anion.

A year later, Wang's group[45] reported further support for the existence of the RCB in metastable multiply charged anions. In this experiment, they demonstrated that multiply charged anions with negative electron binding energies could exist. While examining the photoelectron spectra of the copper phthalocyanine tetrasulfonate tetraanion, $[CuPc(SO_3)_4]^{-4}$, they observed a negative binding energy of the excess electron, i.e. the kinetic energy of photodetached electron was higher than the energy of the incident photon. This important study provided a confirmation for the role of the RCB in metastable multiply charged anions. Similar approaches can be used in case of C_{60}^{2-} dianion. C_{60} anion has been predicted to have a negative electron affinity of the order of

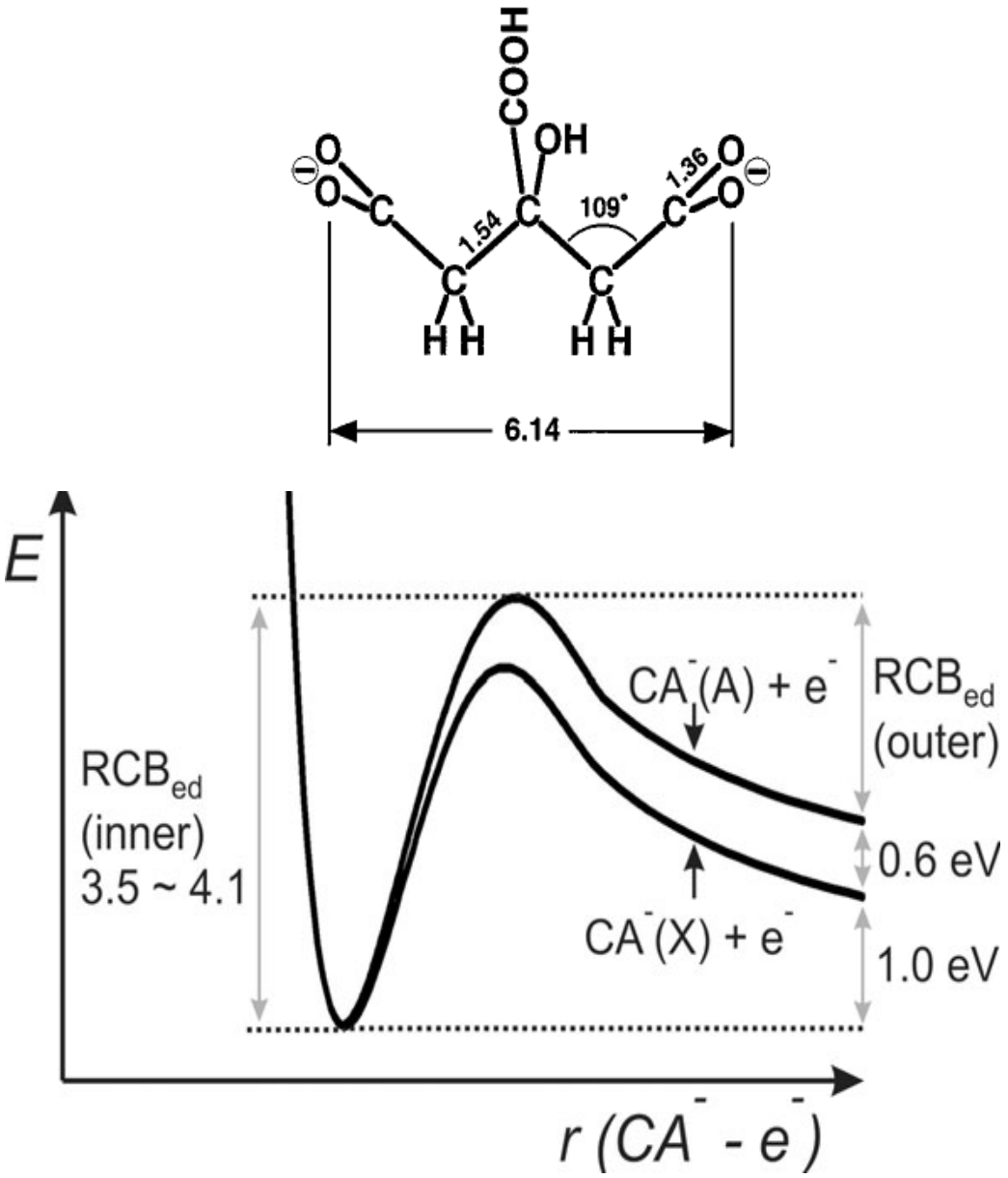

Figure 2.6 Schematic potential energy surfaces illustrating the RCBs for electron detachment of citrate acid dianion, leading to the X and A states of citrate acid monoanion.[54]

0.3 eV[39,40], however C_{60}^{2-} has been observed in the gas-phase with a lifetime greater than 10^{-3} seconds.[23,24,46] Following the first direct proof of the repulsive Coulomb barrier by Wang et al.[44,45], many studies have observed the repulsive Coulomb barrier for electron detachment in many multiply charged anions primarily using photodetachment spectroscopy. [47-49]

Ionic Fragmentation versus Electron Detachment

A wide range of experimental and theoretical studies has focused on the stability of the MCA with respect to electron detachment[25,30,32,50] while the stability of the MCAs toward ionic fragmentation has not been very well explored. Major progress and interest in the stability of MCA toward electron detachment research area have arisen particularly from the photodetachment measurements by Wang's group.[44,45]

In the context of stability of MCAs via ionic fragmentation, the Kappes group have examined the stability of a group of doubly-charged anions (MX_6^{2-}) toward ionic fragmentation. In their first experiment, they examined the stability of $IrBr_6^{2-}$ toward ionic decay employing a collisional excitation of ions isolated within a quadrupole trap.[51] $IrBr_6^{2-}$ was chosen since its RCB (inner) against electron detachment already had been previously estimated to be ~3.0 eV.[52] Photodissociation of $IrBr_6^{2-}$ resulted into Br^-, and $IrBr_5^-$. They provided the first estimate of the RCB (inner) for ionic fragmentation to be about 1.6 ±0.2 eV, and with measuring the released kinetic energy they estimated the height of RCB (outer) to be 2.2 ±0.2 eV. Their results indicated that the RCB for electron detachment is higher (~ 1.4 eV) than RCB for ionic fragmentation meaning that the ionic fragmentation decay pathway is lower than decay against electron detachment. Boxford

and Dessent[5] also investigated the heights of the RCB for some metal complex dianions such as $IrCl_6^{2-}$, $IrBr_6^{2-}$, $ReCl_6^{2-}$, and $PtBr_6^{2-}$. All of these dianions would decay either by electron detachment or ionic fragmentation, i.e., $MX_6^{2-} \rightarrow MX_6^- + e$, or $MX_6^{2-} \rightarrow MX_5^- + X^-$. Interestingly, their results also suggested that for these dianions the RCB for ionic fragmentation lies below the RCB against electron detachment as illustrated in Figure 2.7.

As discussed earlier, the RCB (outer) for the electron detachment was attributed to the Coulomb repulsion energy between the charges and the RCB (inner) to the attractive binding energy of the electron to the monoanion. Boxford and Dessent[54] applied the same analogy and proposed that for the ionic fragmentation the RCB (inner) is associated with the attractive binding energy between of an X^- ion and MX_5^- moiety. Boxford et al.[55] in another similar investigation concluded that for $Pd(CN)_4^{2-}$ ionic fragmentation is the lower energy decay pathway as well. A recent study of sodium chloride clusters dianions exhibited the same result.[56]

As we have seen from the experiments carried out by Boxford's group, the MCA (specifically metal complex dianions) decay through ionic fragmentation, i.e., the RCB (ionic fragmentation) < RCB (electron detachment). To be able to generalize this important feature of the MCAs, more experiments and calculations need to be performed.

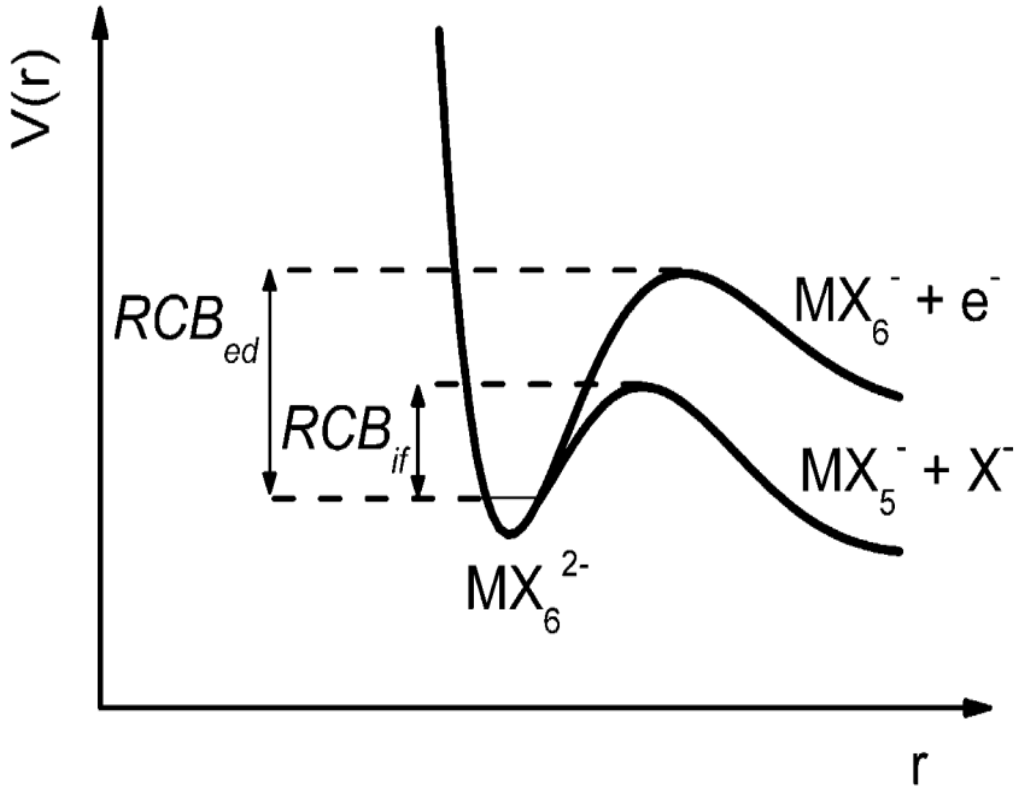

Figure 2.7 Schematic presentation of the potential energy surfaces for decay of MX_6^{2-} via ionic fragmentation and electron detachment. RCB_{if} represents the repulsive Coulomb barrier for ionic fragmentation and RCB_{ed} represents the repulsive Coulomb barrier for electron detachment. [53]

CHAPTER III

Experimental

Introduction

Electrospray mass spectroscopy has attracted wide interest over the past years. It represents one of the fastest growing mass spectrometric techniques for the analysis of biomolecular and macromolecules. Prior to the development of Electrospray ionization (ESI) by Yamashita and Fenn[57], the production of doubly-and triply-charged ions of most large species in the gas phase without fragmentation and/or degradation was rarely reported. In addition to the soft ionization afforded by ESI, a major advantage of ESI is the ability to reduce the m/Q of large molecular weight ions into the low mass region corresponding to the masses of small molecules by increasing the charge Q. ESI provides unique opportunities to the world of analytical biochemistry. For example, mass identification of proteins represents one of the challenging species using other mass spectrometric techniques due to their inherent fragmentation. The importance and applications of electrospray ionization for the study of multiply charged anions, the subject of this thesis, will be discussed in the following chapters. This chapter will focus on the operation of the electrospray ionization source and its production of multiply charged ions. In the following section, collision-induced dissociation theory, which is one of the most important methods applied in this thesis to investigate stability of the multiply charged anions, will be discussed.

Principles of Electrospray Ionization

The various sources of Electrospray ionization (ESI) have undergone extensive development over the years; however, the essential process has remained the same. A brief discussion of the basic ESI method follows: in electrospray ionization, a solution of the analyte is introduced from a syringe pump to a small hole from a capillary (1-4 μm). Typical flow rates are of the order of 3-20 μl/min. The solution passes through a capillary needle that has a high potential difference (typically 3.5 kV for positive ions and 2.5 kV for the negative ions) relative to the entrance to the mass spectrometer. The capillary needle is located 1-3 cm from the counter electrode. The purpose of the high electric field as the solution emerges from the tip is to generate a spray of highly charged droplets, which subsequently pass down an electrostatic potential and pressure gradient toward the analyzer (see Figure 3.1). As the droplets travel from the needle tip to the cone, solvent evaporation occurs. At this point the droplet reaches a critical point, called the Rayleigh limit, such that it can no longer hold the charge (Coulomb explosion) and it blows apart into a cloud of small, highly charged droplets. These small ions resulting from full evaporation "fly" into the mass spectrometry/quadrupole mass spectrometer through the cone (skimmer electrodes) (Figure 3.1). In order to ease the evaporation process a sheath flow of nebulizer gas can be used. A nebulizer gas is commonly used in many ESI commercial instruments. The type of the nebulizer gas can be determined by the flow rate, composition of the solvent and the sign of the capillary voltage.[58]

Although Electrospray ionization is used to produce either positive or negative ions, making a stable negative ion is more difficult due to the possibility of electric discharge at the source needle tip. This could be one of the reasons that most studies reported

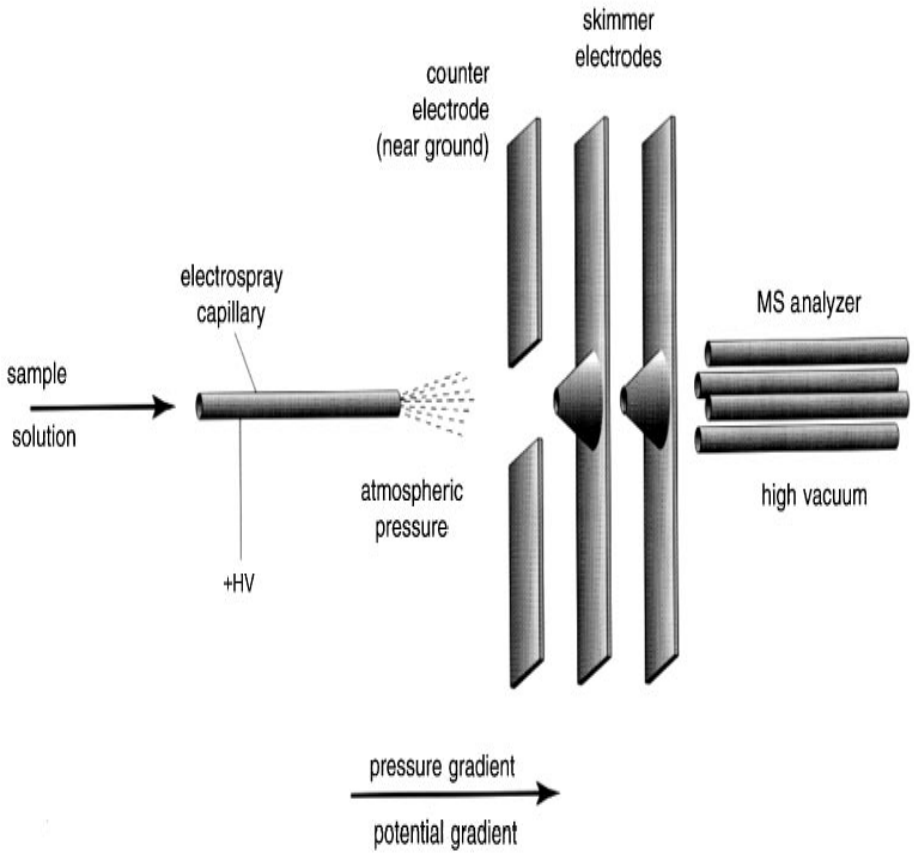

Figure 3.1 A schematic of an electrospray ionization source [58]

employ the positive ion mode. Yamashita and Fenn[59] concluded that the onset of a discharge occurs at a very low field for negative ions. They suggested introducing a gas with a high electron affinity or one that is highly electron attaching over the spray tip would decrease the possibility of the discharge. Some of the reported gasses are O_2[59] and SF_6[60]. Numerous studies have shown that the nature of the solvent in the negative ion mode would lead to the electric discharge as well. An equation by Smith[61] shows that the onset capillary voltage required for different solvents increases with the square root of surface tension as presented in Equation 3.1.

$$E_{on} = \left(\frac{2\gamma \cos\theta}{\varepsilon_0 r_c}\right)^{1/2} \tag{3.1}$$

where E_{on} predicts the electric field at the capillary tip, γ is the surface tension of the solvent, θ is the half angle of the liquid cone at the tip of the capillary, ε_0 is the permittivity of vacuum, and r_c is the outer radius of the capillary. For instance, the onset capillary voltage for the experiments using water as solvent is 1.8 times higher than that for methanol[61] meaning that there is a higher possibility of electric discharge at the needle tip for experiments using water as solvent. Therefore, as a result, when the onset for the capillary voltage for water increases, the chance of the electric discharge at the needle tip will increase. However, a major advantage of using water is that it is generally a perfect solvent for many ionic analytes, especially for multiply charged ions. Wampler[62] and his colleagues in 1992 performed several experiments in the negative ion mode using methanol and water as solvents with and without SF_6. They observed that the electrospray ionization onset voltage (capillary voltage) was much lower when methanol was used as a solvent. This result confirmed the Equation 3.1 derived by Smith[61].

Additionally, they examined that in the presence of SF_6 the onset of the discharge increased for both solvents. For methanol the discharge did not interfere with the ESI operation, but for water (onset voltages ≈onset of electric discharge) performing the experiment without SF_6 was not possible. From the discussion above, it should be noticed that it is necessary to find the right solvent and to discover the proper physical conditions, i.e., capillary voltage, cone voltage, flow rate, etc. in order to obtain reliable results from ESI.

In many experiments, the electrospray source is equipped with three quadrupole mass spectrometers (the instrument used in this study). The so-called triple quadrupole enables researchers to select an ion of interest and perform collision-induced dissociation (CID) in order to obtain structural information such as bond energies or examine the stability of multiply charged ions. In the triple quadrupole mass spectrometer, the first and third quadrupoles are for mass selection filter and the second quadrupole is used as a collision cell.

Figure 3.2 shows a Z-spray electrospray ionization source coupled to three quadrupole mass spectrometers. The Z-spray source consists of two nebuliser and desolvation gas sources. The neubuliser gas usually runs concurrent with sample flow to help create droplets. When a sample is introduce at high flow, droplet are not small enough to produce ions before reaching the sample cone, therefore a heated gas stream known as desolvation gas is introduced into the system to help in further reducing the droplet sizes. In Figure 3.2, Q1 and Q2 are the first and second quadrupole mass spectrometer, respectively. D1 and D2 indicate the electron multiplier detectors for ions

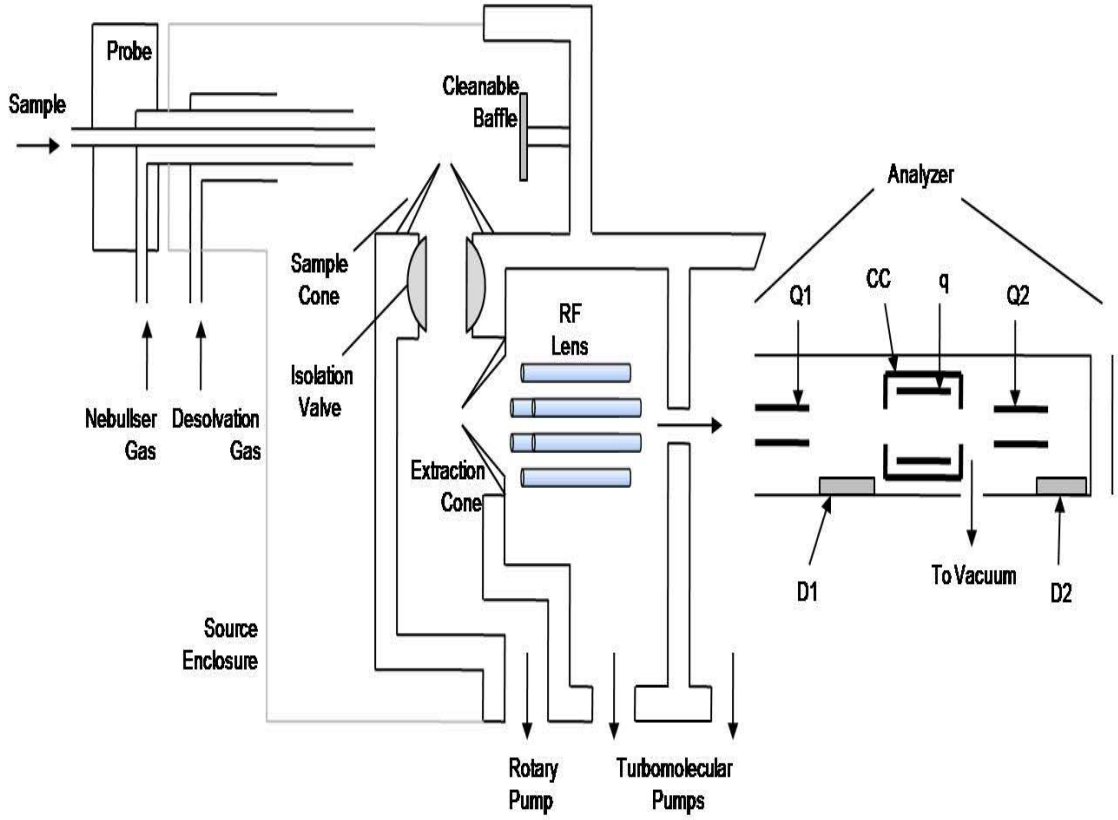

Figure 3.2 A schematic view of a Z-spray electrospray ionization coupled to three quadrupole mass spectrometers. Q1 and Q2 are the first and second quadrupole mass spectrometers respectively. D1 and D1 are the electron multiplier detectors. CC is the collision cell containing a quadrupole ion guide q.

exiting Q1 and Q2 respectively. CC presents the collision cell containing a quadrupole ion guide q.

Theory of Collision-Induced Dissociation

Collision- induced dissociation (CID) of gas-phase charged cluster ions provides a methodology to investigate the thermodynamic properties of the molecular ions such as bond dissociation energies, geometry of clusters and, in particular, measuring the heights of barriers to dissociation. This method consists of colliding the ion of interest with an inert target gas, usually argon or helium, in a collision cell and measuring the probability of the dissociation as a function of collision energy in the center-of-mass frame. Dissociation occurs as a result of conversion of the collision energy into internal energy leading to subsequent decomposition.[63]

The CID technique can be performed for high collision energies (keV) using a tandem sector and time-of-flight mass spectrometer or at low collision energies with (eV range) tandem quadrupole and ion trap instrument.

In the CID method, investigation of the resultant fragments provides information about the structure of the precursor ion. The threshold energy derived for the dissociation provides information on dissociation energy of the fragments if there is no barrier to dissociation such as a Coulomb barrier (multiply charged ions) to the reaction. In addition, another application of the CID method is to examine electron detachment from negatively charged anions.

The total cross-section for the CID reaction, σ_{total}, can be determined employing Beer's Law, along with proper variables for the CID experiments[64],

$$I = I_0 \exp(-\sigma_{total} n \ell) \quad (3.2)$$

where I is the intensity of the outgoing reactant beam, I_0 is the intensity of the incoming beam, n is the number density of the collision gas and ℓ is the path length of the collision cell.

In order to interpret experimental results from the CID method, especially to extract a threshold energy of a reaction, a modeled energy dependent cross-section is needed. In this regard, Armentrout and co-workers[65] developed an expression for the CID cross-section. Their assumed energy dependence cross-section is given in Equation 3.3,

$$\sigma(E) = \sigma_0 \Sigma_i g_i (E + E_i - E_0)^n / E \quad (3.3)$$

where $\sigma(E)$ is the cross-section for formation of the product ion at the center of mass energy E, E_0 is the reaction threshold energy, σ_0 is an independent scaling factor, n is an adjustable parameter, and E_i represents the internal energy of the ion (electronic, vibrational, rotational) having population g_i ($\Sigma_i g_i = 1$). As reflected by σ_0 and n, all relative reactivities of ro-vibrational states are assumed to be equivalent. The density of the ro-vibrational states and population g_i are calculated by the Beyer-Swinehart algorithm[66] applying a Maxwell-Boltzmann distribution at the reactants temperature. The equation $E_{com} = E_{lab}\, m/(m+M)$ is used to convert the energy from the lab frame (E_{lab}) to COM frame (E_{com}), where M and m are the masses of ionic reactants and neutral, respectively.

Although the concept of the CID experiment seems straightforward, many factors must be taken into account in order to extrapolate accurate thermodynamic information such as bond dissociation energy.

Armentrout[67] has presented a review article describing an experimental technique to study reaction cross-section over a wide range of kinetic energy using guided ion beam mass spectrometry. In this article, he points out that many effects such as internal energy and kinetic energy of the reactant ion (electronic, vibrational, and rotational), broadening by the thermal motion of the collision gas (Doppler broadening[68]) and the possibility of multiple collisions should be taken into account. For example, if one does not consider the internal energy of the reactant ions, the threshold energy for dissociation would appear lower than the true threshold. When performing the CID method, the experiment should be carried out under single collision (low pressure) conditions. Armentrout et al.[69] examined the effect of multiply collision conditions (the pressure of the collision gas) on the threshold of the dissociation energy. They noted that multiple collisions would also shift the threshold energy for the dissociation to a lower limit. Their results also showed that multiple collisions have a negligible effect on the dissociation energy threshold of the smaller clusters, but the effect will increase as the size of the cluster increases.

A CRUNCH computer program by P. B. Armentrout and co-workers was provided to the Compton group in order to treat the CID experimental data and to derive the true threshold energy, E_0, for the reaction. The program first chooses a model cross-section applying Equation 3.3, and then accounts for effects such as ion internal energy, Doppler broadening due to the random thermal motion of the collision gas and the kinetic energy distribution of the reactant ion. Finally, the model cross-section is compared to the CID experimental data and fitting parameters are adjusted to give the best least-squares fit. Details of this modeling and the theoretical background are discussed in a paper by Armentrout et al.[64] and references therein.

In a CID experiment involving a multiply charged anion (MCA), the measured threshold energy for the MCA to detach an electron or dissociate into ionic fragmentation, depends upon the inner repulsive Coulomb barrier (RCB) as shown in Figure 3-3. The dissociation energies also can be computed with the aid of available computational methods. As a result, an estimate of the outer repulsive Coulomb barrier can be made, i.e., inner repulsive Coulomb barrier is sum of the computed dissociation energy and the outer repulsive Coulomb barrier.

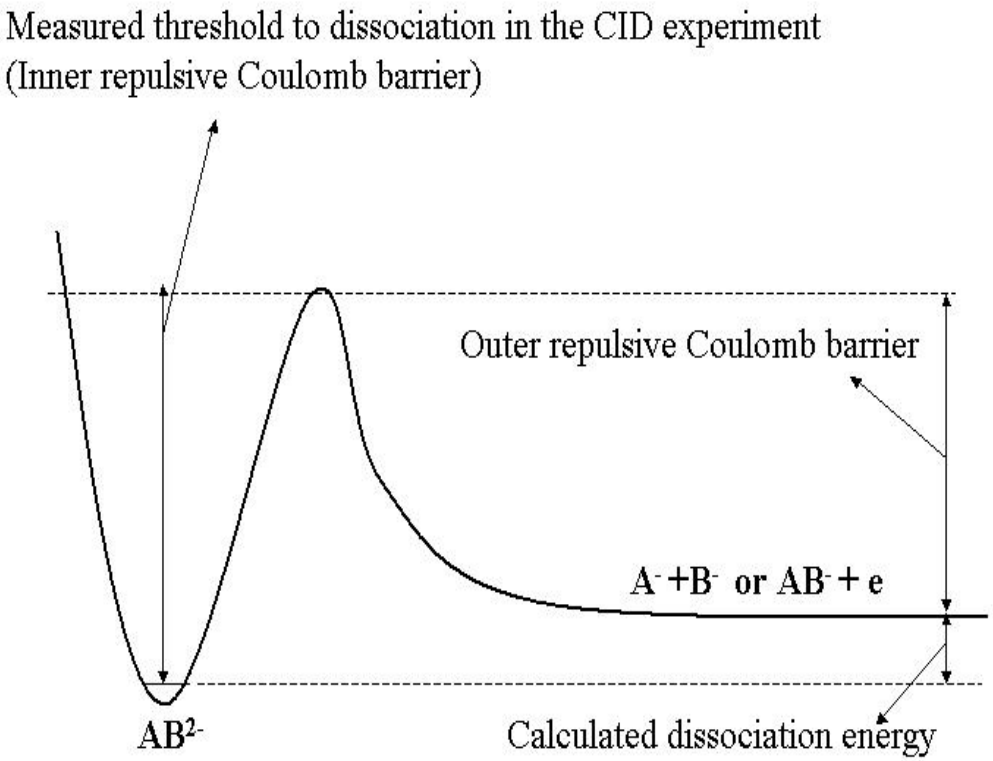

Figure 3.3 A schematic potential curve for an MCA to dissociate via electron detachment or ionic fragmentation. Inner and outer repulsive Coulomb barriers are shown.

CHAPTER IV

A Study of Coulomb Barrier Heights for Dissociation of Doubly-Charged $[Na_xCl_{x+2}]^{2-}$ (x=7& 15) Cluster Ions

Introduction

The electrospray ionization source (ESI) has been demonstrated to be a powerful technique in the study of gas-phase multiply charged anions (MCA). For example, doubly charged of fullerenes and derivatives such as C_{60}^{2-}, C_{70}^{2-}, $C_{60}(CN)_2^{2-}$, $C_{60}(CN)_4^{2-}$, $C_{60}(CN)_6^{2-}$ have been observed using the ESI technique.[71,72] Wang et al. reported the first observation of gas-phase hexahalogenometallate doubly charged anions [ML_6^{2-} where M=Re, Os, Ir, Pt; L=Cl and Br] employing the ESI method.[52] Many more studies have also demonstrated the ability of the ESI method to produce gas-phase multiply charged anions.

The major interest in production of a gas-phase MCA is to study its stability against electron detachment and ionic fragmentation. The study of fragmentation behavior of a MCA also provides valuable structural information. One of the available techniques used to investigate the stability, detailed structural formation, and decay pathways of MCAs is to perform collision- induced dissociation (CID) studies of multiply charged species.

In this regard, Blades and Kebarle[73] investigated the stability of some doubly charged hydrated ions such as $SO_4^{2-}.nH_2O$, $S_2O_6^{2-}.nH_2O$ and $S_2O_8^{2-}.nH_2O$ using an ESI source and triple quadrupole mass spectrometer. CID of these dianions resulted in bare $S_2O_6^{2-}$ and $S_2O_8^{2-}$ dianions; however SO_4^{2-} was not observed. SO_4^{2-} has been reported to be electronically unstable in the gas-phase.[10] Three metal carbonyl cluster anions, $Ru_3Co(CO)_{13}^-$, $Ru_6Co(CO)_{16}^{2-}$, and $Ru_6Co(CO)_{18}^{2-}$ were produced employing the ESI

source and investigated using the CID method. For the doubly-charged species, two competing channels were observed; loss of neutral CO and loss of CO + e.[74]

Tuinman and Compton[75] employed CID method to study the $(C_{60})_n (CN)_m^{x-}$ (n=1-3, m=1-7, and x=1-3) structures. For example, studies of CID of $(C_{60})_3 (CN)_7^{3-}$ showed that the structure of this triply-charged negative ion is $[(C_{60})(CN)_2 \ldots (C_{60})(CN)_3 \ldots (C_{60})(CN)_2]^{3-}$. Their electrostatic calculations also indicated the role of Coulomb barrier as a possible binding force between the components of the clusters. In this work, it was suggested that clusters of cluster anions could be made metastable or even stable as a result of the combined long-range repulsive and short-range attractive forces.

As it was discussed in Chapter II of this thesis, the existence of the repulsive Coulomb barrier is very important for the stability of the MCAs with respect to electron detachment and ionic fragmentation. Clearly, one way to examine such stability is to apply the CID technique. In addition to stability studies, comparison of the order of Coulomb barrier heights for electron detachment and ionic fragmentation is a subject of a very few studies. For instance, the Boxford group[53] investigated the heights of the repulsive Coulomb barrier for electronic decay versus ionic fragmentation performing CID experiments. They demonstrated that for some metal complex dianions ionic fragmentation barrier heights are lower than barrier heights for electron detachment. Yang et al.[76] studied a series of doubly-charged clusters anion, $[Fe_4S_4X_4]^{2-}$ where X= Cl, Br, I, and SC_2H_2. They determined that in the CID experiment of $[Fe_4S_4X_4]^{2-}$ (X= Cl, Br, and SC_2H_2) the only available channel is dissociation into two singly charged ions. The CID products were two symmetric $[Fe_4S_4X_4]^-$ (X= Cl, Br, and SC_2H_2) anions. No electron detachment was observed for the $[Fe_4S_4X_4]^{2-}$ dianions, however electron

detachment was found to be the dominant channel for the $[Fe_4S_4I_4]^{2-}$ dianions. These examples and many more demonstrate the utility of the CID technique to probe the properties of a multiply charged anion.

Experimentalists and theoreticians have shown great interest in the properties of salt clusters, especially those involving alkali halides (subject of this study) for years. Such clusters are believed to exhibit simple ioniclike bonding features that facilitate their production in the lab as well as to model them theoretically. Sodium chloride clusters have also attracted the attention of atmospheric scientists due to the fact that the interaction of this major component of sea salt with nitrogen oxides generates chlorine atoms. The generated chlorine atoms then react with ozone molecules to form chlorine monoxide and oxygen molecules. A study by Oum and his colleagues[77] shows that photolysis of ozone in the presence of the sea-salt particles produces Cl_2, another possible source of chlorine in the atmosphere. Rosenfeld and his co-workers[78] investigated the role of sea spray in cleansing air pollution over the sea through cloud processes. According to their study, raindrops formed by the sea salt increase its concentration by collecting the small clouds resulting from the pollution particles and as a result would clean the sea air. In addition, Bruce[79] has argued that halide ions at the surfaces of atmospheric aerosol particles may control oxidant levels in the oceanic boundary layer of the atmosphere. Bruce points out that atomic ions in salt solutions show a tendency to escape the water/air interface; whereas computational and experimental studies show that atomic ions such as halide anions can be present in the surface region.

A few studies on multiply charged alkali halide clusters exists. A theoretical study by Scheller and Cederbaum[80] examined the stability of the gas-phase salt dianions $M_2X_4^{2-}$

(M=Li, Na, K; X=F, Cl). They reported that these dianions are electronically (electron detachment) and thermodynamically (ionic fragmentation) stable. Friedrich et al.[81] were able to produce singly and doubly charged salt clusters using an electrospray ionization source. They also performed some theoretical investigations of the optimized structures of salt cluster dianions.

In the work presented here, we shall present an investigation of the stability of salt clusters dianions, $Na_nCl_{n+2}^{2-}$ (n = 7, 15), toward ionic fragmentation and electron detachment applying the collision-induced dissociation (CID) technique.

Experimental Method

The instrument employed in this study was a commercial Micromass Quattro II (triple quadrupole) mass spectrometer with an electrospray ionization (ESI) source as descried in the previous chapter (Figure 3-2). The ESI source was a Z geometry design. The "Z" denotes the path of the ions during introduction and analysis. The outcome and performance of this design is exactly the same as one with the linear design. The Z-spray source is used to prevent the source electrodes from contamination especially when one is working with samples such as sodium chloride.

To produce the ions of interest, $(Na_xCl_{x+2})^{2-}$ x =7 & 15, a 40mM solution of sodium chloride in D_2O was introduced into the ESI source at a flow rate of 10 µl/min. The ES capillary voltage was set to -2.5 kV. The cone voltage was varied from 0 to +80 V. The optimum cone voltage in which doubly charged ions were observed was +40 V. The source block temperature was set to 48 $^{\circ}$C and the desolvation temperature was 120 $^{\circ}$C. The nebulizer and desolvation gases were nitrogen with flow rates of 40 and 300

liters/hour, respectively. The electrical discharge was one of the main difficulties encountered in the study due to the fact that the experiment was performed in the negative ion mode and the solvent used in this experiment was D_2O (please note the discussion in previous chapter). The anions to be studied were selected by the first quadrupole (Q1). The reactant ions were guided by an appropriate electrostatic potential into the collision cell (CC). Argon was used as a collision gas. The experiment was carried out under approximately single collision conditions. After performing collision-induced dissociation, the second quadrupole (Q2) was used for secondary ion mass analysis. The experiment was carried out for different collision energies (0 to 50 eV in the lab frame).

In the CID experiment, the potential difference between the ion source and the interaction region determines the ion kinetic energy in the lab frame. The actual ion energy may differ by as much as several electron volts due to contact potential, surface charge effect and other possible voltage reading offsets in the apparatus. In order to calibrate the ion energy scale in our study, a retarding analysis was performed on an atomic ion. A solution of ammonium bromide (NH_4Br) with 5 μM concentration in a mixed solvent of CH_3OH: H_2O = 10000:1 introduced into the electrospray to produce the Br anions. We investigated the threshold energy of Br^- passing through the collision cell with no collision gas applied in order to verify the apparatus "zero energy". In this part of the study, we introduced NH_4Br solution into ESI due the fact that cleaning the system after using the sodium chloride salt is not very convenient. In addition, we could obtain a relatively significant signal of Br^- from NH_4Br solutions.

We performed the retardation graph with a different sample, KBr, and identical results were observed. A retardation curve for the Br^- is shown in Figure 4.1. The kinetic energy distribution and "zero energy" can be obtained by taking the derivative of the retardation curve. Using the retardation method, the energy scale in the experiment has approximately 0.44 eV offset and the full-width, half-maximum of the ion energy was approximately 0.5 eV.

Results and Discussion

A full scan ESI mass spectrum (80 to 900 amu) of the anions produced from electrospraying the sodium chloride in D_2O is shown in Figure 4-2. Singly charged anions, $(Na_xCl_{x+1})^-$ where x=1 to 13, as well as clusters of the form of the $(Na_xCl_{x+2})^{2-}$ where x= 6 to 27 were observed. The intensity of the anions is seen to decrease as the size of the cluster increases. The stoiciometry of each cluster ion was determined from its mass/charge ratio, i.e. the doubly-charged anions peaks are at one-half the mass-to-charge ratio of their parent anions. The most intense ion produced under our experimental conditions was $NaCl_2^-$. The smallest doubly charged ion observed was $Na_6Cl_8^{2-}$. For all of the doubly charged anions, $(Na_xCl_{x+2})^{2-}$, with x being an even number, the peaks are mixed with the peaks from singly charged ions as shown in Figure 4.3; i.e., peaks from $Na_6Cl_8^{2-}$ are odd mass peaks between the peaks from $Na_3Cl_4^-$. For this reason, doubly charged anions with odd number of x, i.e. $Na_7Cl_9^{2-}$and $Na_{15}Cl_{17}^{2-}$, were chosen for the CID experiment. Figure 4.4 highlights two of the dianions with odd number of x. Due to the salt contamination in the system, it was difficult to study complete sets of dianions. As a result of this, only extensive studies for two sets of dianions, $Na_7Cl_9^{2-}$ and $Na_{15}Cl_{17}^2$,

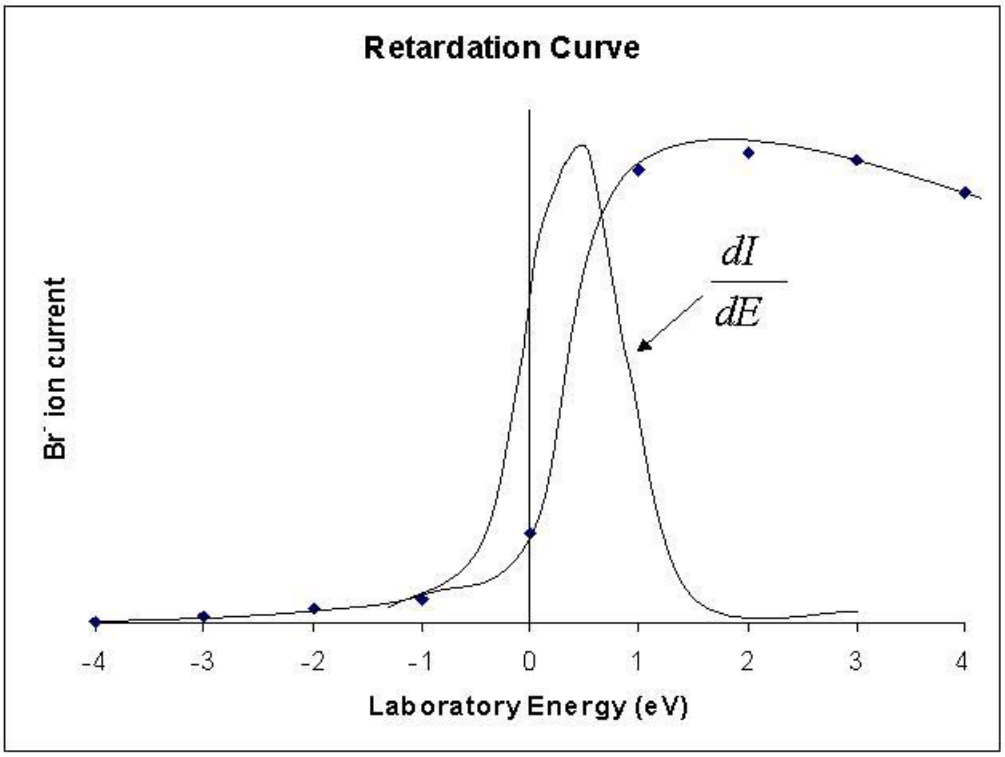

Figure 4.1 Collision- induced dissociation of Br^- with no collision gas (retardation curve). The derivative of the retardation curve, $\frac{dI}{dE}$ is also shown.

were performed. CID of singly charged $NaCl_2$ was also performed. Details of the experiment for $NaCl_2^-$ will be discussed in Chapter V.

Collision-induced dissociation of the $Na_7Cl_9^2$and $Na_{15}Cl_{17}^{2-}$ are shown in Figure 4.5 through 4.8. The collision product ions detected from $Na_7Cl_9^{2-}$ were quite fascinating. Remarkably, at a very low energy (~1 eV) $Na_7Cl_9^{2-}$ dissociates into conjugate ion pairs of the type $NaCl_2^-(NaCl)_x + NaCl_2^-(NaCl)_{5-x}$ for x= 0,1,2 (see Figures 4.5 & 4.6)) were observed. Investigating the fragment ions leads to information on the structural geometry of the clusters. From the observed dissociation, we conclude that $NaCl_2^-$ represents the main core of the cluster with the rest of the cluster built around this unit. In the future we will abbreviate the ions such as $NaCl_2^-$, and $Na_7Cl_9^-$ as (1,2) and (7,9) for brevity. During the experiment it was observed that at the dissociation threshold energy, the first pair (1,2 and 6,7) appeared, as the collision energy increased, the (3,4 and 4,5) pairs appear at higher energy followed by (2,3 and 5,6). In the CID experiments, $Na_{15}Cl_{17}^{2-}$ also dissociates into conjugate ion pairs of the type $NaCl_2^-(NaCl)_x + NaCl_2^-(NaCl)_{13-x}$ for n = 0,1,2,3,4,5,6 (Figures 4.7 & 4.8). In Figure 4.9, threshold curves for daughter ions from collision-induced dissociation of parent $Na_7Cl_9^{2-}$ is demonstrated. Threshold curves of $Na_{15}Cl_{17}^{2-}$ were not extrapolated to zero signal due to the fact that the dianions had a very low intensity and fragmentations occur in a very low threshold. The CRUNCH program (discussed in Chapter III) was not used in this study to correct for ion internal energy, Doppler broadening and other effects for two reasons. First it was difficult to calculate some of the necessary inputs for the CRUNCH program (i.e., vibrational frequencies of the cluster dianions). Second, some of the assumption to fit the data in CRUNCH program is less valid for the energies near zero in the laboratory frame.

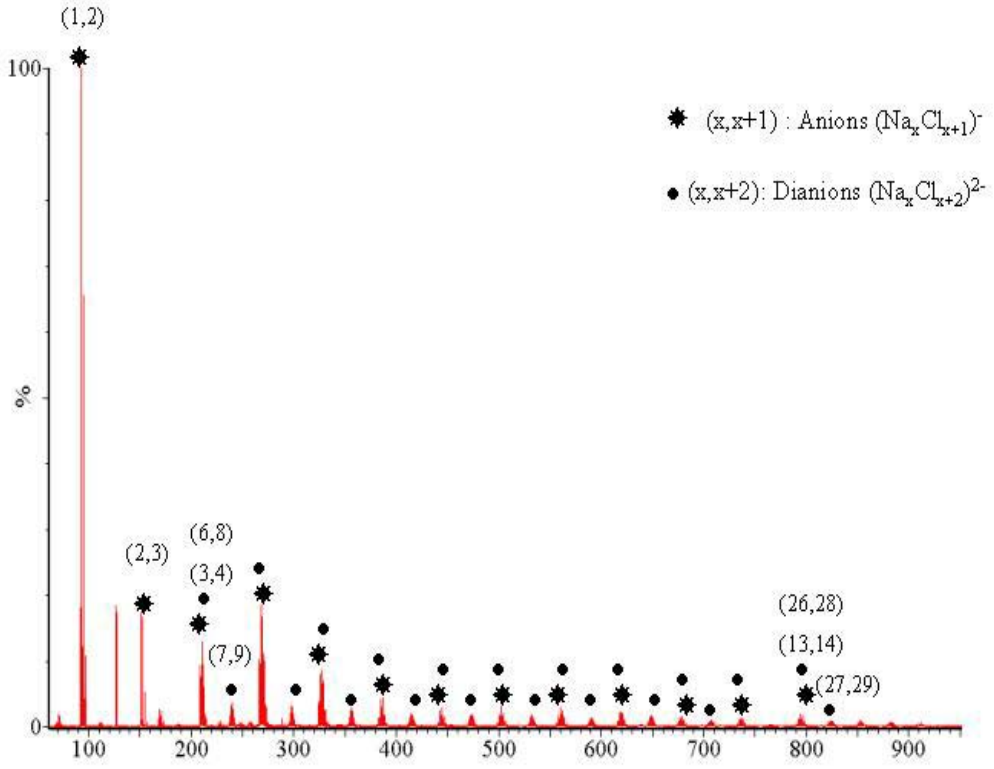

Figure 4.2. Full scan ESI mass spectrum of spraying NaCl solution in D_2O. The dianions are presented as filled stars and monoanions are denoted as filled circles.

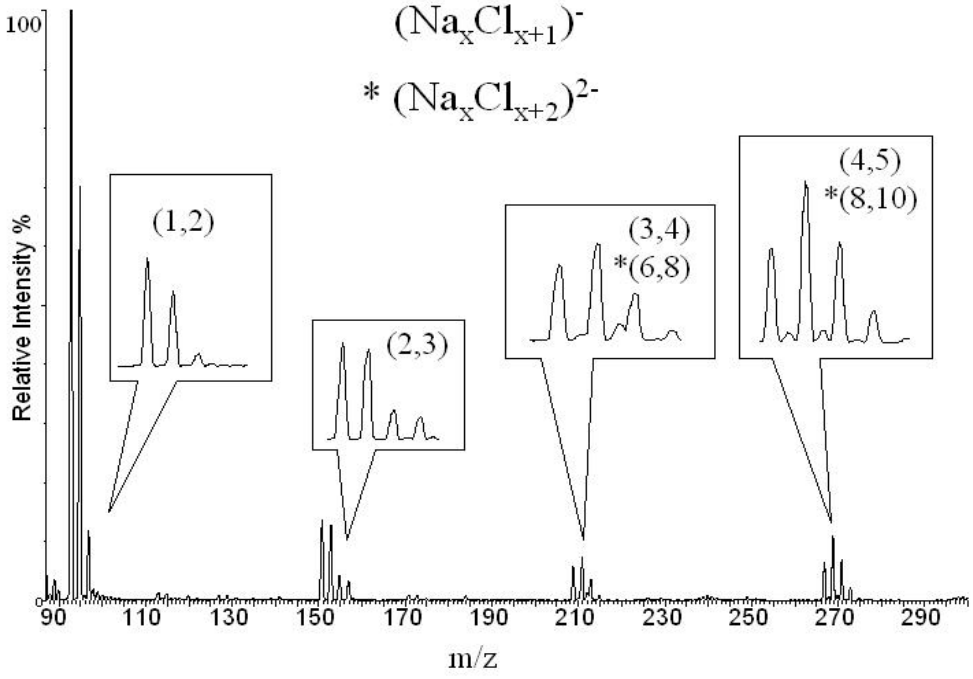

Figure 4.3 Selected mass spectrum of salt spray emphasizing the monoanions and dianions (*). Peaks from $Na_6Cl_8^{2-}$ are odd mass peaks between the peaks from $Na_3Cl_4^-$, and peaks from $Na_8Cl_{10}^{2-}$ are odd mass peaks between the peaks from $Na_4Cl_5^-$ singly-ion.

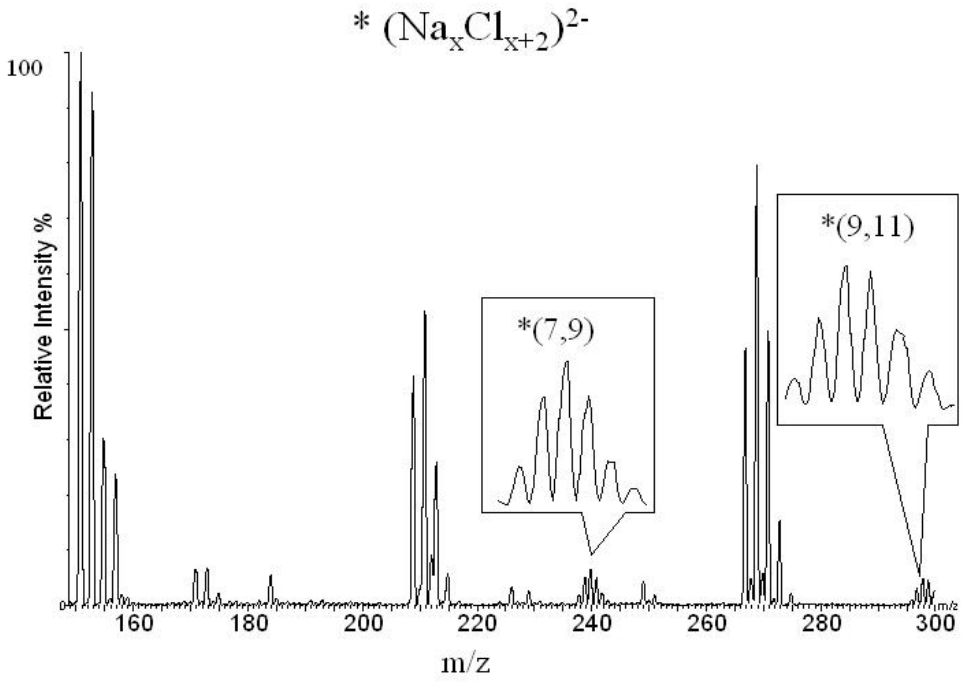

Figure 4.4 Mass spectrum of salt spray highlighting the dianions in the region of the 7,9 and 9,11 dianions. $Na_7Cl_9^{2-}$and $Na_9Cl_{11}^{2-}$ are abbreviated as (7,9) and (9,11) for brevity.

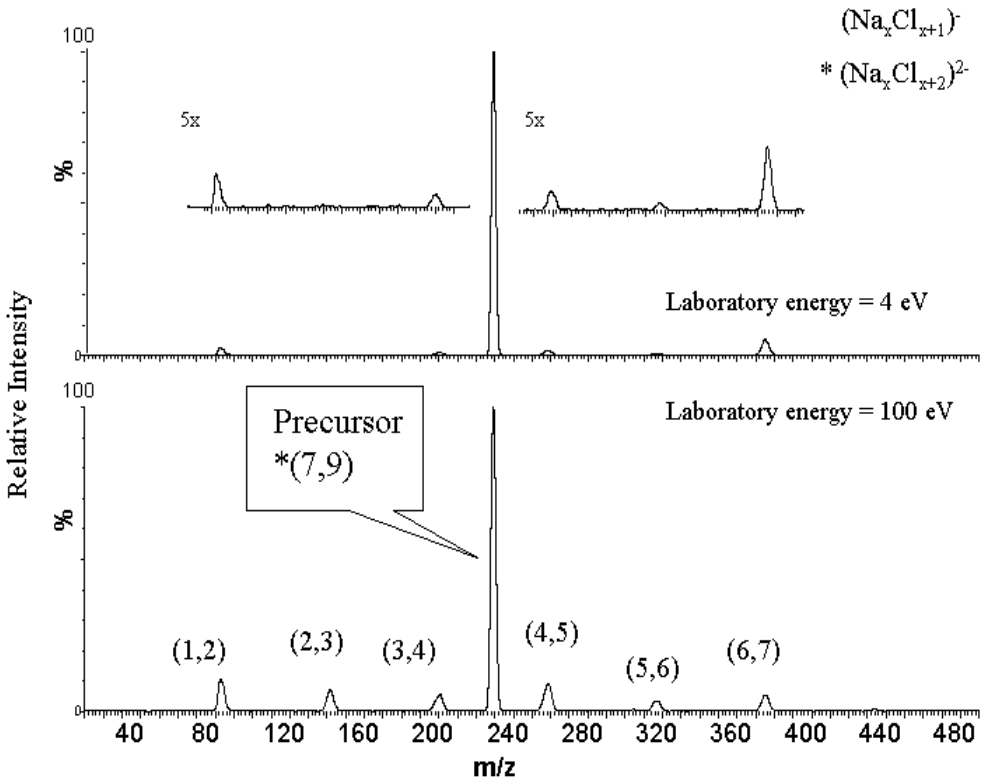

Figure 4.5 Collision-induced dissociation of $Na_7Cl_9^{2-}$ (240 amu) at laboratory energies of 4 and 100 eV. We abbreviated the ions such as $NaCl_2^-$, and $Na_6Cl_7^-$ as (1,2) and (6,7) for brevity.

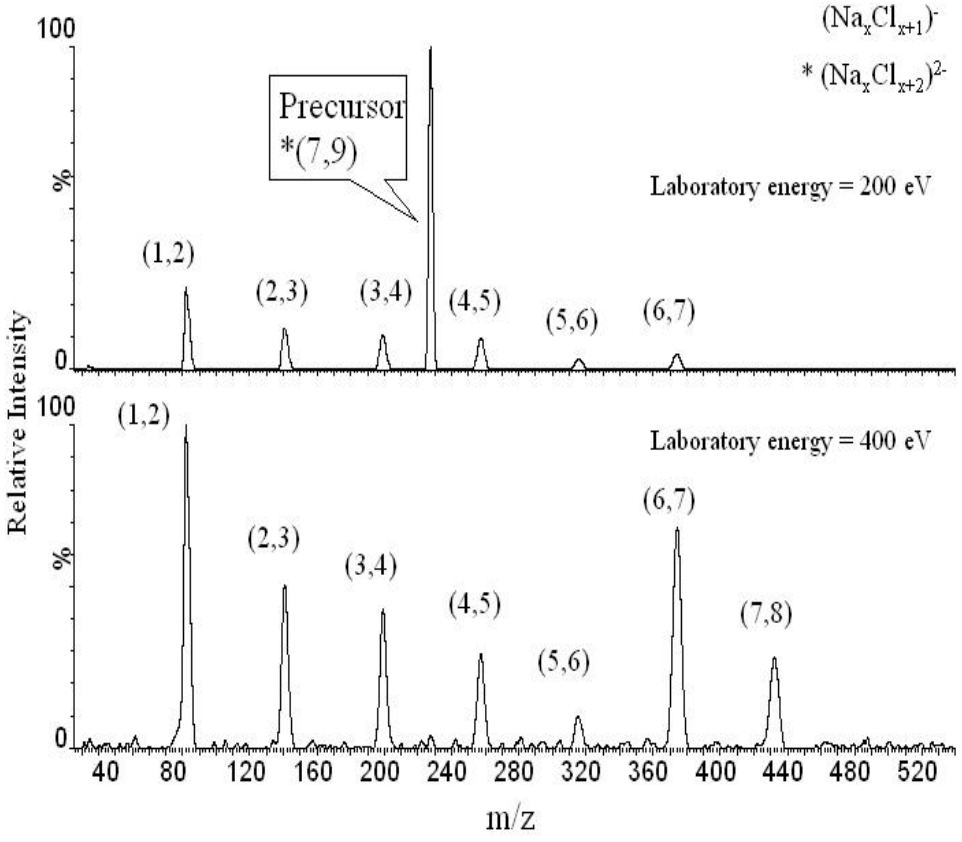

Figure 4.6 Collision-induced dissociation of $Na_7Cl_9^{2-}$ (240 amu) dianions at laboratory energies of 200 and 400 eV. We abbreviated the ions such as $NaCl_2^-$, and $Na_7Cl_8^-$ as (1,2) and (7,8) for brevity.

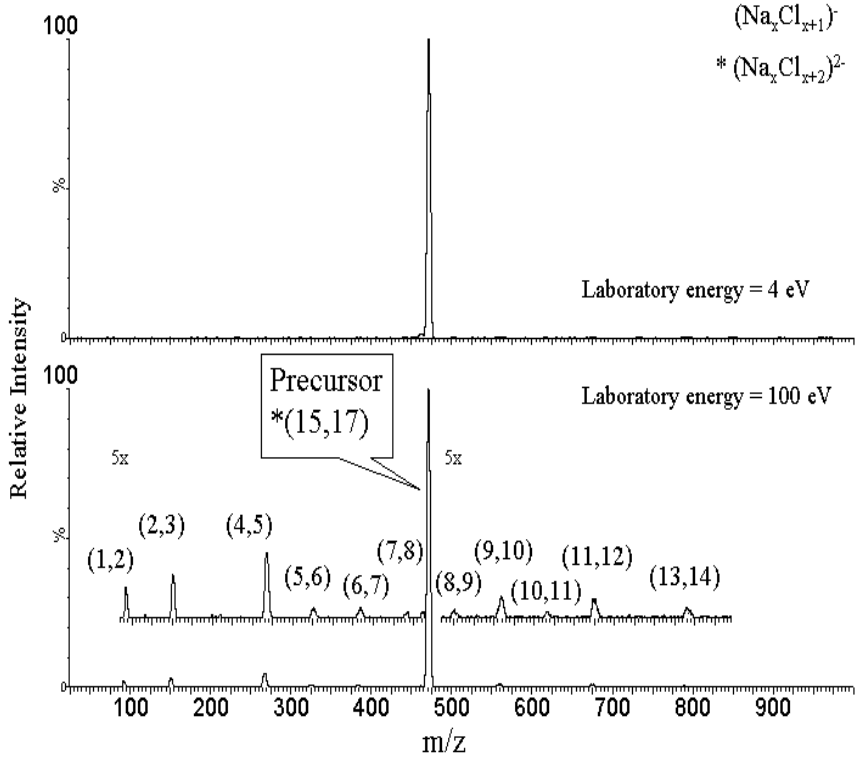

Figure 4.7 Collision-induced dissociation of $Na_{15}Cl_{17}^{2-}$ (474 amu) dianions at laboratory energies of 4 and 100 eV. We abbreviated the ions such as $NaCl_2^-$, and $Na_7Cl_8^-$ as (1,2) and (7,8) for brevity.

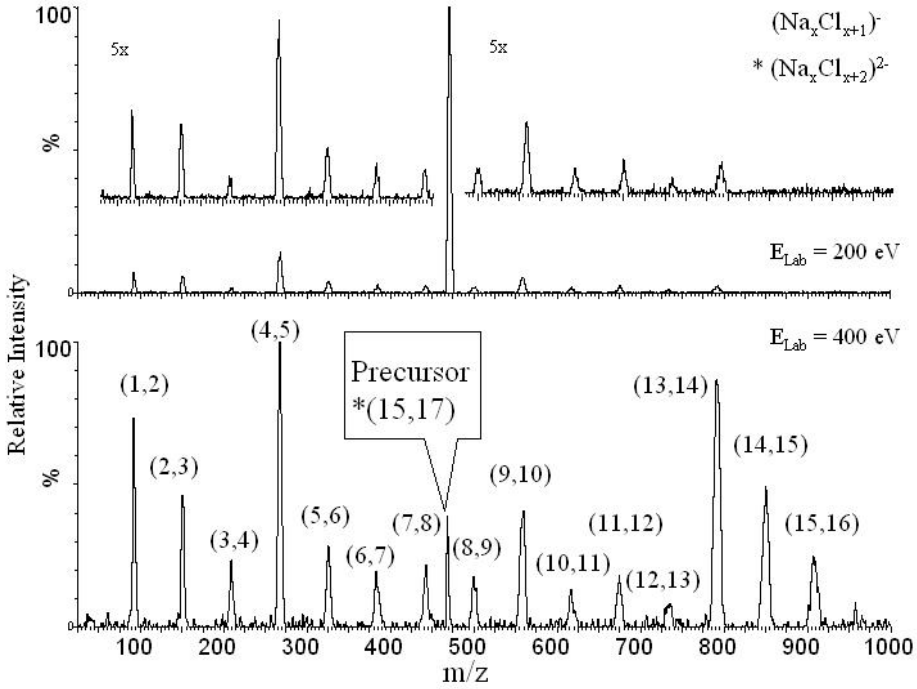

Figure 4.8 Collision-induced dissociation of $Na_{15}Cl_{17}^{2-}$ (474 amu) at laboratory energies of 200 and 400 eV. We abbreviated the ions such as $NaCl_2^-$, and $Na_7Cl_8^-$ as (1,2) and (7,8) for brevity.

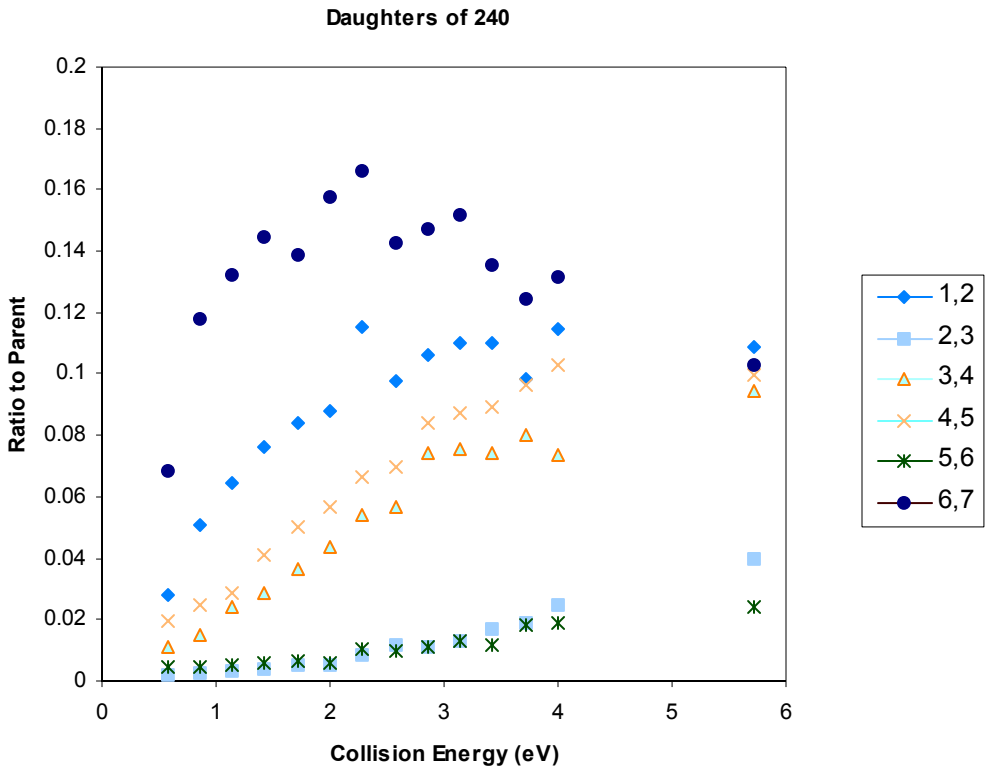

Figure 4.9 Cross-section for collision-induced dissociation of $Na_7Cl_9^{2-}$ (240 amu) in center-of-mass frame. We abbreviated the ions such as $NaCl_2^-$, and $Na_6Cl_7^-$ as (1,2) and (6,7) for brevity.

A significant result of this study was that ions corresponding to the detachment of an electron from the doubly-charged ions were not observed ($Na_7Cl_9^-$ at 480 amu and $Na_{15}Cl_{17}^-$ at 947 amu). The fact that electron loss was not observed might be due to the fact that singly-charged ions ($Na_7Cl_9^-$ and $Na_{15}Cl_{17}^-$) are very unstable toward fragmentation and collisions provide the necessary energy for these ions to dissociation. This assessment is supported by the fact that the $Na_7Cl_9^-$ or $Na_{15}Cl_{17}^-$ ions were not observed in the mass spectrum prior to adding the collision gas. If these ions were stable, one would expect their appearance in the primary electrospray ion spectrum. A closer look at Figure 4.9 also supports this assumption since the conjugate ions do not have the same ratio. However the collection efficiency varies for the different mass ranges involved, making it difficult to attribute the unevenness in the intensities only to the loss of electron.

Friedrich and his coworkers[81] investigated the stability of some alkali halide cluster dianions toward fragmentation. One of the dianions of interest was $Na_7Cl_9^{2-}$. They computed dissociation energies for this dianions toward loss of Cl^-, $NaCl_2^-$, $Na_2Cl_3^-$, and $Na_3Cl_4^-$ as shown in Table 4.1. According to their calculations, $Na_7Cl_9^2$ is stable against dissociation into $NaCl_2^-$ (0.016 eV) and unstable toward other fragmentations (negative dissociation energies). However based upon our study; $Na_7Cl_9^2$ is a metastable dianion with respect to all monoanion pairs. In their calculations, they calculated the difference between total energies of the parent dianions and its fragmentations. The question arises here is "what factor binds these dianions together and render them stable toward fragmentation?" As discussed previously, stability of the doubly-charged anions is

Table 4.1 Calculated dissociation energies for $Na_7Cl_9^{2-}$ toward loss of Cl^-, $NaCl_2^-$, $Na_2Cl_3^-$, and $Na_3Cl_4^-$. According to the dissociation energy calculations, $Na_7Cl_9^2$ is stable against dissociation into $NaCl_2^-$ (0.016 eV) and unstable toward other fragmentations (negative dissociation energies).

	Cl^- -loss	$NaCl_2^-$ - loss	$Na_2Cl_3^-$ - loss	$Na_3Cl_4^-$ - loss	Units
$Na_7Cl_9^{2-}$	-7.3[81]	1.5[81]	-13.7[81]	-62.1[81]	KJ/mol
	-0.076	0.016	-0.14	-0.64	eV
Threshold energies	95[this work]	76[this work]	----------	----------	KJ/mol
	0.99[this work]	0.79[this work]	----------	----------	eV

attributed in part to the repulsive Coulomb barrier. With this assumption, it is clear that exploring the repulsive Coulomb barrier of the anions toward dissociation channels provides considerable insight. In this connection, Drs Weis and Kappes from the University of Karlsruhe in Germany explored the barrier heights for dissociation of $Na_7Cl_9^{2-}$ into Cl^- and $Na_7Cl_8^{2-}$ and also dissociation of $Na_7Cl_9^{2-}$ into $NaCl_2^-$ and $Na_6Cl_7^-$. The other dissociation channels for $Na_7Cl_9^{2-}$, and $Na_{15}Cl_{17}^{2-}$ were not performed due to the complexity of the calculations. In their calculations, they obtain structures and fragmentation energies using density functional theory. The TURBOMOLE package with the same functional (BP-parameterization) and basis set was employed similar to that in reference 81.

There are two possible structures for $Na_7Cl_9^{2-}$. The lowest minimum structure found for $Na_7Cl_9^{2-}$ has C_{2v} symmetry and is shown in Figure 4.10 (the first structure in Figure 4.10). The next isomer (second structure 2 in Figure 4.10) of this dianion is based on a 2 x 2 x3 Na_6Cl_6 cuboid with an extra Cl^- and $NaCl_2^-$ in two opposite corners, however this isomer has 6.3 KJ/mol energy higher than the optimized structure. Two possible structures for $Na_7Cl_8^{2-}$ are also shown in Figure 4.10 (third and fourth structures in Figure 4.10) with an energy difference of 15.8 KJ/mol.

Both isomers of $Na_7Cl_9^{2-}$ were stable against electron loss. The respective $Na_7Cl_9^-$ monoanions were 2 eV higher in energy. However, this dianion was stable against dissociation into $NaCl_2^-$ (0.016 eV) and unstable toward other fragmentations (negative dissociation energies) as was presented in reference 81.

Figure 4.11 shows the dissociation pathway for $Na_7Cl_9^{-2}$ into Cl^- and $Na_7Cl_8^-$ ($Na_7Cl_9^{-2} \rightarrow Cl^- + Na_7Cl_8^-$). In this computation, the energy is being calculated as the

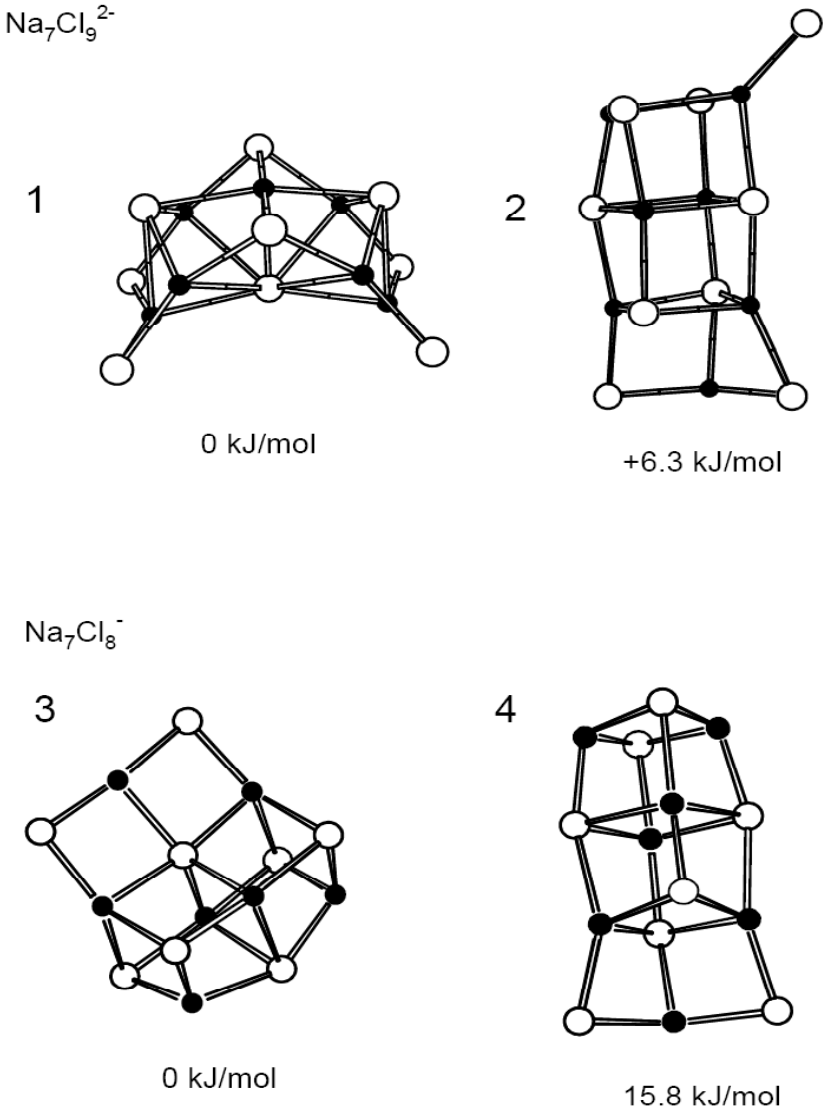

Figure 4.10 Optimized structures of $Na_7Cl_9^{2-}$ and $Na_7Cl_8^{2-}$ and their isomers.

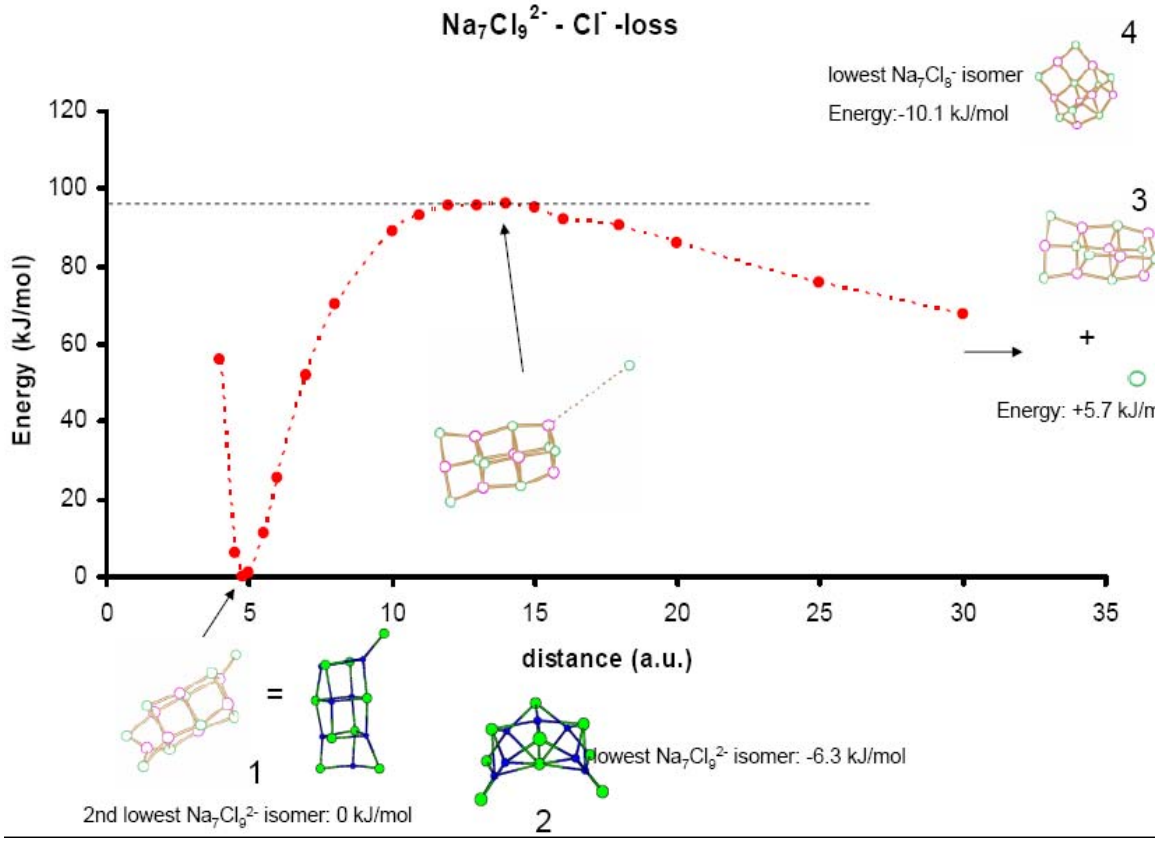

Figure 4.11 Barrier potential for dissociation of $Na_7Cl_9^{2-}$ into $Na_7Cl_8^-$ and Cl^-. The barrier height for the loss of Cl^- is about 95 KJ/mol (0.99 eV).

distance between the Cl^- and $Na_7Cl_9^{-2}$ core increases. In this graph, the barrier height for the loss of Cl^- is about 95 KJ/mol (0.99 eV); however, experiments were carried out up to 50 eV collisional energy with no observable Cl^- ions. Dissociation of $Na_7Cl_9^{2-}$ into Cl^- + $Na_7Cl_8^-$ was not observed, however, at higher energy electron loss into $Na_7Cl_8^-$ was observed (Figure 4.6). This result suggests that at higher collision energy, electron detachment of $Na_7Cl_9^{2-}$ occurs resulting in $Na_7Cl_9^-$ and due to the inherent instability of this anion, it decays to $Na_7Cl_8^-$ + Cl.

In Figure 4.12, the dissociation pathway for $Na_7Cl_9^{-2}$ into $NaCl_2^-$ and $Na_6Cl_7^-$ ($Na_7Cl_9^{-2} \rightarrow NaCl_2^- + Na_6Cl_7^-$) is shown. In this calculation the barrier height was calculated by again increasing the distance between $NaCl_2^-$ unit and $Na_6Cl_7^-$ core in a stepwise fashion. The calculated barrier height is approximately 0.79 eV (below 1 eV) and is in a good agreement with the dissociation threshold derived from the experimental results.

Conclusion

The present experimental results show that salt dianions produced in this experiment are metastable toward dissociation at least on the time scale of microseconds. The repulsive Coulomb barrier is believed to play an essential rule in the stability of these dianions. Dissociation of salt clusters dianions can occur as a result of tunneling through the Coulomb barrier and the lifetime of the dissociation depends on the height and width of the Coulomb barrier. As far as stability of these dianions toward the electron detachment is concerned, we did not observe direct evidence of the loss of the electron to

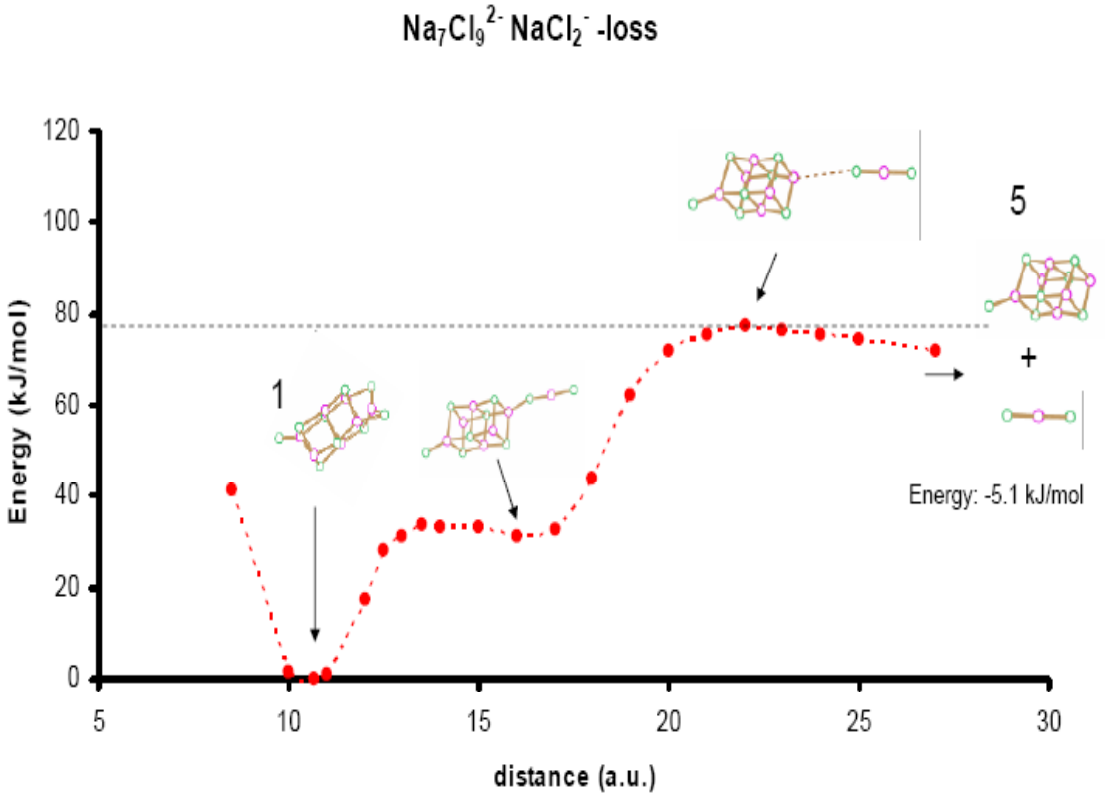

Figure 4.12 Barrier potential for dissociation of $Na_7Cl_9^{2-}$ into $Na_6Cl_7^-$ and $NaCl_2^-$. The barrier height is calculated to be about 76 KJ/mol (0.79 eV).

produce a singly-charged anions; however as discussed earlier some observations suggest that these dianions are also metastable toward electron detachment.

In conclusion, these results demonstrate that electrospray ionization along with collision-induced dissociation method provides a valuable introduction into the molecular bonding, structure and stability of the gas-phase multiply-charged anions.

CHAPTER V

The Dissociation Energy of $NaCl_2^-$ into NaCl and Cl^-

Introduction

Thermochemical properties of molecules play a pivotal role in the foundation of chemistry. One of the most important thermochemical properties of a molecule is its bond dissociation energy (BDE). The BDE characterizes the structure and energetic properties of the molecule. In the chemical literature, BDE is introduced as the sum of all attractive electric forces between atoms in a molecule. The bond dissociation energy (BDE) is also known as bond dissociation enthalpy or simply bond enthalpy. Although the bond dissociation energy is one of the critical concepts in chemistry, it still remains one of the most complicated quantities to measure. However, many empirical methods and ab initio theories have been developed in order to calculate the BDE.

In order to determine the BDEs experimentally, investigation of one of two processes is often considered: (a) the process of the formation of a bond (b) the process of breaking a bond. It might appear that the first method is a more direct and easy method to measure the bond dissociation energy. One could assume that measuring the heat produced in a recombination process from a calorimetric method would be a fundamental approach in measuring the bond dissociation energies. However, this approach has its own technical difficulties such as generation of the radicals, evaluation of their concentrations, modes of reaction radicals, temperature rise in the calorimeter, and so on. In 1928 Bichowsky and Copeland[82] applied a direct calorimetric method to determine the recombination heat for hydrogen atoms resulting in the formation of hydrogen molecules. From this study, they reported the recombination heat of hydrogen atoms to be 105 ± 3.5 Kcal/mole (4.55±

0.15 eV). Later in 1930 Copeland [83] attempted to also estimate the dissociation energy for the oxygen molecule using calorimetric technique, but the reported value was not reliable. Since the technical difficulties of the first method (formation of a bond) make this technique very complex and impractical, bond-breaking process is widely used to determine BDEs. Many techniques have been developed to determine BDEs by applying the bond-breaking method; however here we only categorize three approaches to investigate BDEs of molecules: (1) the study of chemical kinetics, in this study an estimation of the bond dissociation energy is carried out by measuring the equilibrium constant for the reaction, (2) photochemical method, in this technique the energy to break a bond is supplied in the form of radiation. Investigation of the absorption spectra, predissociation phenomena, fluorescence, photo-decomposition, photo-sensitized, and etc. can result in an estimation of the bond dissociation energy. Analysis of absorption spectra or predissociation phenomena is usually limited to smaller molecules since for the larger molecules this method of investigation can be very complex. The method based on photo-decomposition measures only the upper limit for the bond dissociation energies since the applied energy is enough to break the bond, but it might be an amount greater than the actual bond dissociation energy. The third method (3) is the electron impact method. In this method, electron kinetic energy supplies the necessary energy to break the bond. In many cases dissociation into ions also can occur. There is also a review article by Compton and Bardsley[84] extensively studies the dissociation of molecules by slow electrons. Another method in this category can also be referred to as ion-pair formation. Ion–pair formation occurs when the incident electron has enough kinetic energy to decompose the molecule into positive and negative ions, i.e., $AB + e \rightarrow A^+ + B^-$

+ e. In electron impact measurements, the threshold energy (electron energy) for this decomposition is the ionization potential of the positive ion plus the bond dissociation of the molecule minus the electron affinity of the negative fragment. To be able to measure the bond dissociation, accurate values for ionization potential of the positive ion and electron affinity of the negative ion are necessary. We shall also include one more method to measure the BDE employing electron impact method: dissociative electron detachment. In this process, the energy of the incident electron decomposes the molecule into a negative ion fragment and a neutral, i. e., AB+ e →A+ B^-. In 1942, Stevenson[85] measured the first C-H bond dissociation energy in methane using electron impact technique.

Recent developments in mass spectroscopy, especially electrospray ionization mass spectrometry, have introduced a very important and effective method to measure the BDEs: collision-induced dissociation. The experimental threshold energy in a collision-induced dissociation experiment can be assigned as the thermodynamic bond dissociation energy of the reaction if there are no potential barriers for the dissociation (i.e. multiply charged ions), and there are no other reactions competing with the dissociation.

Collision-induced dissociation (CID) has proven to be a valuable technique to determine the BDE of ionized molecules[86-95] and clusters[96-101]. For instance, Wu and Tiernan[86] measured bond dissociation energies of CO_3^- and NO_3^-, using the CID technique. They determined the bond dissociation energy $D_0(CO_2 - O^-)$= 2.5 ± 0.1eV, and $D_0(NO_2 - O^-)$= 4.8± 0.1 eV. Prior to the Wu and Tiernan experiment, a lower value for the CO_3^- bond dissociation (> 1.85 eV) was reported by Vestal and Mauclaire[102] from a photo-destruction experiment. Sunderlin and coworkers[94] reported a value of 0.59 ±

0.07eV for dissociation of $Cl_2O_2^+$ into Cl_2^+ and O_2 using the CID technique. Before the Sunderlin experiment[94], there were no other experiment values for the $Cl_2O_2^+$ bond energy. Nizzi et al.[12] also applied the CID method to measure BDEs of three hypervalent polyhalide ions. Their experimental values for $D_0(Cl_2 - Cl^-)$, $D_0(Br_2 - Br^-)$, and $D_0(Br_2 - Br_3^-)$ were estimated to be 1.025 ±0.05 eV, 1.316 ±0.07 eV, and 0.41 ±0.07 eV respectively. There were no direct experimental measurements of bond dissociation energies of Cl_3^-, Br_3^-, and Br_5^- prior to the CID experiments.

There are many more studies in the literature that indicate collision-induced dissociation can assist scientists to measure the bond dissociation energies of molecules, ionized molecules and clusters. In many experiments, the CID bond dissociation energies are in a good agreement with the bond dissociation energies obtained from other experimental methods[70, 103-104]. More importantly, this method has a great potential to allow one to measure the bond dissociation energies of singly or multiply charged species.

The smallest negative ions of alkali halide clusters, MX_2^- (where M=Na, Li; X = F, Cl), have been predicted to have very large adiabatic electron affinities[105]. Simons and coworkers[105] calculated the adiabatic electron affinities (EA_{ad}) of LiF_2, $LiCl_2$, NaF_2, and $NaCl_2$ to be 5.45eV, 4.97eV, 5.12eV, and 4.69 eV, respectively. Such compounds having electron affinities greater than that of halogen atoms (3.0-3.6 eV) are known as superhalogens. In 2004, Wang and his colleagues[106] employed photoelectron spectroscopy to obtain the vertical electron detachment energy for $NaCl_2^-$ to be 5.6 eV. In their study, they also measured the vertical electron detachment energies for $Na_2Cl_3^-$, $Na_3Cl_4^-$, and $Na_4Cl_5^-$ to be 6.46 eV, 6.3eV, and 7.0eV, respectively. These results also

revealed that the electron binding energies of the $Na_xCl_{x+1}^-$ cluster increase with the cluster size. A few studies in the literature[31, 105, 106] have attempted to obtain the adiabatic electron affinity and vertical electron detachment of $NaCl_2^-$, and among these few investigations only the work of the Wang et al.[106] has examined the vertical electron detachment experimentally.

Presently, there is no experimental value for the bond dissociation energy of $NaCl_2^-$ into NaCl and Cl^-. The only available theoretical value for the BDE of $NaCl_2^-$ is 2.23 eV computed by Simons and coworkers[105] using CCSD(T) level of theory.

In this study, we present an investigation of the bond dissociation energy of $NaCl_2^-$ produced in the gas-phase using electrospray ionization source and employing the collision-induced dissociation technique.

Empirical Intermolecular Potential (Morse potential)

The only bonding interaction between atoms in a diatomic molecule is a bond stretch between the atoms. The Harmonic oscillator model is the simplest demonstration of the stretching potential, i. e.

$$V(r) = V(r_e) + \frac{1}{2} f_r (r - r_e)^2 \qquad (5.1)$$

where f_r is the bond force constant, and r_e is the equilibrium bond length.

The vibrational frequency for the harmonic stretch is given by:

$$\nu_e = \frac{1}{2}\sqrt{\frac{f_r}{\mu}} \qquad (5.2)$$

where μ is the reduced mass of the diatom.

And the energy levels of the harmonic oscillator are:

$$E(n) = (n + \frac{1}{2})\, h\nu_e \quad \text{where } n = 0, 1, 2, 3 \ldots \tag{5.3}$$

However, the harmonic oscillator potential accuracy is based on small displacements of r from the equilibrium bond length. As displacement, r, increases the real potential of the diatomic molecule differs from the simple harmonic oscillator. The difference between the real potential and simple harmonic potential at larger distances is known as "anharmonic effect". To incorporate the anharmonicity effect in the simple harmonic potential, a Taylor series expansion of the potential can be written to generalize the potential for all distances, i. e.,

$$V(r) = V(r_e) + (\frac{\partial V}{\partial r})_{r=r_e}(r-r_e) + \frac{1}{2}(\frac{\partial^2 V}{\partial r^2})_{r=r_e}(r-r_e)^2 + \frac{1}{6}(\frac{\partial^3 V}{\partial r^3})_{r=r_e}(r-r_e)^3$$

$$+ \frac{1}{24}(\frac{\partial^4 V}{\partial r^4})_{r=r_e}(r-r_e)^4 \tag{5.4}$$

A Physicist, Philip McCord Morse, introduced an approximately simple potential called Morse potential for the diatomic molecule for all values of r. Morse potential describes the bond stretch potential as follow:

$$V(r) = D_e\,[1 - \exp\{-\beta e\,(r-r_e)\}]^2 \tag{5.5}$$

Where r is the distance between the atoms, r_e is the equilibrium bond distance, D_e is the well depth, and β_e is a parameter that governs the width of the well.

β_e is related to the bond force constant (f_r) through the following equation:

$$\beta_e = \sqrt{\frac{f_r}{2D_e}} \tag{5.6}$$

Vibrational energy levels for the Morse potential can be written by:

$$E(n) = (n + \frac{1}{2})\, h\nu_e - (n+\frac{1}{2})^2\, h\nu_e\chi_e \qquad n= 0, 1, 2, 3, \ldots \tag{5.7}$$

where χ_e known as anharmonicity is defined as

$$\chi_e = \frac{h\nu_e}{4D_e} \tag{5.8}$$

One of the advantages of representing the diatomic molecule's potential with Morse potential (Figure 5.1) is that the potential directly includes the bond dissociation energy. In Equation 5.5, D_e has a direct correlation with the bond dissociation energy. The bond dissociation energy can be calculated by subtracting D_e, well depth, from the zero-point energy, E_{zp}, of the molecule, i.e.

$$D_0 = D_e - E_{zp} \tag{5.9}$$

In comparison to diatomic molecules, representing a potential energy for polyatomic molecules becomes much more complex due to the fact that for the polyatomic system, there are more degrees of freedom. For the simplicity of our study, we present $NaCl_2^-$ with a diatomic potential. One can assume $NaCl_2^-$ as diatomic molecule model with two parts, NaCl and Cl^-. This is a valid assumption since we are studying dissociation of $NaCl_2^-$ into NaCl and Cl^-.

Experimental Method and Data Analysis

The experimental details of the collision-induced dissociation experiment of salt clusters have been described previously in Chapter IV of this thesis. In brief, a 40mM solution of sodium chloride in D_2O was introduced into the ESI source of a commercial Micromass Quattro II (triple quadrupole) mass spectrometer with an electrospray

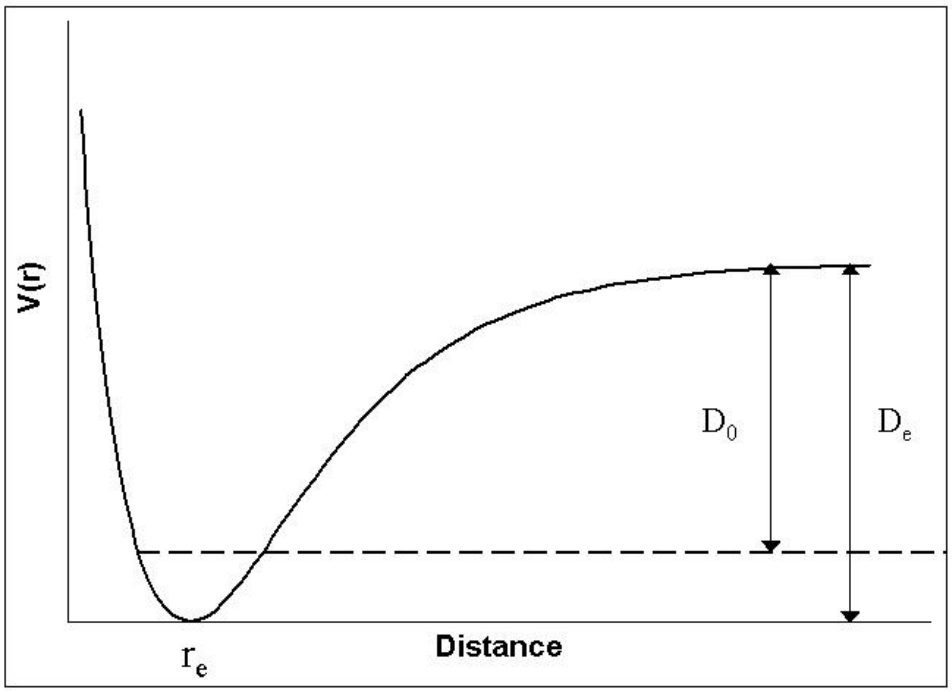

Figure 5.1 The Morse potential, V(r), as a function of distance for a diatomic molecule. r_e is the equilibrium distance. D_e represents the well depth, and D_0 is the bond dissociation energy. The dashed lines represent the zero-point energy level of the molecule.

ionization (ESI) source (Figure 3-2). The capillary and cone voltages were -2.5 kV and 40 V, respectively. Clusters of singly charged and doubly charged ion of sodium chloride clusters were observed in the mass spectrum as demonstrated in Chapter IV. $NaCl_2^-$ ions have the highest signal intensity in the mass spectrum (see e.g. Figure 4.2).

$Na^{35}Cl_2^-$ produced from the ESI source (Figure 5.2) was selected in the first quadrupole (Q_1), and then collided with a collision gas at various collision energies. The resulting Cl^- fragment was analyzed in the last quadrupole (Q_2). Cl^- ion was the only fragment ion observed in the CID experiment. No $NaCl^-$ ion was observed. The experiment was performed under approximately single collision conditions. For CID experiment, two different collision gasses were used: argon and nitrogen.

The threshold data for CID of $NaCl_2^-$ was determined by modeling the intensity of the ratio of the product ions (Cl^-) to parent ions ($NaCl_2^-$) as a function of the collision energy in the center-of-mass frame. To derive the CID threshold energy, the threshold data was fitted to the model function described in Chapter III, i.e.,

$$\sigma(E)= \sigma_0 \Sigma_i g_i(E+E_i-E_0)^n /E \qquad (5.10)$$

where $\sigma(E)$ is the cross-section for formation of the product ion at the center-of-mass energy E, σ_0 is the scalling factor, n is an ajustable parameter, and E_0 is the threshold energy. The summation is over rotational and vibration states of the reactants having energy E_i, and Boltzman population, g_i,where $\Sigma g_i =1$.

The CRUNCH program[64] was used to fit the data into the model in Equation 5.10. In CRUNCH data analysis, a model cross-section is first chosen and then the effects of broadening due to the thermal motion of the collision gas (Doppler broadening), internal

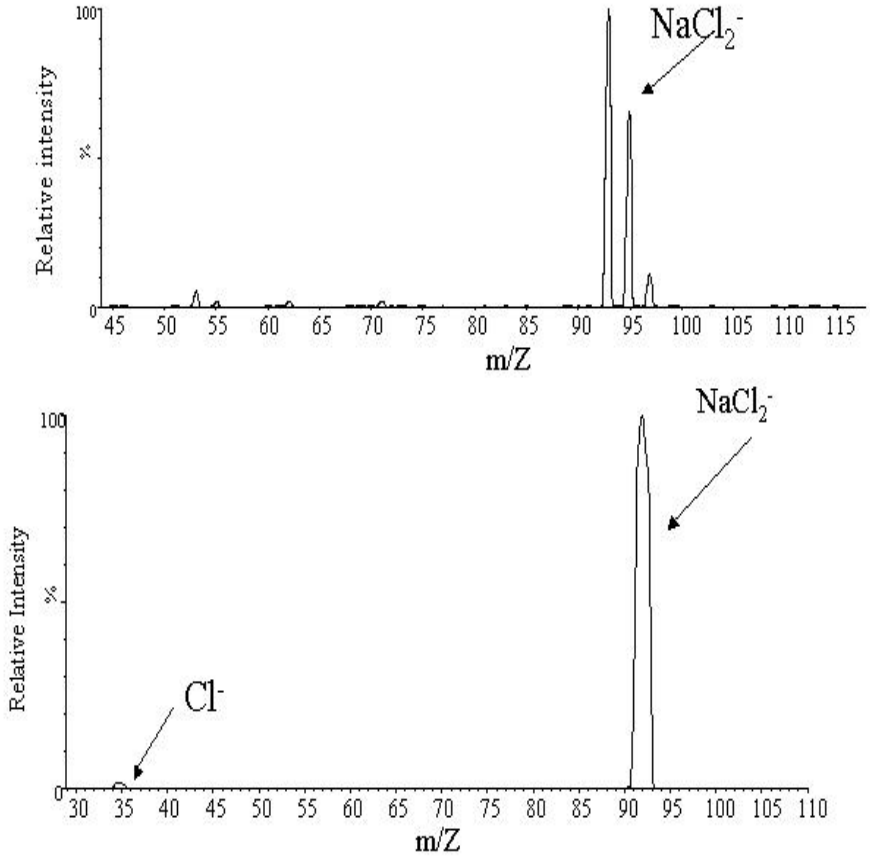

Figure 5.2 Above figure shows the mass spectrum of $NaCl_2^-$ emerging from the first quadrupole. The figure below shows collision-induced dissociation of $Na^{35}Cl_2^-$ into Cl^- at laboratory energy of 20 eV.

energy of the reactant, and the kinetic energy distribution of the reactant are taken into account by convoluting the model cross-section. Then, the adjustable parameters, σ_0 and, n are varried to get the best least-squares fit to the experimental data. Experimental vibrational and rotational frequencies are not known for reactants and products of this study, therefore computed vibrational and rotational frequencies were used to calculate internal energies. To examine the effect of inaccuracies in the frequencies on the threshold energy, all frequencies were multiplied by 0.9 and 1.1 factor. Also the different sets of frequencies from different methods were used as input in the CRUNCH program. The uncertainty of the threshold energy due to the different sets of frequencies is within 0.01 uncertainties in the threshold energy, E_0. The calibration of the collision energy, zero energy, (0.44 eV, details in previous chapter) and the full-width, half-maximum (FWHM) of the ion energy (0.5 eV, details in previous chapter) also were accounted for in the data analysis. The energy scale is determined from a retardation analysis on the Br^- ion in the ion source. The representative data in Figure 4.1 shows an energy scale correction of 0.44 eV. However, the retardation curve could overestimate this correction due to decreasing ion signal as the energy approaches zero. Thus our energy calibration of 0.44 eV could be too large. This represents one of the major potential systematic errors in the experiment and should be considered in the discussion of the data. Therefore, a potential inaccuracy of the threshold energy due to zero-energy and FWHM was evaluated by varying the zero-energy and FWHM to ± 0.2 eV and ± 0.5 eV, respectively. These parameters have an effect of ± 1 eV on the threshold energy.

In Figures 5.3 and 5.4, the threshold energy for dissociation of $NaCl_2^-$ into Cl^- and NaCl as a function of energy in center-of-mass frame is shown. The convoluted model is

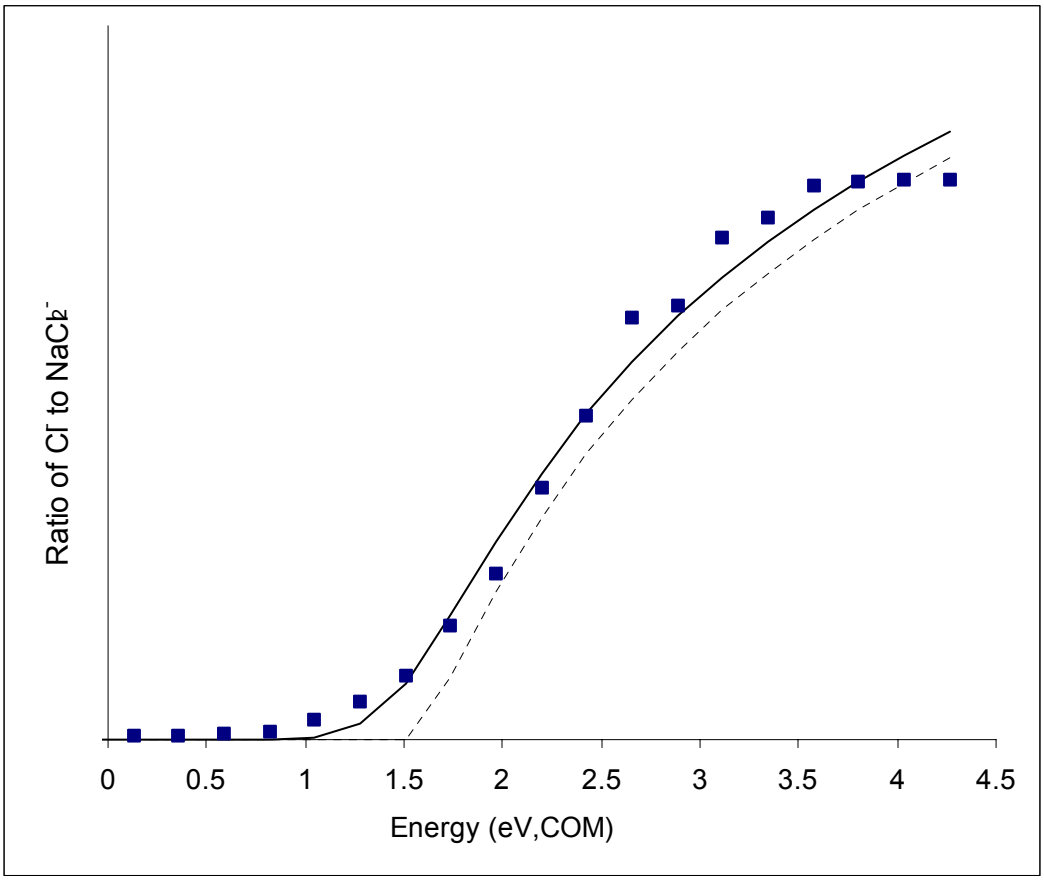

Figure 5.3 Experimental collision-induced dissociation threshold energy for dissociation of $Na^{35}Cl_2^-$ as a function of energy in the center-of-mass frame. Nitrogen gas was used as a collision gas. The filled squares are the experimental data; solid and dashed lines represent convoluted and unconvoluted line fits to the experimental data, respectively.

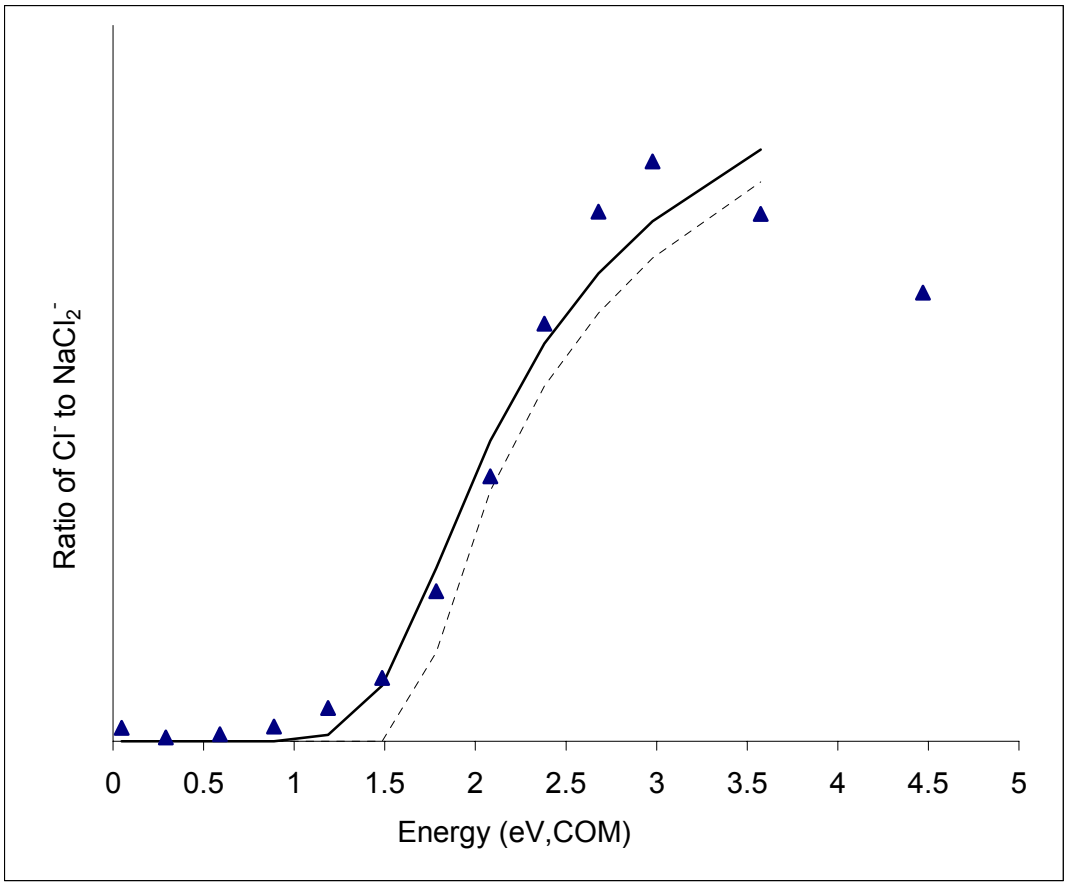

Figure 5.4 Experimental collision-induced dissociation threshold energy for dissociation of $Na^{35}Cl_2^-$ as a function of energy in the center-of-mass frame. Argon gas was used as a collision gas. The filled triangles are the experimental data; solid and dashed lines represent convoluted and unconvoluted line fits to the experimental data, respectively.

shown with solid line and unconvoluted model is presented with dashed line. Figure 5.3, is the data analysis of the collision of $NaCl_2^-$ with nitrogen gas. The threshold energy appears to be about 1.51 eV. The best fitting parameters, σ_0 and n were found to be 0.014 and 1.10, respectively.

Figure 5.4, demonstrates the threshold dissociation energy for $NaCl_2^-$ using argon gas as the collision gas. In order to use the CRUNCH program to extrapolate the convoluted and unconvoluted models, energy range from zero to 3.5 eV was only considered since there is a drop off in the intensity when energy exceeds 3.5 eV. The threshold energy using Ar gas is about 1.48 eV.

The threshold energy for the dissociation of $NaCl_2^-$ into NaCl and Cl^- was obtained to be $E_0 = 1.5 \pm 0.2$ eV. The uncertaintiy in the threshold energy has been estimated by the root sum squares of the uncertainties in the lab energy, internal temperature, the rotational and vibrational frequencies.

Computational Method

All computational work on geometry optimizations and frequency calculations were carried out using a PC and the Gaussian G03 suite of programs[107]. The calculations were performed using three different theoretical levels: the density functional theory (B3LYP), the second-order Møller-plesset (MP2), and the infinite-order coupled-cluster method (CCSD). Two different basis sets, 6-311+G* and aug-cc-pVDZ, were employed for all three levels of theory.

The well depth (D_e) was obtained as the difference of total energy of the reactant ion ($NaCl_2^-$) and sum of the fragments energies (NaCl and Cl^-), i.e.,

$$D_e = E_{tot}(NaCl_2^-) - [E_{tot}(NaCl) + E_{tot}(Cl^-)] \quad (5.11)$$

where E_{tot} represents total energy.

The zero point energy (E_{zp}) was calculated from:

$$E_{zp} = \frac{1}{2}\sum_{i=1}^{n} h\upsilon_i \quad (5.12)$$

where h is the Planck's constant, ν is vibrational frequency and n denotes the number of the degrees of freedom. Finally, the dissociation energy of $NaCl_2^-$ into NaCl and Cl^- (D_0) was calculated from D_e-E_{zp}.

The optimized geometry calculated at the DFT, MP2, and CCSD levels of theory predict a triangular geometry for neutral $NaCl_2$ (Figure 5.5). The optimized geometrical parameters of $NaCl_2$ are listed in Table 5.1. The calculated bond distances between Na and Cl are in a close agreement ~ 2.5 Å. However, the valence angle of $NaCl_2$ is somewhat different. It ranges from 67° to 61°, depending on the level of theory and basis set employed. The optimized geometry for $NaCl_2^-$ for all three levels of theory was found to be linear (Figure 5.6). The computational results from three different levels of theory are shown in Table 5.2. The structure of the $NaCl_2^-$ ion is rather different from its neutral. Since $NaCl_2$ has 15 valence electrons and the $NaCl_2^-$ negative ion possesses 16 valence electrons, this change of structure from bent to linear can be predicted from Walsh's rule.[108]

In Table 5.3, the calculated bond dissociation energies of $NaCl_2^-$ for loss of Cl^- are listed. The BDE of $NaCl_2^-$ calculated at three levels of theory agrees with each other within 0.01 Å. The computed BDE was found to be 2.15 ± 0.01 eV. Table 5.4 presents

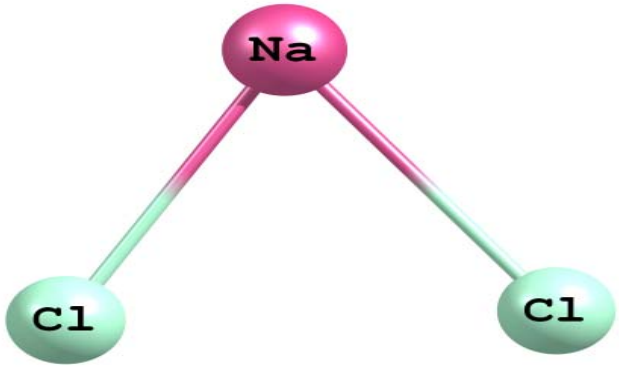

Figure 5.5 Optimized structure of neutral $NaCl_2$.

Table 5.1. Equilibrium geometry of $NaCl_2$ calculated at the DFT (B3LYP), MP2, and CCSD levels of theory with two different basis sets. The bond lengths (R) are in Å, zero point energy (E_{zp}) in eV, and total energies (E_{tot}) in Hartree. Valence angles are in degrees. For comparison the computed values by Simons and coworkers[105] are also presented.

Method /Basis set	E_{tot}	R (Na-Cl)	R (Cl-Cl)	∠ ClNaCl	E_{zp}
B3LYP/6-311+G*	-1082.814	2.54	2.80	67.1°	0.044
B3LYP/aug-cc-pVDZ	-1082.809	2.54	2.77	65.8°	0.043
MP2/6-311+G*	-1081.196	2.52	2.69	64.4°	0.048
MP2/aug-cc-pVDZ	-1081.226	2.59	2.66	61.8°	0.047
CCSD/6-311+G*	-1081.220	2.52	2.72	65.07°	0.043
CCSD/aug-cc-pVDZ	-1081.252	2.59	2.69	62.47°	0.044
B3LYP/6-311+G(d)[105]	-1082.814	2.53	2.80	67.2°	0.042
CCSD/6-311+G(d)[105]	-1081.222	2.52	2.72	65.1°	0.045
CCSD(T)/6-11+G(d)[105]	-1081.431	2.53	2.67	63.7°	0.046

Figure 5.6 Optimized structure of $NaCl_2^-$ ion.

Table 5.2 Equilibrium geometry of $NaCl_2^-$ calculated at the DFT (B3LYP), MP2, and CCSD levels of theory with two different basis sets. The bond lengths (R) are in Å, zero point energies (E_{zp}) are in eV, and total energies (E_{tot}) are in Hartree. For comparison the computed values by Simons and coworkers[105] are also presented.

Method /Basis set	E_{tot}	R (Na-Cl)	E_{zp}
B3LYP/6-311+G*	-1082.943	2.51	0.044
B3LYP/aug-cc-pVDZ	-1082.936	2.52	0.043
MP2/6-311+G*	-1081.321	2.49	0.046
MP2/aug-cc-pVDZ	-1081.359	2.55	0.041
CCSD/6-311+G*	-1081.343	2.49	0.046
CCSD/aug-cc-pVDZ	-1081.384	2.55	0.042
B3LYP/6-311+G(d)[105]	-1082.986	2.51	0.044
CCSD/6-311+G(d)[105]	-1081.390	2.49	0.046
CCSD(T)/6-311+G(d)[105]	-1081.889	-----	0.040

Table 5.3 Well depth, D_e, zero point energy, E_{zp}, and bond dissociation energy of $NaCl_2^-$ are shown using three different levels of theory and two different basis set: 6-311+G* and aug-cc-pVDZ. All values are in eV. For comparison the computed values by Simons and coworkers[105] are also presented.

Method	B3LYP		MP2		CCSD		CCSD(T)
Basis set	6-311+G*	aug-cc-pVDZ	6-311+G*	aug-cc-pVDZ	6-311+G*	aug-cc-pVDZ	WMR
D_e	2.21	2.19	2.34	2.18	2.2	2.2	2.27[105]
E_{zp}	0.044	0.043	0.046	0.041	0.046	0.042	0.040[105]
D_0	2.17	2.15	2.29	2.14	2.15	2.16	2.23[105]

Table 5.4 Calculated vibrational and rotational frequencies of $NaCl_2$ and $NaCl_2^-$ ion using different levels of theory and aug-cc-pVDZ basis set. All values are in cm^{-1}.

Method	B3LYP/aug-cc-pVDZ	MP2/aug-cc-pVDZ	CCSD/aug-cc-pVDZ
$NaCl_2^-$ Vib. Freq.	88, 88, 179, 338	81, 81, 175, 331	82, 82, 176, 332
$NaCl_2^-$ Rot. Freq.	0.0380, 0.0380	0.0382, 0.0382	0.0367, 0.0367
NaCl Vib. Freq.	353	344	345
NaCl Rot. Freq.	0.213	0.213	0.206

the vibrational and rotational frequencies of $NaCl_2^-$ and NaCl. These frequencies were used in data analysis of the experimental section.

Results and Discussion

In this study using the collision-induced dissociation method, we report that $NaCl_2^-$ is a thermodynamically stable ion and possesses a dissociation energy of 1.5 ± 0.2 eV for dissociation into NaCl and Cl^-. The theoretical value for this dissociation using three different levels of theory is approximately 2.15 ± 0.01 eV, in a fair agreement with the computed value from the work of Simon et al. (2.23 eV).[105]

The experimental value of 1.5 ± 0.2 eV is considerably smaller than the values calculated from theory. The inconsistency between the two results can be related to many possible factors. Since at this point there are no other experimental values available for the dissociation threshold energy of $NaCl_2^-$, our main source of comparison is with the theoretical approaches. Although the theoretical approach is a valuable tool to estimate the dissociation bond energy, it does not always correlate well with the experimental results. We have examined the accuracy of the theoretical levels used here with applying them to some known bond dissociation energies. There are not many negative ions bond dissociations experimentally available at this point so the justification of the theories is based on a few negative ions dissociation bond energies. For instance, the measured energy for dissociation of NO_3^- into NO_2 and O^- is 4.8 eV[86], however the computed value using all three levels of theory is found to be about 4.2 eV. Another example is dissociation energy of Cl_3^- and Br_3^-. Sunderlin and coworkers[93] measured D_e ($Cl_2 - Cl^-$) = 1.026±0.05 eV and D_e ($Br_2 - Br^-$) = 1.316±0.07 eV, but the predicted dissociation

energies by theory for Cl_3^- and Br_3^- are 1.69 eV and 1.79eV, respectively. Note that theory is too low for the first case and too high for the second. These few examples emphasize the difficulty in obtaining an accurate computational (or experimental) value for bond dissociation energy.

Another approach to investigate the bond dissociation energy of $NaCl_2^-$ can be as follow. If one considers the potential energy curves for negative and neutral $NaCl_2$ as shown in Figure 5.7, $NaCl_2^-$ bond dissociation energy can be written using a thermochemical relationship, i.e.,

$$D_0(NaCl_2^-) = D_0(NaCl_2) + EA_{ad}(NaCl_2) - EA_{ad}(Cl) \quad (5\text{-}13)$$

where $D_0(NaCl_2^-)$ is $NaCl_2^-$ dissociation energy into Cl^-, $D_0(NaCl_2)$ is $NaCl_2$ dissociation energy into Cl, $EA_{ad}(NaCl_2)$ is adiabatic electron affinity of $NaCl_2$, and $EA_{ad}(Cl)$ is the chlorine atom electron affinity. It should be mentioned that since the neutral and negative geometries of $NaCl_2$ are rather different, the potential energy curves would not be as simple as shown in Figure 5.7.

In Equation 5.13, the only experimentally known value is the electron affinity of Cl, 3.613[109]. Other values in Equation 5.13 have been computed and summarized in Table 5.5. Calculating the bond dissociation of $NaCl_2^-$ applying Equation 5.13, gives a range of $NaCl_2^-$ bond dissociation energy from 2.29eV to 1.85eV. Obviously, we are using calculated values for bond dissociation and electron affinity of $NaCl_2$ and the same uncertainty for the calculations are valid here.

Let us assume that the threshold energy of the dissociation is a reasonable value, thereby applying Equation 5.13, an adiabatic electron affinity of $NaCl_2$ can be calculated.

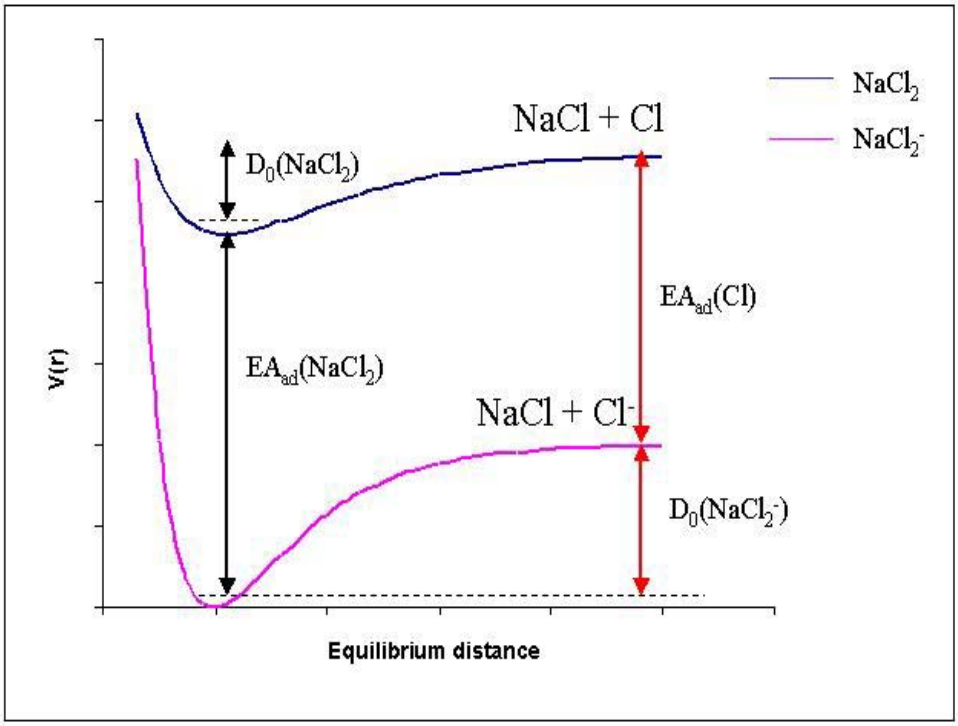

Figure 5.7 Hypothetical potential curves for $NaCl_2$ neutral and anion. EA_{ad} is $NaCl_2$ adiabatic electron affinity. D_0 ($NaCl_2^-$) and D_0 ($NaCl_2$) are bond dissociation energy of $NaCl_2^-$ and $NaCl_2$, respectively.

Table 5.5 Calculated bond dissociation energy of $NaCl_2$ into NaCl and Cl using three levels of theory in this work and reference 110. Adiabatic electron affinity of $NaCl_2$ is also presented. All values are in eV.

	Method	eV
$D_0(NaCl_2 \rightarrow NaCl + Cl)$	MBPT(4)/6-311+G(d)[110]	0.89
	CISD/6-311+G(d)[110]	0.82
	CCSD(T)/WMR[110]	1.05
	B3LYP/aug-cc-pVDZ [thiswork]	1.267
	MP2/aug-cc-pVDZ [thiswork]	0.964
	CCSD/6-311+G* [thiswork]	0.848
	CCSD/aug-cc-pVDZ [thiswork]	0.896
EA_{ad} ($NaCl_2$)	CCSD/6-31+G(d)[105]	4.56
	CCSD(T) /6-31+G(d)[105]	4.60
	B3LYP/aug-cc-pVDZ [thiswork]	4.60
	MP2/aug-cc-pVDZ [thiswork]	4.74
	CCSD/6-311+G* [thiswork]	4.53
	CCSD/aug-cc-pVDZ [thiswork]	4.71

With the bond dissociation energy of 1.5 eV for $NaCl_2^-$, a value of 4.2 ±0.1 eV for the adiabatic electron affinity can be predicted. Wang et al.[106] measured the vertical electron detachment of $NaCl_2^-$ (5.6eV). Their photoelectron spectrum is shown in Figure 5.8. Analysis of the photoelectron spectrum demonstrates that there is a possibility of 4.2 eV adiabatic electron affinity for $NaCl_2$. Keep in mind that the structure of $NaCl_2^-$ differs from its neutral so the photoelectron spectroscopy method can be very unfavorable in determining the adiabatic electron affinity of $NaCl_2$ experimentally due to a poor Frank-Condon overlap.

Assuming the value for bond dissociation energy computed with three different levels of theory is a reasonable value, then the question arises here is what kind of effects in our CID experiment and data treatment might lower the true threshold energy for the dissociation. One of the most critical conditions in the CID experiments is carrying the experiment under single collision conditions. In our experiment, the apparatus did not have a capability of reading the pressure of the collision gas especially below 10^{-4} mbar. To be able to vary the pressure in the system, we had to use a knob to change the amount of the gas going through the collision cell. The experiment was started off with no collision gas in the cell, and gradually the pressure was increased until we observed the dissociation to occur. The pressure reading was $< 10^{-4}$ mbar. We believed that we performed the experiment under single collision conditions. The apparatus used in this experiment was a multiple-use system and we could not employ any modification on the system to be able to obtain a better reading of the pressure. However, if one has a capability of reading the pressure in the system, data can be taken at several pressures and

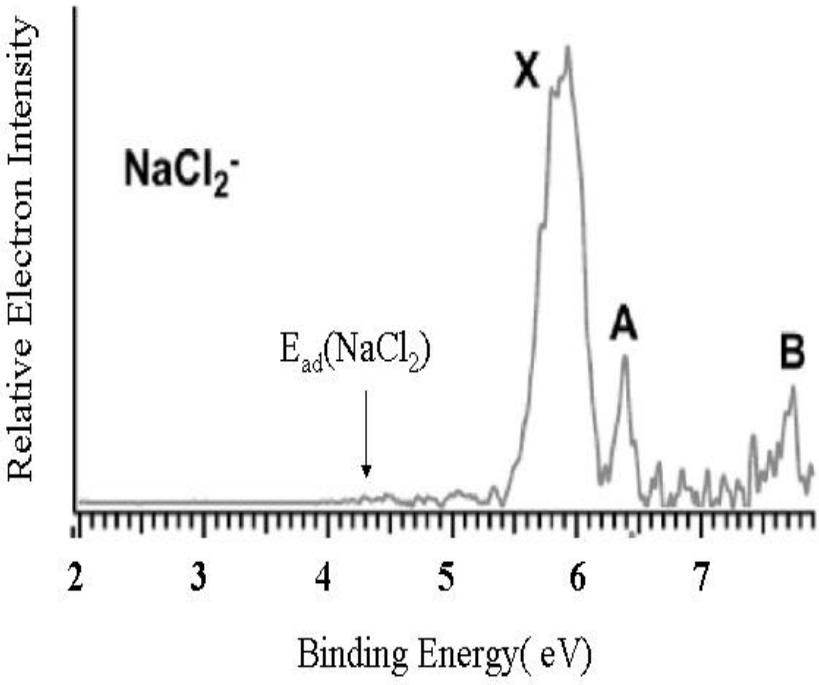

Figure 5.8 Photoelectron spectrum of $NaCl_2^-$ at 157 nm (7.866 eV). Three bands (X, A, B) are shown.[106]

then extrapolate to a zero pressure cross-section to avoid the effects of multiply collisions. We repeated the experiment in relatively higher pressure, i.e., opening the knob one more turn; we did not observe any changes in the threshold energy. In this regard, Armentrout et al.[69] examined the effect of multiply collision conditions on the threshold of the dissociation energy and concluded that multiple collisions has a negligible effect on the dissociation energy threshold of small clusters, but the effect will increase as the size of the cluster increases.

In a CID experiment, the raw data from the experiment requires a careful data treatment such as including the effect of internal energies and kinetic energy distribution of the reactants, Doppler broadening and many more as discussed in Chapter III. In the present experiment, the CRUNCH program was used to treat the experimental data, and accuracy of the results relies on a theoretical treatment of the program. However, the effect of this treatment should not be large enough to explain the inconsistency between the experimental and computed results. On the other hand the CRUNCH program has proven to do a fairy good job in the treatment of collision-induced dissociation data[65-70].

One also argues that during the collision between the collision gas and $NaCl_2$ ions, the collision energy ($E_{collision\ energy}$) could be consumed to break the bond (E_0), and provide the collision gas with some kinetic energy (KE), however if that is the case, then the observed threshold should be higher than the real threshold i.e., $E_{collision\ energy} = E_0 + KE$ (collision gas).

Overall, to verify the inconsistency between the theory and experiment, one needs to improve the experimental conditions, i.e., a better control of the pressure, and apply an advanced and sophisticated theory to calculate the bond dissociation energy.

Conclusion

The current work demonstrates that $NaCl_2^-$ is a stable anion. The calculations confirm that $NaCl_2^-$ ion has a linear geometry that is different from its neutral parent (triangular), and has a higher bond dissociation energy than its neutral. Its bond dissociation is approximately 1.5±0.2 eV and its adiabatic electron affinity can be predicted to be higher than 4.2 eV, showing that it belongs to the class of superhalogens. This work demonstrates the importance of continuous research on the CID and computational methods regarding bond dissociation energies. The CID technique has a great potential in measuring one of the most difficult molecular properties, bond dissociation of singly, doubly and even higher charged anions.

CHAPTER VI

Collision-Induced Dissociation of Dicarboxylate and Disulfonic Dianions

Introduction:

Carboxylic acids are characterized by the presence of a carboxylic group. The carboxylic group is a carbonyl group (C=O), bonded to a hydroxyl group, OH. This group is attached to one of the carbons in the rest of the molecule. Carboxylic acids are usually written as R-COOH or RCO_2H, where R is an H or an organic group. These acids are widely distributed in the nature and also important industrial chemicals. Carboxylic acids are very weak acids so they partially dissociate into H^+ and $RCOO^-$ in water. As a result an equilibrium exists in water, i.e., R-COOH $\leftrightarrow$ $RCOO^-$ + H^+. Carboxylic acids have important derivatives such as esters, acid halides, salts, acid amides and etc.

Dicarboxylic acids are organic compounds that are consisted of two carboxylic functional groups, HOOC-R-COOH. Dicarboxylic acids are used in a variety of industrial applications such as adhesive and powder coating, pharmaceutical, modifying rigidity in plastics, plasticizer for polymers, etc. Dicarboxylic acids are also well known to be one of the important groups of organic compounds in the study of doubly charge negative ions since producing doubly-charged dianions of this group in the gas phase is relatively easy.

In 1989, Mass and Nibbering[20] for the first time were able to generate doubly-charged dicarboxylate negative ions in the gas phase from singly-charged carboxylate negative ions employing collision-induced “ion pair” formation. In their experiment, they produced doubly-charged α, ω-alkane dicarboxylate negative ions from aliphatic α, ω-dicarboxylate esters using helium as the target gas. They pointed out the importance of

charge separation in the dianions. As mentioned before in order to have a stable dianion, the Coulomb repulsion energy between the charges in the dianion should be smaller than the binding energy of the second electron to the singly-charged anion. According to Mass and Nibbering calculations, the generated dicarboxylate dianions were stable when the distances separating the two charges were larger than about 5 Å.

There are several studies regarding the dicarboxylate dianions stability toward electron detachment. Following the observation of Maas and Nibbering, Wang et al.[44] investigated a dependency of the excess electron binding energy to the equilibrium charge separation for a group of linear dicarboxylate dianions, $^{-}O_2C(CH_2)_nCO_2^{-}$ (n=3-10). They assumed that two charges are localized on the oxygen atoms of the carboxylate groups. They reported that as the distance between two charges increases, the electron binding energy also increases since the Coulomb repulsion between two charges is expected to decrease. They also demonstrated that the electron binding energy (EB) and charge separation distance fits a linear functional form, i.e., EB (eV) =3.21 (4)-16.7(3)/r_n where r_n is the average distance between the oxygen atoms in Å. The electron binding energy becomes negative for a critical value of n=2 corresponding to a charge separation of 5.3 Å that is in accord with the Mass and Nibbering value (5 Å)[20]. In this study, they also estimated an inverse relation between the outer repulsive Coulomb barrier and distance between two charges for the linear dicarboxylate dianions as RCB (eV) = 0.00(5) + 16.8 (3)/r_n. One can simply employ the Coulomb repulsion equation as $e^2/ 4\pi\varepsilon_0 r$ where r is the distance between two charges. If we set ε_0=1(vacuum), the Coulomb repulsion will be 14.4 (eV.Å) /r(Å) . The equation extrapolated by Wang et al.[44] has a

16.7 coefficient that is higher than 14.4. This slight difference likely is result of overestimating the imprecise distance between two charge distributions. In the linear dicarboxylate dianions, charges are actually delocalized on CO_2 ligands not oxygen atoms and are certainly not point charges.

Generally, a doubly-charged anion is expected to be stable toward electron detachment as long as the Coulomb repulsion between the two isolated charges is lower than the electron binding energy of the second electron (electron affinity of the monoanion). With this assumption, stability of a large-molecule dianion toward electron detachment is more or less expected. However, it is not exactly clear how delocalization of charges on a dianion would affect the repulsive Coulomb barrier. Does delocalization increase or decrease the repulsive Coulomb barrier? There are only a few studies examining that how molecular structure and electronic properties of a doubly-charged dianion would affect its stability toward electron detachment. In this regard, Skurski et al[111], experimentally and theoretically examined the stability of two small dicarboxylate dianions having similar molecular size, geometry, and atomic structure: [(O_2C─C ≡ C─CO_2)$^{2-}$ (AD^{2-}) and (O_2C─CH_2─CH_2─CO_2)$^{2-}$ (SD^{2-})]. In this work electrospray mass spectrometry, photodetachment spectroscopy, and ab initio calculations were employed. In their experiment, the SD dianions were very difficult to produce whereas they reported large signals of AD dianions even though the chemical structure suggested they both have the same charge separations. Furthermore, their calculations showed that SD dianions are unstable toward electron detachment (negative adiabatic electron affinity) whereas AD dianions are stable with 0.418 eV adiabatic and 0.69 eV vertical electron binding energies. Their calculations also suggested that for AD dianions, two charges are

delocalized into the –CC- π-type orbitals while for SD dianions, charges are localized on the CO_2^- groups. Their results indicated that even though the charge delocalization on AD dianions increases the Coulomb repulsion, the D_{2d} structure of the AD dianions allows interaction between carboxylate group and the –CC- π-type orbitals, therefore increasing the stability of the AD dianions and minimizing the Coulomb repulsion.

In 2003, Schwerdtfeger et al.[112] performed a theoretical study regarding the stability of some dianions with similar atoms and structure, but slightly different electronic structure, i.e., $^-O\text{-}(CH_2)_n\text{-}O^-$, $^-O\text{-}(HC{=}CH)_n\text{-}O^-$, and $^-O\text{-}(C{\equiv}C)_nO^-$ where n is the number of carbon-carbon pairs (i.e., C-C, C=C, or C≡C). Their Density Functional theory calculations revealed that aliphatic dialkoxides, $^-O\text{-}(CH_2)_n\text{-}O^-$, are unstable toward electron detachment up to a chain length of n= 22 (charge separation of 30 Å) . While for $^-O\text{-}(HC{=}CH)_n\text{-}O^-$, and $^-O\text{-}(C{\equiv}C)_nO^-$ stable dianions exist for n=10 and n=6, respectively. In an effort to explain the necessary charge separation for these species to overcome the Coulomb repulsion, Schwerdtfeger and his co-workers plotted the highest occupied molecular orbitals for stable $^-O\text{-}(C \equiv C)_6\text{-}O^-$ and $^-O\text{-}(HC{=}CH)_{10}\text{-}O^-$, and compared them to the unstable $^-O\text{-}(CH_2)_{22}\text{-}O^-$. Their results showed that distribution of the charges over the carbon-carbon chain would *reduce* the Coulomb repulsion, while Skurski et al[111] found out that charge delocalization *increases* the Coulomb repulsion.

According to the present studies in the literature[111,112], there is still no clear correlation between the charge delocalization and electronic stability of a dianion. This situation is even more acute in considering the stability of a dianion toward ionic

fragmentation. To the best of our knowledge there are no studies investigating the stability of a dianion with delocalized charge separation toward ionic fragmentation.

The goal of present study is to investigate the stability of a group of dicarboxylate and disulfonic dianions with respect to electron detachment and ionic fragmentation employing a collision-induced-dissociation methodology. These two groups of dianions were chosen as a result of their different electronic properties. As it will be discussed later, the two excess charges are delocalized on dicarboxylate dianions whereas they are more localized on disulfonic dianions. This work attempts to address some of the posed questions regarding the correlation between charge distribution and stability of dianions.

Experimental Method

Collision-induced dissociation (CID) studies were conducted with a Micromass Quattro II (triple quadrupole) mass spectrometer in conjunction with an electrospray ionization source (ESI). Details and set-up of the apparatus (Figure 3.2) have been discussed in chapter III. The dianions studied were formed from 20 μg/ml solutions of potassium benzene-1,2-disulfonate [$C_6H_4(SO_3)_2K_2$], 2,6-naphthalenedisulfonic acid disodium salt [$C_{10}H_6(SO_3)_2Na_2$], terephthalic acid disodium salt [$C_6H_4(CO_2)_2Na_2$], 2,6-naphthalenedicarboxylic acid dipotassium salt [$C_{10}H_6(CO_2)_2K_2$] , and 4-sulfobenzoic acid potassium salt [$C_6H_4(SO_3)_1(CO_2)_1KH$] (Figure 6.1) in 50/50 water and methanol mixture and were introduced to the ESI at a rate of 5 μl/min. Salt samples were purchased from Sigma-Aldrich (USA) and used with no further purification. The source block temperature and desolvation temperature were set to be 80 °C and was 120 °C,

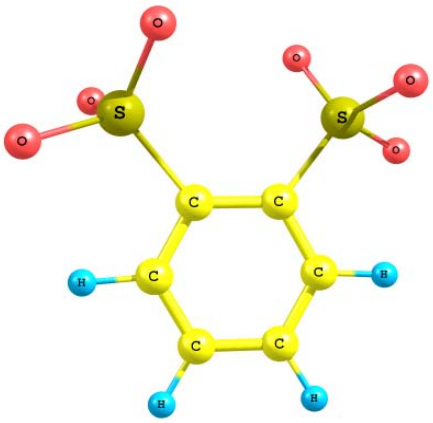

Fig. 6.1(a) 1,2-disulfonate dianion

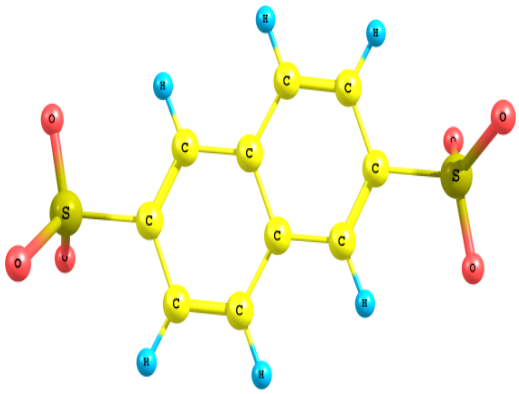

Fig. 6.1(b) 2,6-naphthalenedisulfonic dianion

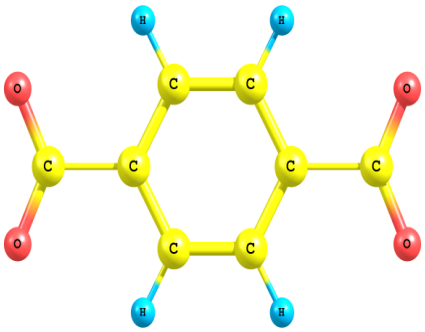

Fig. 6.1(c) Terephthalic dianion

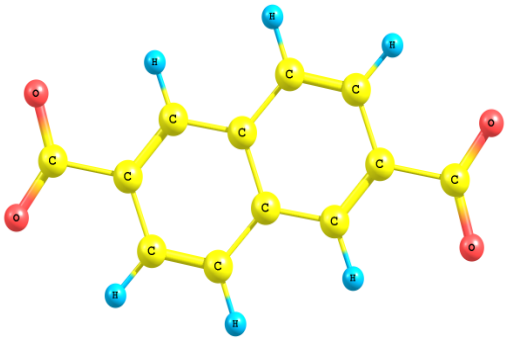

Fig. 6.1(d) 2,6-naphthalenedicarboxylate dianion

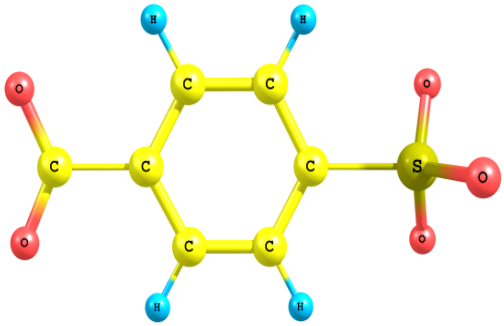

Fig. 6.1(e) 4-sulfobenzoic dianion

Figure 6.1 Geometric structures of the doubly-charged studies in this work.

respectively. The optimum cone voltage for extraction of the dianions studied was empirically found to be 20 V. The collision-induced dissociation experiment was performed using argon as the target gas under approximate single collision conditions. The collision energies ranged from 0 to 60 eV in the lab frame. Further details of the apparatus and energy calibration have been described previously in chapter IV and remain unchanged. The energy scale and ion energy resolution (FWHM ~ 0.5 eV) was obtained by employing a retardation analysis on various ions as presented in Figure 4.1.

Computational Method

Full geometry optimization of the neutral and anionic species were performed on the level of Density Functional Theory (B3LYP) and 6-311++G** basis set. All calculations were performed using the Gaussian 03 code.[107]

To investigate the stability of the dianions toward electron detachment, the second electron affinity of each species was computed as a difference in total energies between the dianion and the singly anion. Zero-point energies were not included in the calculations.

To explore the dissociation pathways of each dianions into two singly ions, i.e. $AB^{2-} \rightarrow A^- + B^-$, the potential curves as a function of distance between the two singly ions were constructed. Each ion-ion interaction potential was obtained by stepwise increasing the distance between the two singly charged ions, i.e. A^- and B^-. In all calculations, only the coordinate corresponding to the distance between the ions was varied. All other geometrical parameters were fully optimized to minimize the energy at each point.

In the CID experiment, the measured threshold energy for a dianion to dissociate into two singly-charged ions represents the inner repulsive Coulomb barrier (RCB). In order to determine the outer repulsive Coulomb barriers an estimation of dissociation energy of the dianion into two singly-charged ions is necessary (see Figure 3.3). In this regard, energies to dissociate the dianions into two singly charged ions were determined calculating the energy difference between the optimized dianions and singly-charged ion fragmentations.

Experimental Results

The primary electrospray mass spectra along with post-collisional mass spectra of the dianions studied are shown in Figures 6.2 to 6.7. We have attempted to identify some of the peaks in the mass spectra prior to collision, however, due to the fact that some of the peaks are from reaction between the sample and solvent made it difficult to unambiguously identify all of the peaks.

The mass spectra of the dianions prior to collision were optimized to the most intense signal of doubly-charged anions (cone voltage = 20V). For the optimized conditions, the dicarboxylate and disulfonic samples do not show singly charged ions of the doubly charged, however, singly charged ions along with hydrogen were observed as shown in Figure 6.2. The only exception was that for 2,6-naphthalenedisulfonic dianions, there is no singly charged anion with or without hydrogen at the optimized cone voltage (Figure 6.3). However, as the cone voltage was varied the signal of negative ions along with hydrogen for this sample was observed as well. In general, it was concluded that the singly charged anion of the corresponding dianions are not stable and not observed in the

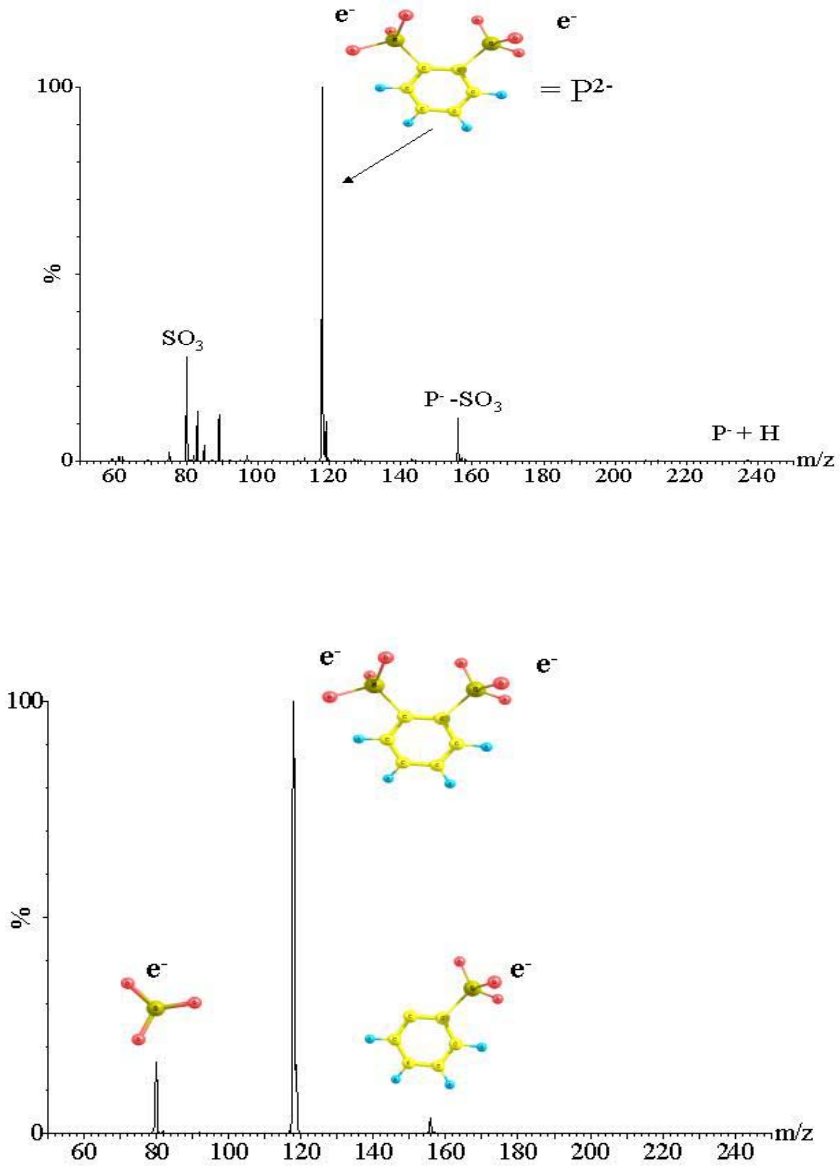

Figure 6.2 Top: Electrospray mass spectrum of potassium benzene-1,2-disulfonate in 50/50 water and methanol mixture. Bottom: Mass spectrum of secondary ions produced by collisions of the parent dianions with argon at laboratory energy of 60 eV.

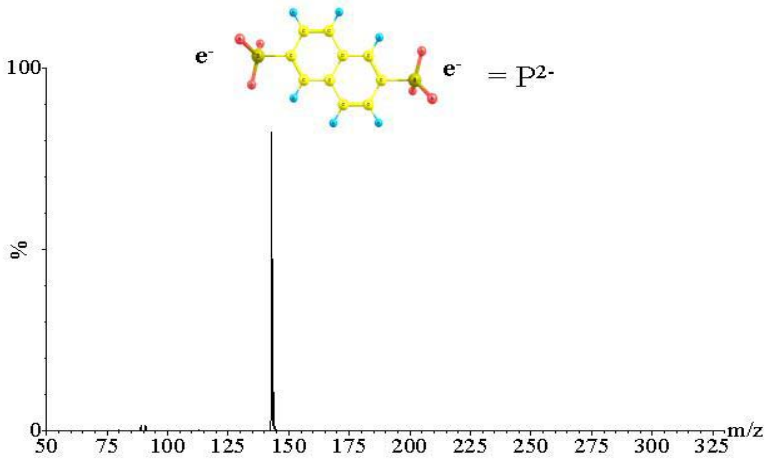

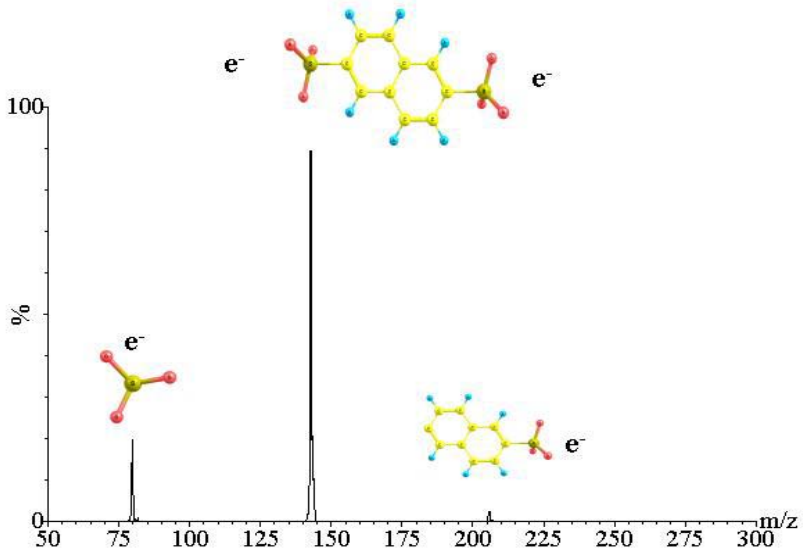

Figure 6.3 Top: Electrospray mass spectrum of 2,6-naphthalenedisulfonic acid disodium salt in 50/50 water and methanol mixture. Bottom: Mass spectrum of secondary ions produced by collisions of the parent dianions with argon at laboratory energy of 60 eV.

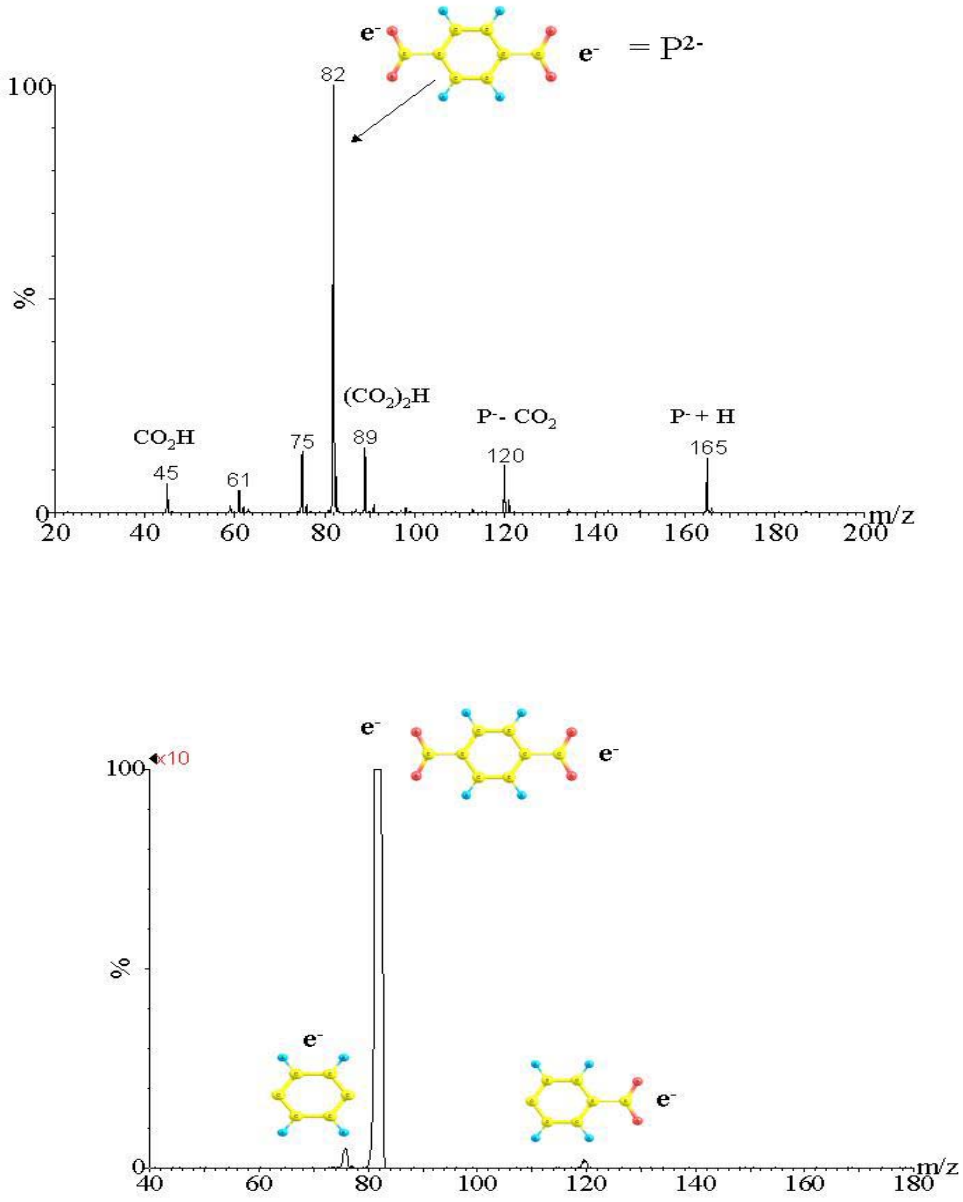

Figure 6.4 Top: Electrospray mass spectrum of terephtahlic acid disodium salt in 50/50 water and methanol mixture. Bottom: Mass spectrum of secondary ions produced by collisions of the parent dianions with argon at laboratory energy of 60 eV.

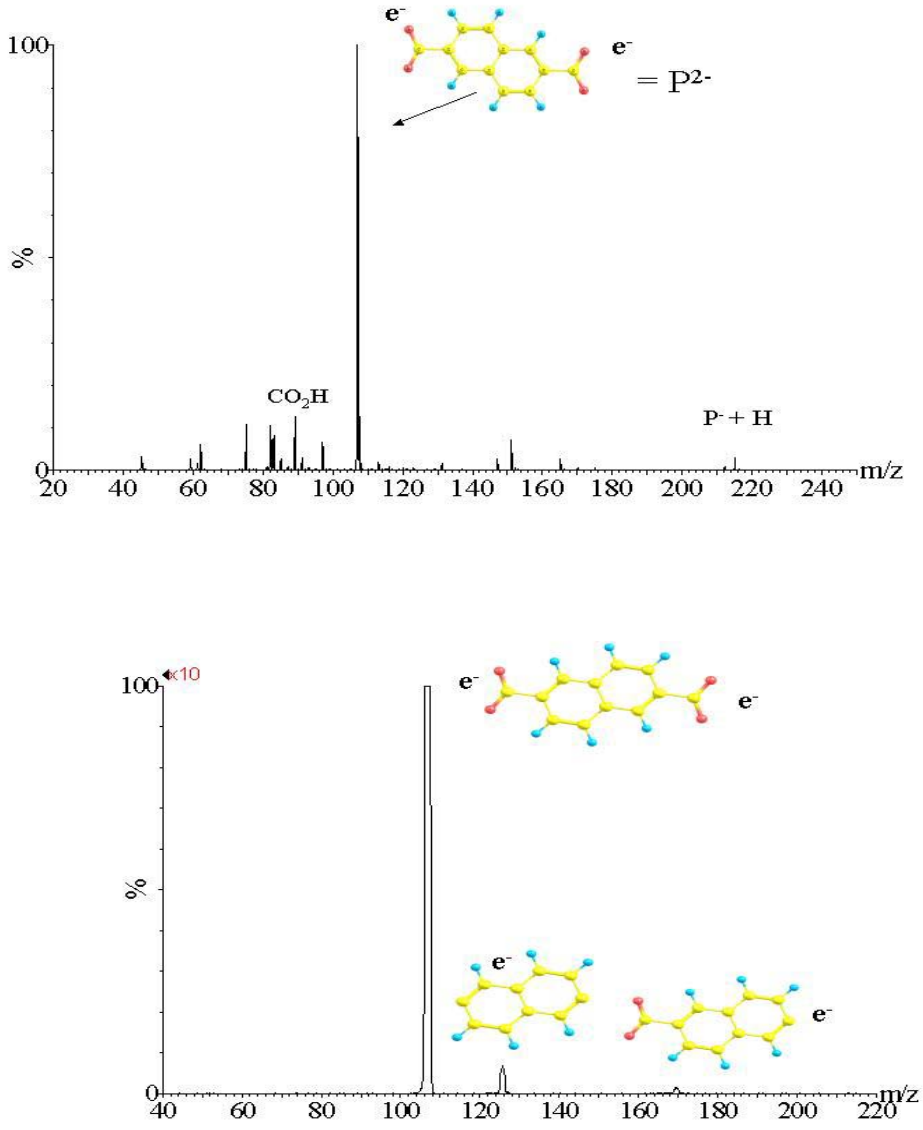

Figure 6.5 Top: Electrospray mass spectrum of 2,6-naphthalenedicarboxylic acid dipotassium salt in 50/50 water and methanol mixture. Bottom: Mass spectrum of secondary ions produced by collisions of the parent dianions with argon at laboratory energy of 60 eV.

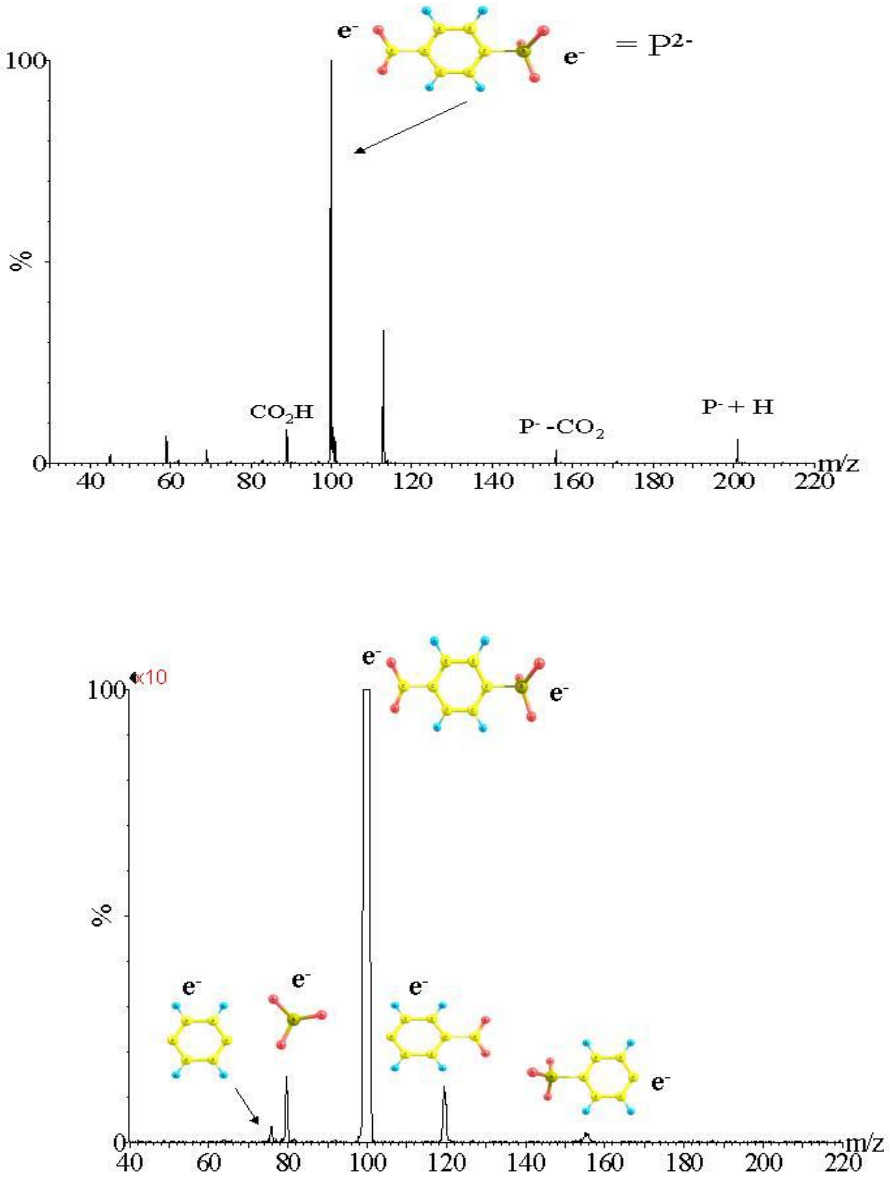

Figure 6.6 Top: Electrospray mass spectrum of 4-sulfobenzoic acid potassium salt in 50/50 water and methanol mixture. Bottom: Mass spectrum of secondary ions produced by collisions of the parent dianions with argon at laboratory energy of 60 eV.

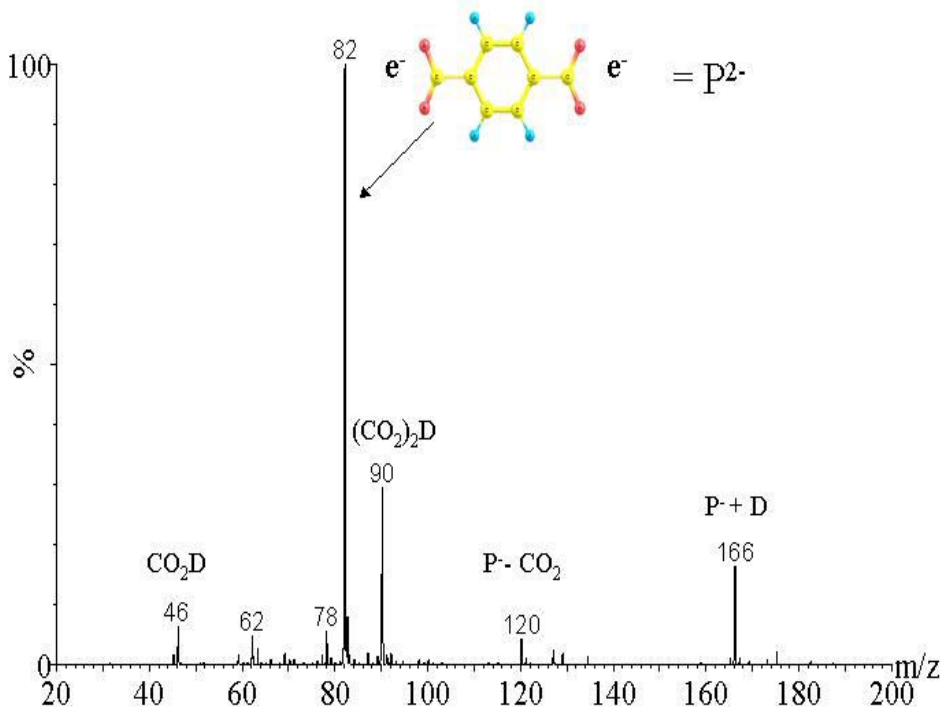

Figure 6.7 Electrospray mass spectrum of terephtahlic acid disodium salt in 50/50 deuterated water and deuterated methanol mixture.

mass spectra before collision. To verify that the signal observed is singly-charged along with hydrogen, 20 μg/ml of solution of terephthalic acid disodium salt in 50/50 deuterated water and deuterated methanol mixture was introduced to the ESI. As a result the peaks presented in Figure 6.4, singly-charged ion plus H, changed to singly-charged ion plus deuterium as shown in Figure 6.7. This result also shows that the hydrogen along with the singly-charged peaks coming from the solvent not from the terephthalic acid disodium salt.

The CID of disulfonic dianions shows a single dissociation pathway, leading to the SO_3^- anion and its conjugate ion for both molecular species (Figures 6.2& 6.3). The dicarboxylate dianions showed fragmentation resulting in singly charged anions without one or both CO_2 ligands (Figures 6.4& 6.5). Anions of the carbon ring structure corresponding to the case where both SO_3 ligands are fragmented are not observed in the collisional dissociation of the disulfonic dianions. Long-lived CO_2 ions were also not observed within the experimental time window available, which is estimated to be in the order of ms. The CO_2 anion is known to be metastable with respect to autodetachment with a lifetime varying between 20-90 μseconds depending upon the internal ro-vibrational energy present in the CO_2^- ion[113]. The dianion containing both SO_3 and CO_2 ligands showed the most complicated fragmentation pattern. The SO_3^- anion is formed along with its conjugate ion. The loss of CO_2 is again seen without CO_2^- signal. As with the dicarboxylate dianions singly charged ring anions are left after loss of both the SO_3 and CO_2 ligands (Figure 6.6). Autodetachment or collisional electron detachment of these dianions was not observed up to 60 eV (lab frame). This would imply that dissociation represents the lower energy pathway for decay.

The collisional energy dependencies for the formation of each of these ionic fragments were investigated. The relative fragment signal was taken as the ratio of the fragment signal to the remaining parent, such that variances in signal intensity from experiment to experiment could be accounted for. These signals were then plotted with respect to collision energy in the center-of-mass (COM) energy to probe the energy thresholds for fragmentation. The fragmentation of the SO_3^- anion from the disulfonic dianions showed a clear threshold (Figures 6.8 &6.9). These thresholds are estimated to be 2.32 eV and 3.48 eV, respectively. The loss of a CO_2 ligand and an electron from the dicarboxylate dianions appeared with no clear threshold (Figures 6.10 &6.11). In this case there is signal at "zero" collision energy implying that these ions are metastable. However, later experiments to be described indicate that these dianions in their ground state are stable.

The single ringed dicarboxylate dianion showed significant loss of a single CO_2 ligand and electron, as well as loss of both CO_2 ligands (along with the loss of one or two electrons, respectively), to a lesser extent, at the lowest collisional energies. The dianion containing two rings (naphthalenedicarboxylate dianion) showed a small, but measurable, signal for both fragmentation pathways at the lowest collision energies (and at zero pressure). Both singly and doubly ringed dicarboxylate dianions exhibited a peak due to the signal from loss of a single CO_2 ligand and electron as the signal for loss of both CO_2 ligands and an electron began to increase. The dianion containing both CO_2 and SO_3 ligands showed results in concurrence with the other dianions (see Figure 6.12). The signal from loss of a CO_2 and electron again appears at the lowest collision energies and

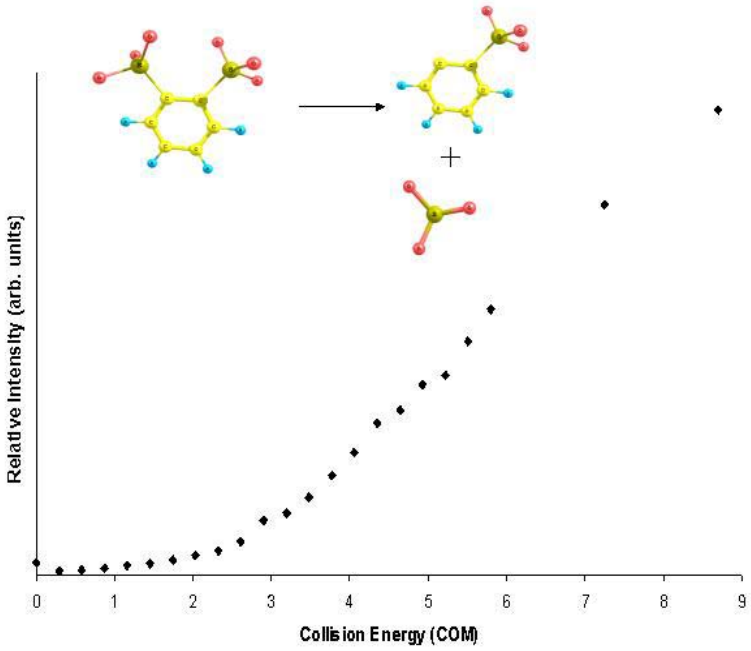

Figure 6.8 Cross-section for CID of 1,2- disulfonate dianion in the center-of-mass frame.

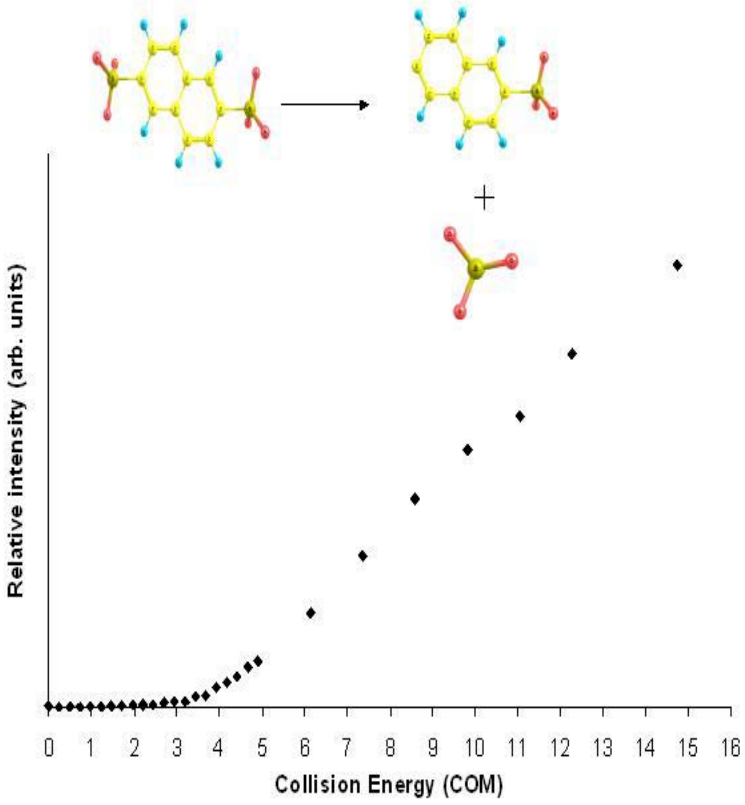

Figure 6.9 Cross-section for CID of 2,6-naphthalenedisulfonic dianion in the center-of-mass frame

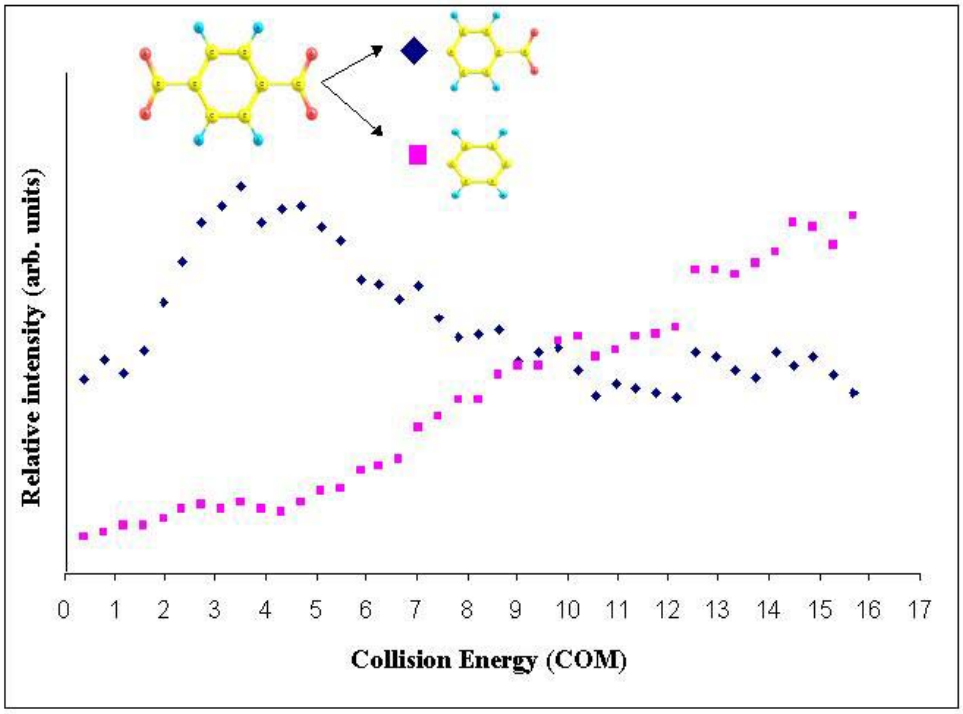

Figure 6.10 Cross-section for CID of terephtahlic dianion in the center-of-mass frame

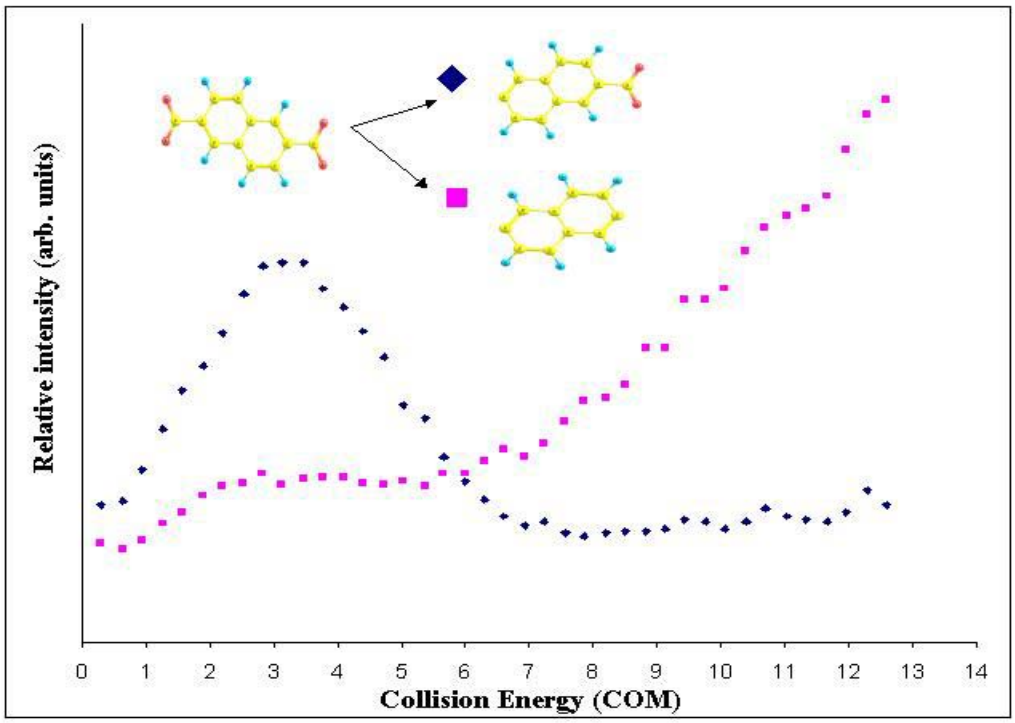

Figure 6.11 Cross-section for CID of 2,6-naphthalenedicarboxylate dianion in the center-of-mass frame

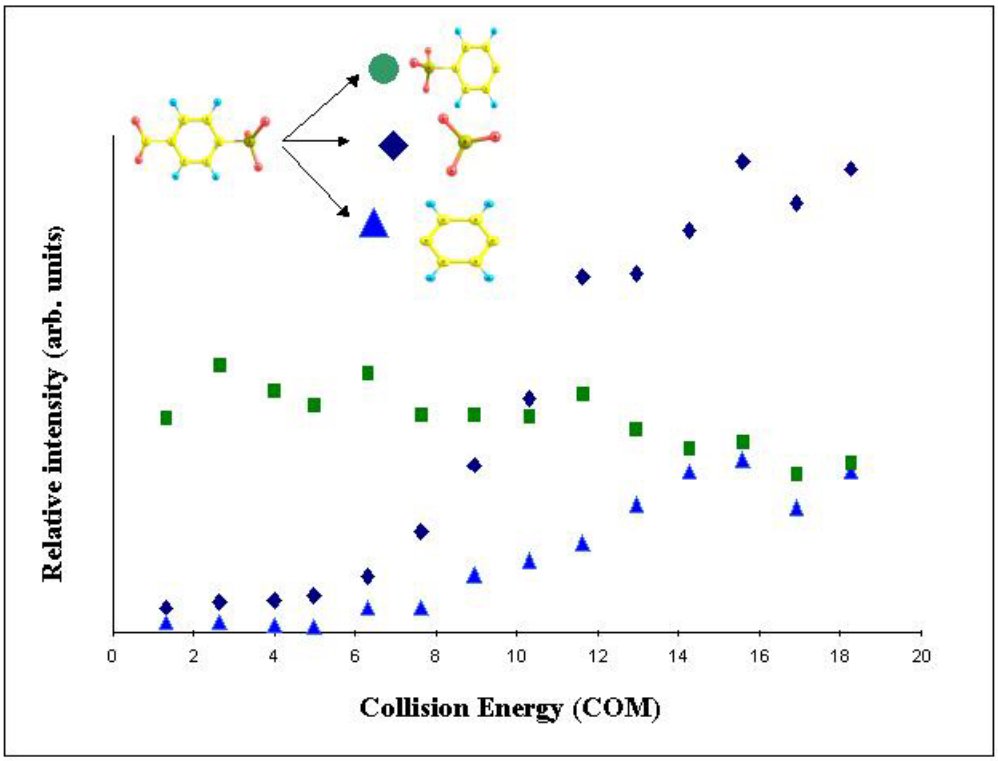

Figure 6.12 Cross-section for CID of 4-sulfobenzoic dianion in the center-of-mass frame.

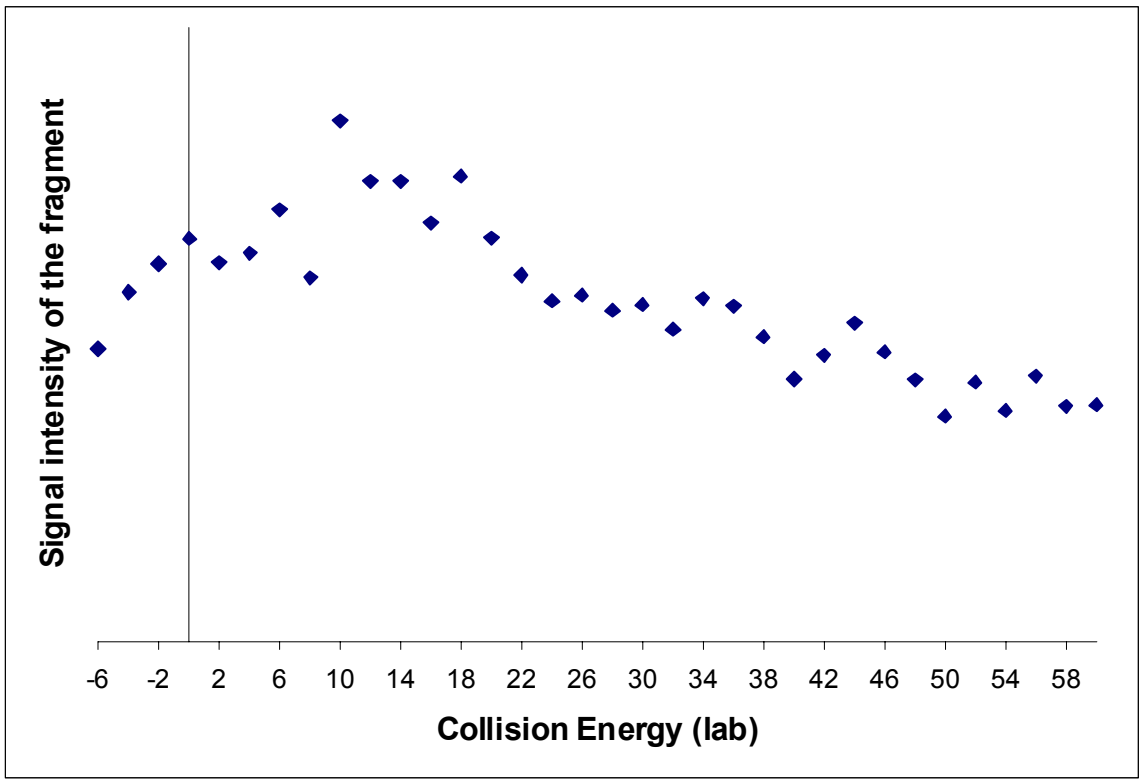

Figure 6.13 Signal intensity of the singly fragment ion from terephthalic dianion in collision-induced dissociation experiment with no collision gas.

in this case remains relatively unchanged over the energies studied. The loss of SO_3^- appears with a clear threshold, as does the loss of both ligands (see Figure 6.12).

Calculation Results

Table 6.1, presents the computed electron bonding energies for the dianions studied in this work. All these dianions have a positive electron binding energy predicting that they are adiabatically stable.

The dissociation pathways of all dianions toward ionic fragmentation are presented in Figures 6.14 through 6.18. All dissociation pathways exhibit a Coulomb barrier that is approaching the 1/r asymptote as the distances between the two singly ions are increased. The heights of the inner repulsive Coulomb barrier (RCB) are summarized in Table 6.1. The computed inner RCBs for 1,2-disulfonate and 2,6-napthalenedisulfonic dianions are approximately 2.68 eV and 3.77 eV, respectively. The experimental inner RCB for these dianions were estimated to be 2.32eV and 3.48eV (Figures 6.8 and 6.9). Comparing to the experimental results, the computed values represent an overestimate of the heights of the inner RCB for both dianions by about 0.3 eV. This difference could be attributed to the fact that the zero-point energies were not included in the calculations. It is also interesting to note that the RCB for the 2,6-naphthalenedisulfonic dianion is much wider than that for 1,2-disulfonate dianion.

The computed inner RCBs for terephtahlic, 2,6-naphthalenedicarboxylate, and 4-sulfobenzoic are roughly the same: 2.92eV, 2.75eV, and 2.82eV, respectively. The width of the RCB for all of these dianions appears to be similar. A theoretical analysis of these potentials in terms of their shapes and widths is not a straightforward task and required a

Table 6.1 Calculated electron binding energies (second electron affinities) and inner repulsive Coulomb barriers (RCB) for the dianions toward ionic fragmentation are presented. Density Functional theory (B3LYP) with 6-311++G** basis set was used. All values are in eV.

Dianion	Electron binding energy	Inner RCB
1,2- disulfonate	0.91	2.68
2,6-naphthalenedisulfonic	2.08	3.77
Terephthalic	0.61	2.92
2,6-naphthalenedicarboxylate	1.65	3.77
4-sulfobenzoic	1.11	2.68

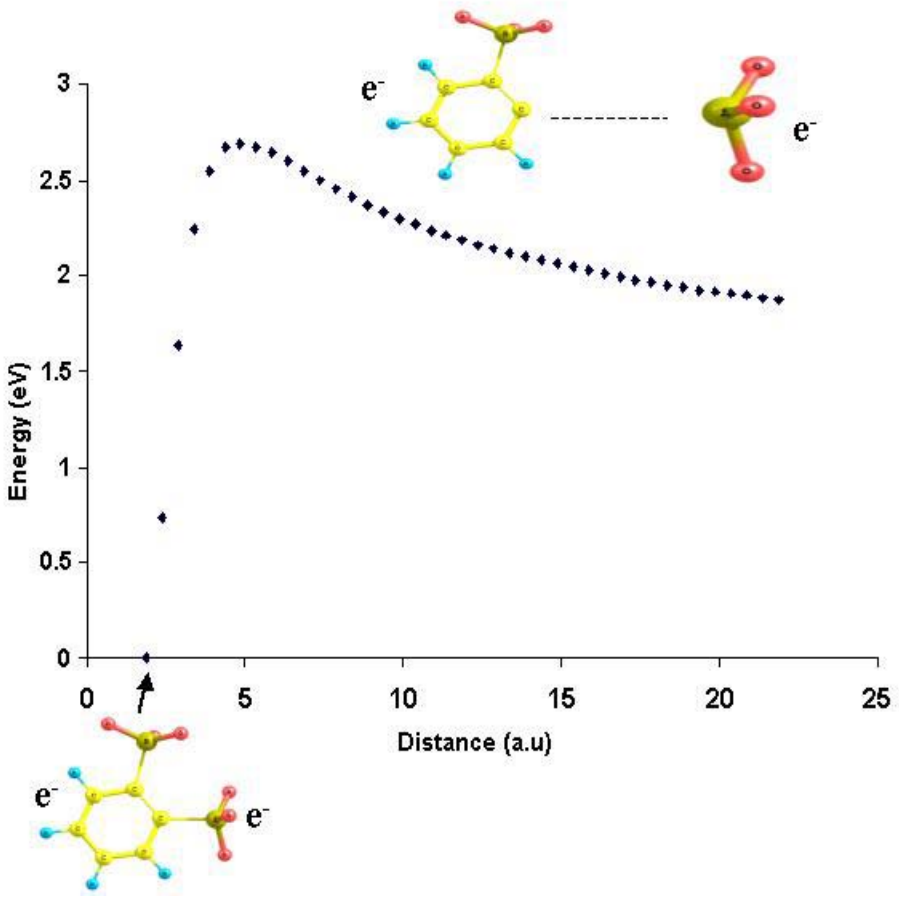

Figure 6.14 Dissociation pathway of 1,2- disulfonate dianions into SO_3^- ion and $C_6H_4(SO_3)^-$ ion. The curve is obtained by stepwise increasing the distance between SO_3^- ion and $C_6H_4(SO_3)^-$ ion. All other geometrical parameters were fully optimized to minimize the energy at each point. The zero-point of the energy scale corresponds to the energy of the optimized dianion.

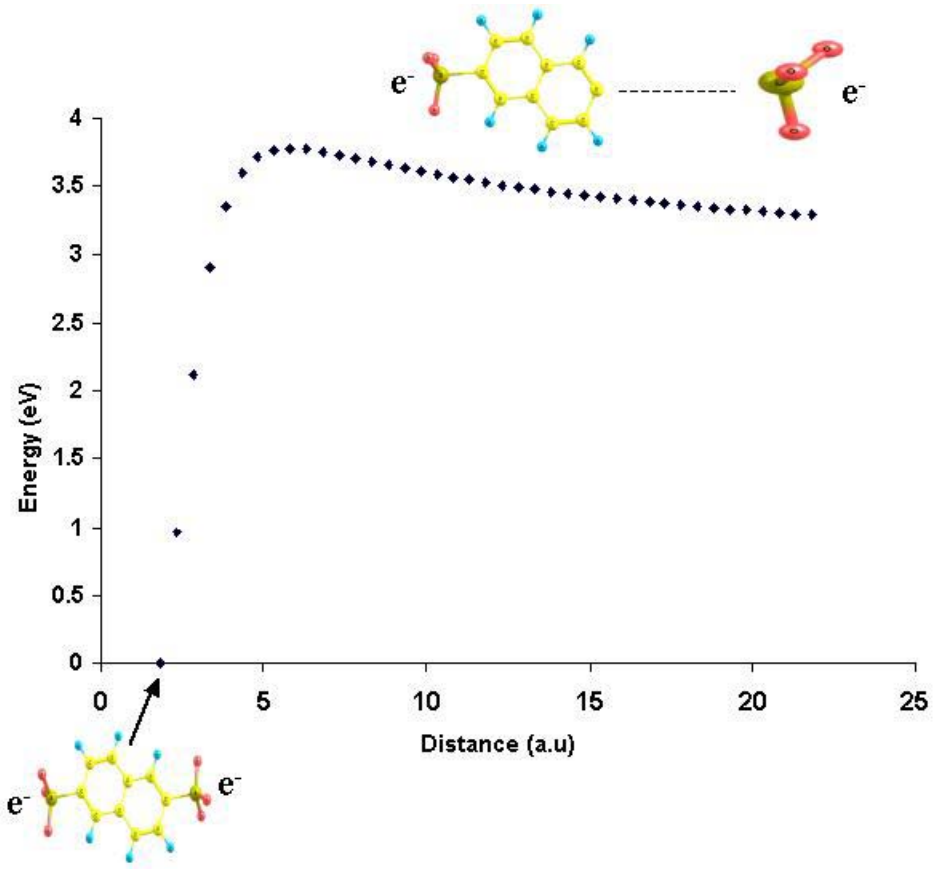

Figure 6.15 Dissociation pathway of 2,6-naphthalenedisulfonic dianion into SO_3^- ion and $C_{10}H_6(SO_3)^-$ ion. The curve is obtained by stepwise increasing the distance between SO_3^- ion and $C_{10}H_6(SO_3)^-$ ion. All other geometrical parameters were fully optimized to minimize the energy at each point. The zero-point of the energy scale corresponds to the energy of the optimized dianion.

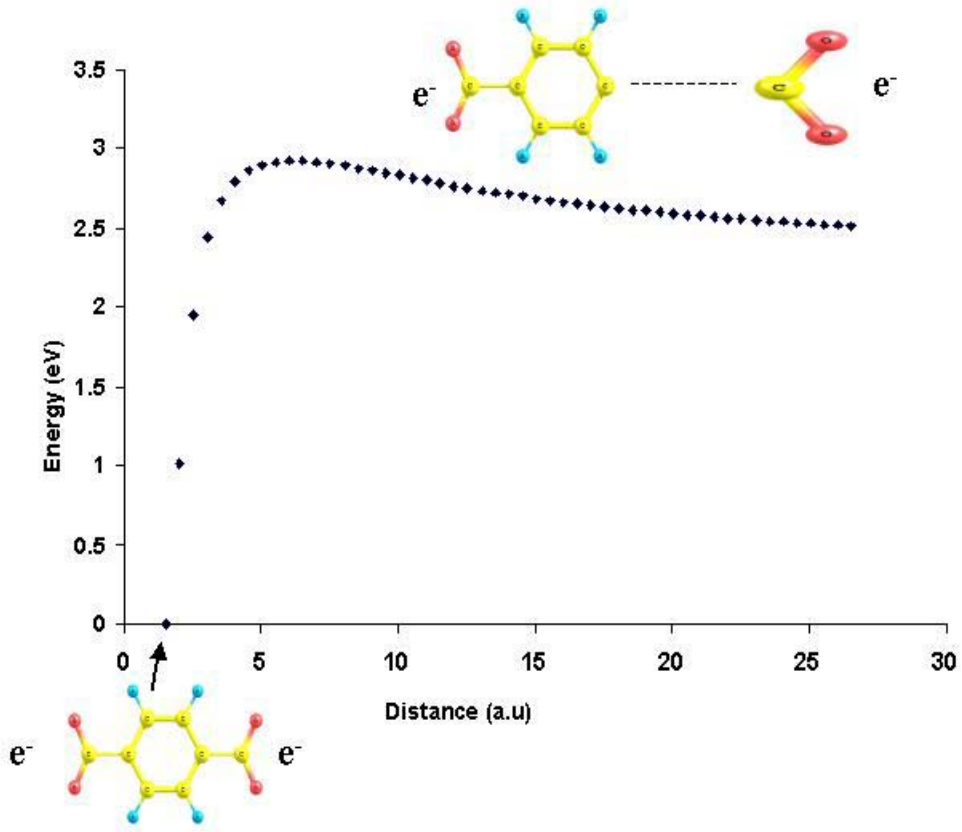

Figure 6.16 Dissociation pathway of terephtahlic dianion into CO_2^- ion and $C_6H_4(CO_2)^-$ ion. The curve is obtained by stepwise increasing the distance between CO_2^- ion and $C_6H_4(CO_2)^-$ ion. All other geometrical parameters were fully optimized to minimize the energy at each point. The zero-point of the energy scale corresponds to the energy of the optimized dianion.

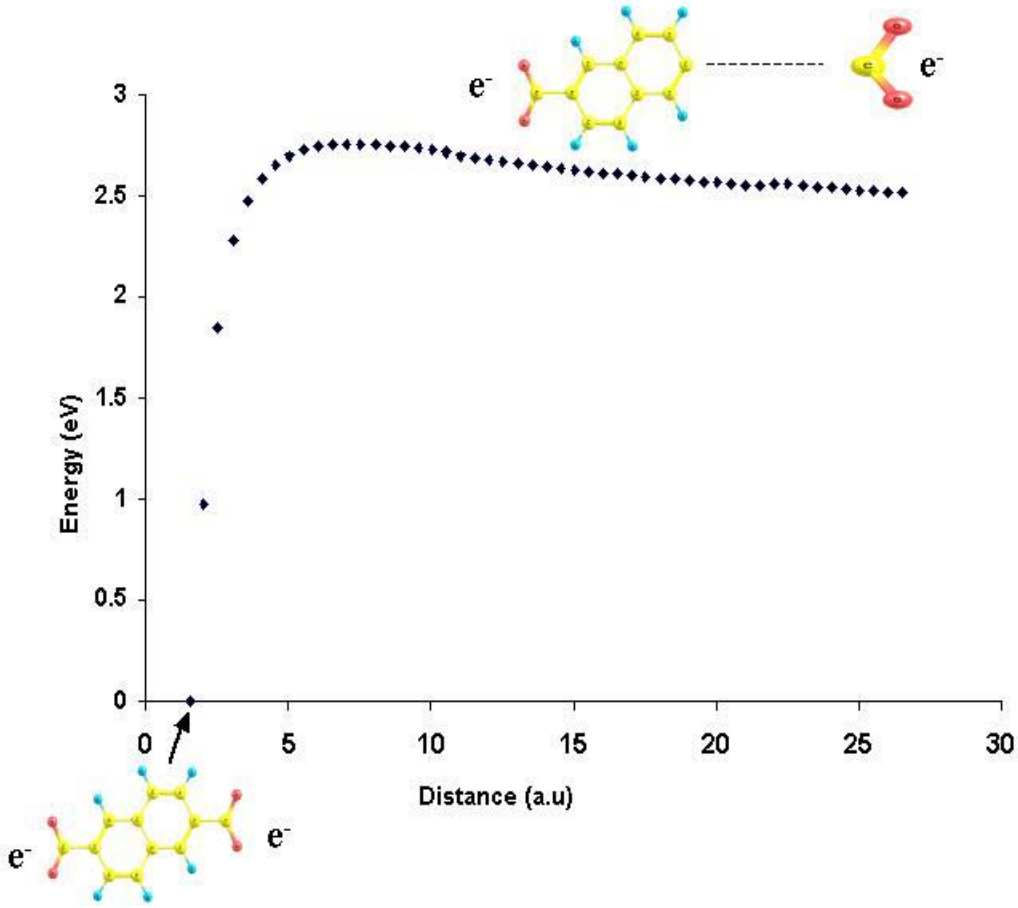

Figure 6.17 Dissociation pathway of 2,6-naphthalenedicarboxylate dianion into CO_2^- ion and $C_{10}H_6(CO_2)^-$ ion. The curve is obtained by stepwise increasing the distance between CO_2^- ion and $C_{10}H_6(CO_2)^-$ ion. All other geometrical parameters were fully optimized to minimize the energy at each point. The zero-point of the energy scale corresponds to the energy of the optimized dianion.

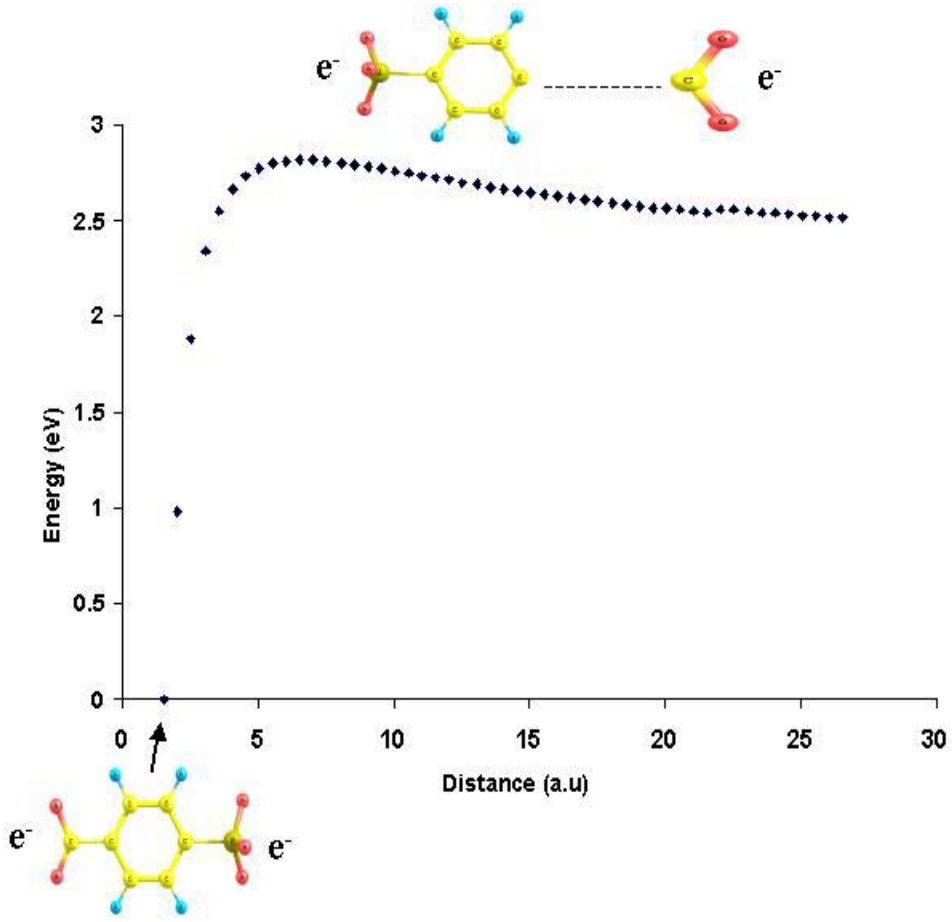

Figure 6.18 Dissociation pathway of 4-sulfobenzoic dianion into CO_2^- ion and $C_6H_4(SO_3)^-$ ion. The curve is obtained by stepwise increasing the distance between CO_2^- ion and $C_6H_4(SO_3)^-$ ion. All other geometrical parameters were fully optimized to minimize the energy at each point. The zero-point of the energy scale corresponds to the energy of the optimized dianion.

precise quantum treatment. There are still no clear theoretical formalisms to relate the appearance of a RCB to the electronic properties of its corresponding dianion.

The width of a repulsive Coulomb barrier is an important feature of multiply-charged anions. The height and width of the RCB determine the lifetime of a metastable MCA since the lifetime is a result of tunneling through the Coulomb barrier. The tunneling probability and lifetime of a metastable MCA can be determined using a model such as semi-classical WKB (Wentzel, Kramers, and Brillouin)[114] theory. According to this model, probability of the tunneling through the RCB inversely is proportional to the width of the barrier. The tunneling probability gets smaller for the wider RCB, resulting in a longer lifetime.

Discussion

Collision-induced dissociation studies demonstrate that dicarboxylate dianions are metastable toward fragmentation i.e., they fragment with no collision gas present (Figure 6.13). However, dissociation is generally enhanced at higher collision energy.

Disulfonic dianions are stable toward ion fragmentation and clear energetic thresholds are seen in the dissociation cross-sections. Interestingly, the dianions resulting from 4-sulfobenzoic (containing both CO_2 and SO_3 ligands) were stable toward SO_3^- and metastable toward loss of CO_2 + e.

The fact that no CO_2^- ions were detected in CID experiment for the dicarboxylate dianions raises an interesting question as to the lowest possible pathway for ionic fragmentation. From these experiments, it is not possible to determine whether the

dicarboxylate dianions are simultaneously losing CO_2 and an electron or autodetachment of CO_2^- ligand is occurring. In this regard there are two group of experiments[115,116] that represent dicarboxylate dianions decay with loss of a neutral molecule (CO_2), e.g. ^-O_2C - $(CH_2)_nCO_2^- \rightarrow {}^-O_2C$ - $(CH_2)_n^- + CO_2$. As mentioned before the CO_2^- anion is metastable (adiabatic electron affinity = -0.6 ± 0.2 eV[117]) and has a lifetime of ~ 60 μs[113], therefore would not be detectable in the experimentally available time window (on the order of ms). Our calculations indicate that dicarboxylate dianions are stable toward ionic dissociation (Figures 6.17& 6.18). These dianions are also calculated to be adiabatically stable, i.e., have a positive electron bonding energy (Table 6.1). Relying on the computed results and the evidence of loss of a neutral CO_2 presented in other experiments[115,116], we believe that the decay of dicarboxylate dianions in our CID experiment is through loss of neutral CO_2 and electron simultaneously. Since the electron affinity of CO_2 is ~ - 0.6 eV ions of CO_2 and electron is the lowest energy pathway.

An interesting result from the collision-induced dissociation studies is the detection of the *p*-benzyne anion (C_6H_4, m=76 amu, EA= 1.265±0.008 eV[118]) in dicarboxylate and 4-sulfobenzoic (containing both CO_2 and SO_3 ligands) dianions, but no *p*-benzyne fragmentation from disulfonic dianions. In order to compare these dianionic species and to attempt to understand this interesting feature, orbital calculations of these dianions using the Gaussian G03 suite of programs[107] at the Density Functional level of theory with 6-311++G^{**} basis set was employed. The results are demonstrated in Figures 6.19 through 6.23. Orbital visualization of these dianions shows that for dicarboxylate dianions the two electrons are distributed between the CO_2 and the benzyne ring while

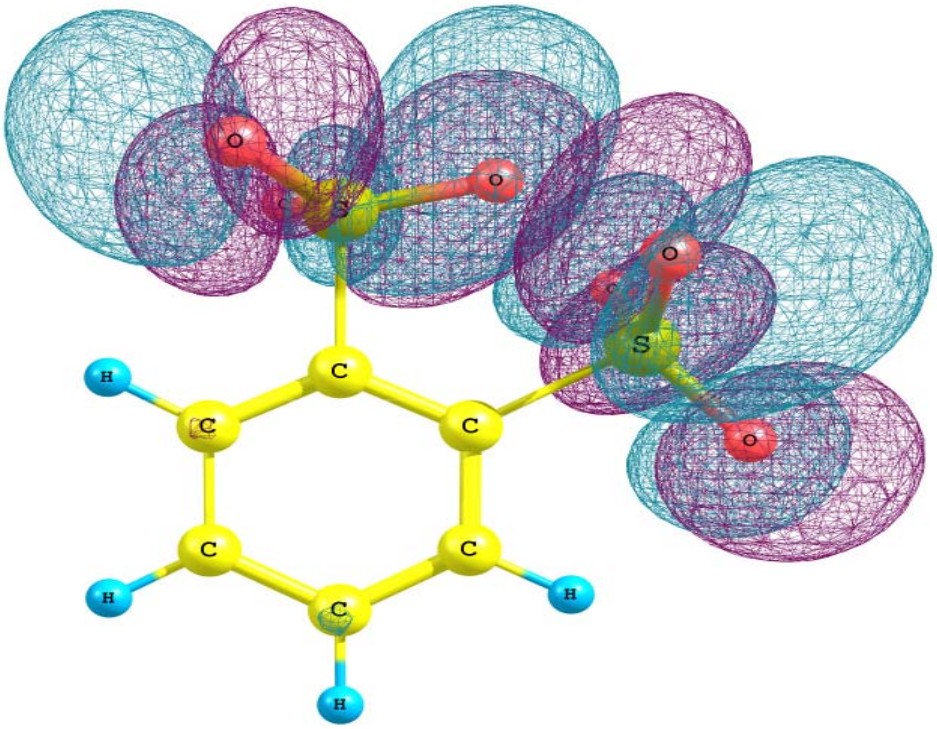

Figure 6.19 Highest occupied molecular orbital visualization for 1,2- disulfonate dianion using Density Functional theory (B3LYP) and 6-311++G** basis set.

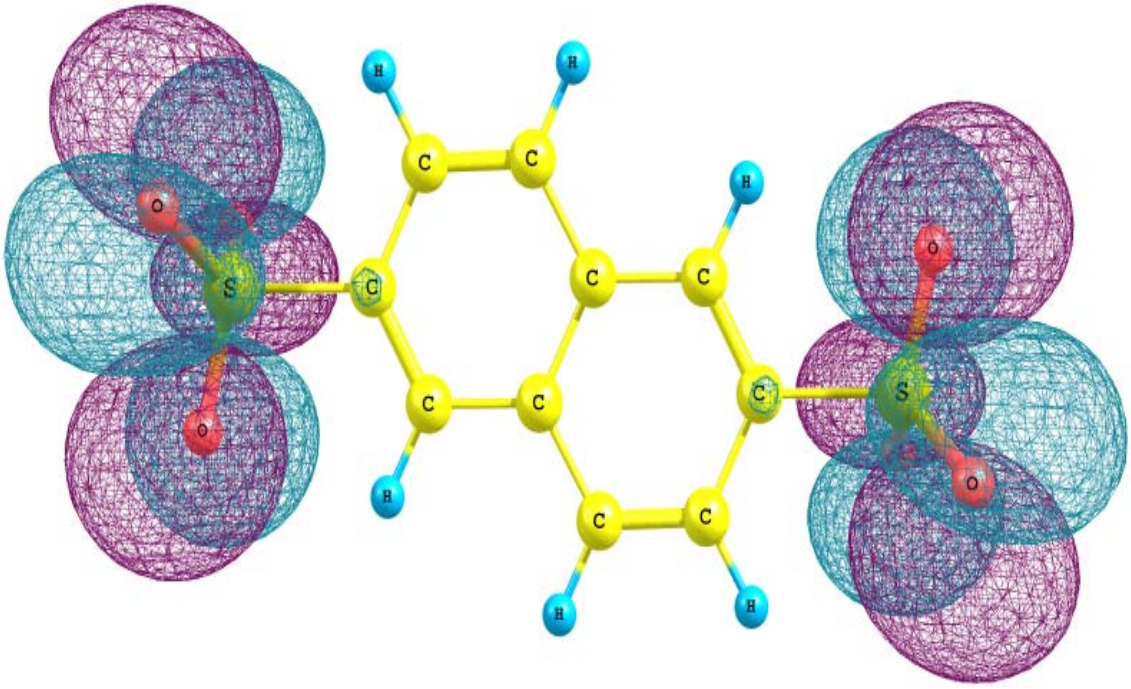

Figure 6.20 Highest occupied molecular orbital visualization for 2,6-naphthalenedisulfonic dianion using Density Functional theory (B3LYP) and 6-311++G** basis set.

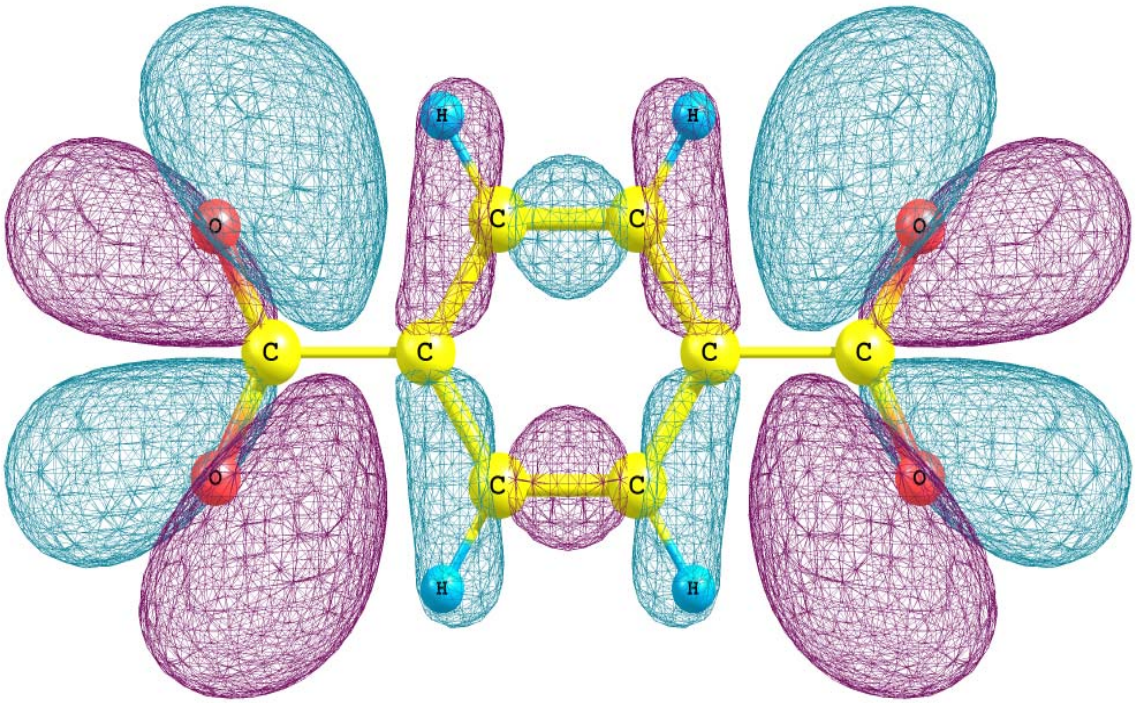

Figure 6.21 Highest occupied molecular orbital visualization for terephtahlic dianion using Density Functional theory (B3LYP) and 6-311++G** basis set.

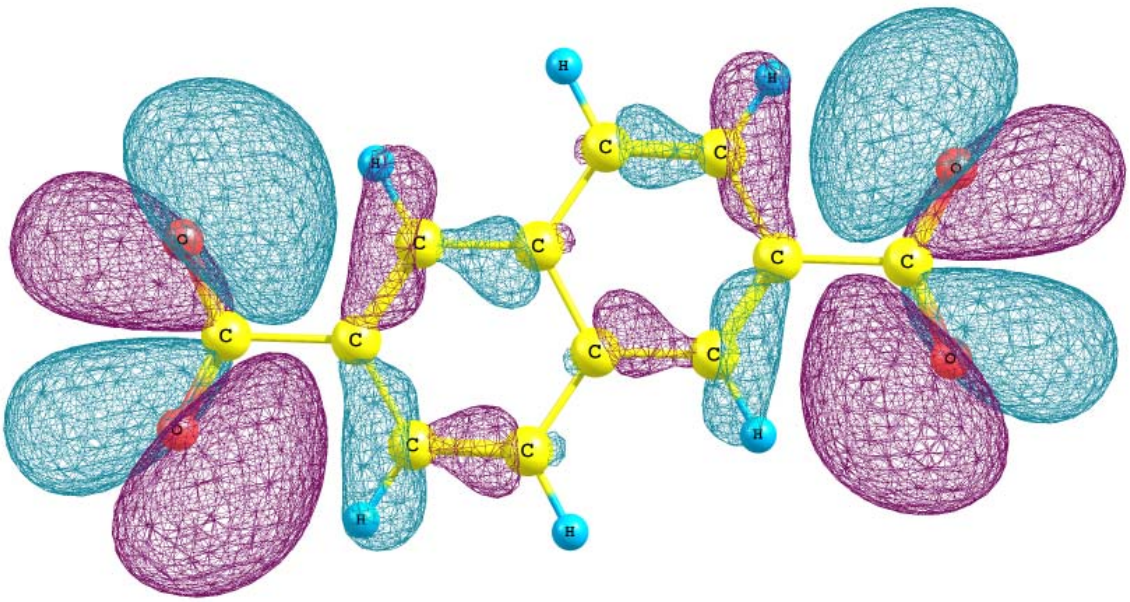

Figure 6.22 Highest occupied molecular orbital visualization for 2,6-naphthalenedicarboxylate dianion using Density Functional theory (B3LYP) and 6-311++G** basis set.

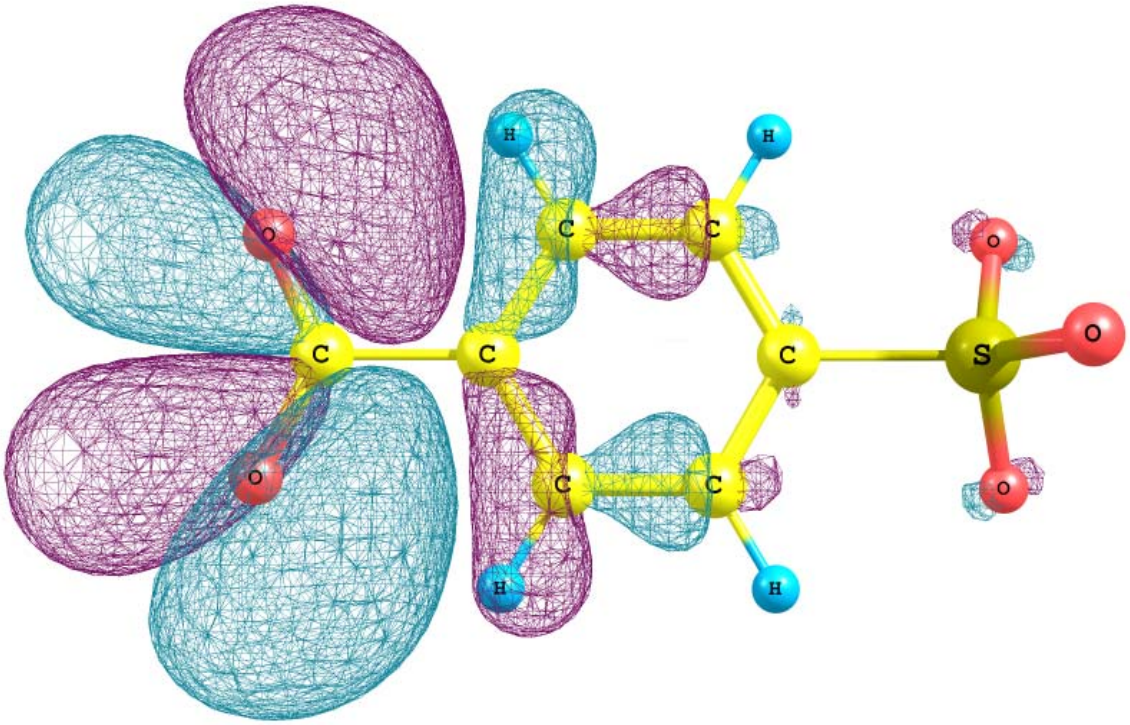

Figure 6.23 Highest occupied molecular orbital visualization for 4-sulfobenzoic dianion using Density Functional theory (B3LYP) and 6-311++G** basis set.

for the disulfonic dianions the two electrons are mainly reside on the SO_3 moieties. For the 4-sulfobenzoic dianion the two electrons are found mostly on the CO_2 moiety as well as the benzyne ring as shown in Figure 6.23. Using these calculations one can notice that for dicarboxylate and 4-sulfobenzoic dianions, the two electrons are partially localized on the benzyne ring allowing for the formation of the *p*-benzyne anion while for disulfonic dianions there is very little electron distribution on the benzyne ring.

For the dicarboxylate dianions, there are no clear thresholds for the ionic fragmentation and therefore no information is available regarding the Coulomb barrier heights for these dianions. Also, it should be mentioned that if loss of CO_2 neutral is the lowest pathway for the dicarboxylate dianions dissociation, there is no barrier for the dissociation. On the other hand, for the disulfonic dianions, it is possible to extrapolate the Coulomb barrier heights toward ionic fragmentation. As stated in Chapter III, the collision-induced dissociation threshold energy (inner repulsive Coulomb barrier) is sum of the outer repulsive Coulomb barrier and the adiabatic energy required to dissociate the dianion into two singly charged ions. Table 6.2 shows the resulting inner and outer repulsive Coulomb barriers for two disulfonic dianions as well as their dissociation energies. In this table, the inner RCBs are the measured threshold energy in the CID experiment and the dissociation energies are computed values using Density Functional theory. The outer RCBs are determined as the difference between the inner RCBs and the dissociation energies. As presented in Table 6.2, the calculated dissociation energy for 1,2-disulfonate dianion is a negative value meaning that this dianion is unstable toward ionic fragmentation, however, as shown in the CID experiment, this dianion appears to be

Table 6.2 Inner and outer repulsive Coulomb barriers (RCB) and dissociation energies for 1,2-disulfonate and 2,6-naphthalenedisulfonic dianions are presented. In this table, the inner RCBs are the measured threshold energy in the CID experiment. The dissociation energies are computed using Density Functional theory. The outer RCBs are determined as the difference between the inner RCBs and the dissociation energies. All values are in eV.

	1,2- disulfonate dianion	2,6-naphthalenedisulfonic dianion
Inner repulsive Coulomb barrier (CID threshold energy)	2.32	3.48
Calculated dissociation energy	-0.25	1.43
Outer repulsive Coulomb barrier	2.57	2.06

stable. This is an evidence of the existence of the repulsive Coulomb barrier and how this barrier can render an unstable dianion to be long-lived toward dissociation. For 2,6-naphthalenedisulfonic, the repulsive Coulomb barrier increases the stability of the dianion. The outer repulsive Coulomb barriers for dissociation of 1,2-disulfonate and 2,6-naphthalenedisulfonic dianion are ~ 2.57eV and 2.06 eV, respectively as shown in Table 6.2. If we assume that the outer repulsive Coulomb barrier is the repulsive Coulomb potential between two charges, then the above results are expected. The distance between two charges in 1, 2-disulfonate dianion is smaller than the distance between two charges in 2, 6-naphthalenedisulfonic dianion and as a result the outer repulsive Coulomb barrier for 1, 2-disulfonate (2.57 eV) is larger than the outer repulsive Coulomb barrier for 2,6-naphthalenedisulfonic dianion (2.6eV).

Finally, we need to examine the apparent metastability of the dicarboxylate dianions in this study. According to the experimental evidence terephthalic and 2,6-naphthalenedicarboxylic dianions appear to be metastable. In order to investigate the stability of a dianion, one has to study an internally (i.e., vibrationally) cold dianion. For instance, if the terephthalic dianions produced in this study are vibrationally hot, then the vibrational excitation can lead to cleavage of its chemical bond, i.e., assuming loss of neutral CO_2. To investigate the influence of the internal energy on the stability of the dianions, Dr Steen B. Nielsen from University of Aarhus, Denmark, attempted to measure lifetimes of terephthalic and 2,6-naphthalenedicarboxylic dianions. Lifetime measurements carried out using an Electrostatic Ion Storage Ring (ELISA).[119] In this experimental setup dianions are produced with an electrospray ionization source and then transported to an ion trap filled with helium buffer gas for nearly 0.1 second for

accumulation and cooling. The ions are then accelerated to 22 kV and mass-to-charge selected by a bending magnet. Finally, the ions are injected into the storage ring. Metastable decay as well as collisions with residual background gas leds to the production of neutral fragments, which are counted by a micro-channel plate detector if formed in the injection side of the ring. Dr. Nielsen measured the lifetime of 2,6-napthalenedicarboxylate dianion to be about 1.5 second (Figure 6. 24). The 1.5 second decay time is attributed to collisional dissociation with the very low pressure background gas (10^{-10} torr) in the ELISA apparatus. Thus this ion is essentially stable under the conditions of their experiment. Dr. Nielsen was not successful in measuring the lifetime for terephthalic dianion. Lifetime of the terephthalic dianion was very short to make it to the storage ring. It takes about 100 microseconds for the dianion to travel from the source to the storage ring. It shows that although the terephthalic dianions were collisionally cooled with helium gas, their lifetimes were still shorter than 100 microseconds. This could indicate that terephthalic dianions are actually metastable as shown in our experiment. A comparison between the CID experiment and the lifetime measurements indicates that the produced dicarboxylate dianions are vibrationally hot in the ESI source. An ideal experiment to verify stability of the ground state of these dianions would be cooling the dianions by a background gas before introducing them to the collision cell in the CID experiment.

Conclusion

In this study collision-induced dissociation was employed to study the dissociation pathways for dicarboxylate and disulfonic dianions. For disulfonic dianions a single

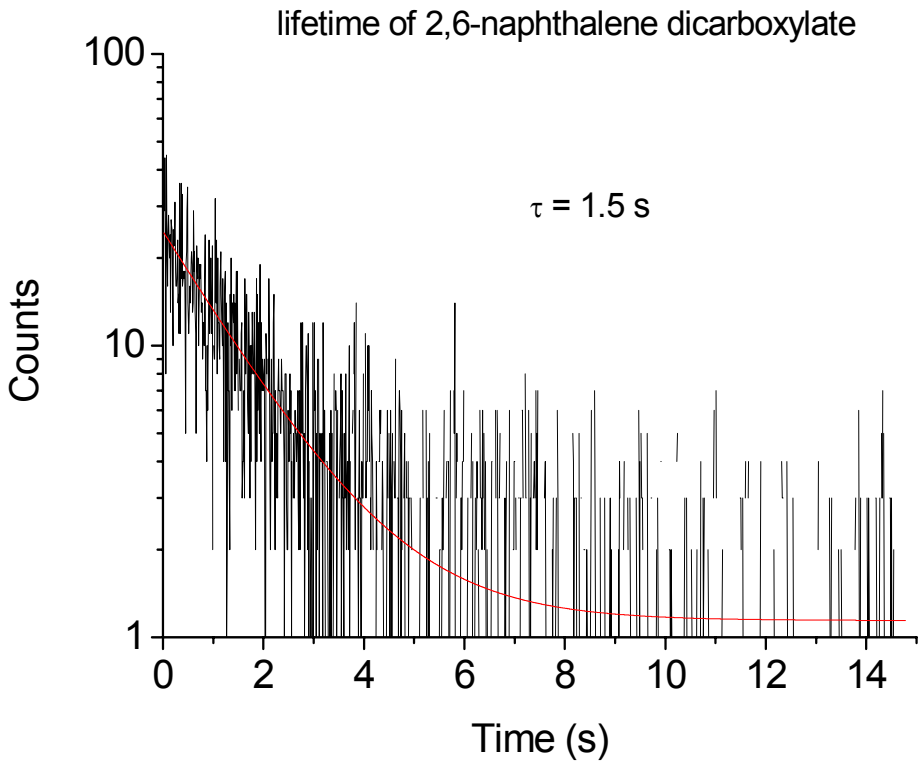

Figure 6.24 Lifetime spectrum of 2,6-naphthalenedicarbxylate dianion measured by Dr. Steen B. Nielsen from University of Aarhus, Denmark employing ELISA experiment.

dissociation pathway, loss of SO_3^- was observed. The inner and outer repulsive Coulomb barriers of disulfonic dianions toward ionic fragmentation were estimated. Our calculations predicted the heights and shapes of the repulsive Coulomb barrier of the ionic dissociation for these dianions.

The dissociation decay for the dicarboxylate dianions is believed to be through loss of neutral CO_2 and an electron . This is a very interesting result since the stability of dianions is generally observed to occur through electron detachment and/or ionic fragmentation. More experiments in order to find other similar dianions, which decay through neutral species, are encouraged.

Although our purpose was to obtain a correlation between the stability and charge delocalization on dicarboxylate dianions, the loss of neutral decay channel and metastability of the dianions in our experiment did not allow us to fulfill this purpose. We hope our experimental and theoretical results will encourage more studies on the dicarboxylate dianions and their stabilities.

CHAPTER VII

Ionic and Vibrational Properties of an Ultra-Low Ionization Potential Molecule, Tetrakis(dimethylamino)ethylene

Introduction

The ionization potential (IP) of most organic compounds lie in the range from 7 to 15 eV. However, a photoionization study indicated that the organic molecule, tetrakis(dimethylamino)ethylene ($C_{10}H_{24}N_4$, TDAE), has a very low ionization potential, i.e., IP $\leq 5.36 \pm 0.02$.[120] Such a low IP, which is comparable to that of the lithium alkali atom (5.39 eV), has attracted a great deal of interest over the past decade. Since TDAE readily gives up an electron, it has found many applications in various applied and research areas such as plasma technology, semi-conductivity, and electrospray mass spectroscopy.

In many areas of plasma research, a central focus is on the study of high-density, low temperature plasmas (about $10^{11\text{-}13}$ cm^{-3}) at atmospheric pressure. Many applications of these plasmas have been proposed. For instance, plasma sheaths have been considered to reduce drag on supersonic vehicles and to modify the radar cross-section of an aircraft by forming a microwave absorbing or reflecting medium.[121-123] The main difficulty of producing these plasmas is a requirement of high power budget in order to initiate and sustain an air-plasma discharge. The high power budget can be reduced to some extent by the choice of seed gas. For the first time, Woodworth et al.[124] proposed the generation of a plasma using low ionization potential organic molecules and employing ultraviolet lasers as the means of ionization. One of the attractive organic molecules in which to generate such a plasma is TDAE. For example, the Scharer group[125,126] produced plasmas

with densities of about 10^{13} cm^{-3} in TDAE vapor using 193 nm laser photoionization. They also examined the conditions required to sustain the high-pressure plasma produced from TDAE, as well as other methods to extend the plasma's lifetime.

TDAE has found very important applications in particle physics and medical imaging. An alternative to expensive photomultiplier tubes in the detection of ultraviolet (UV) photons is to employ photosensitive gases.[127,128] Detectors based on photosensitive gases can be employed to detect UV photons over large areas with a reasonable cost. In designing a detector based on these photosensitive gases, the absorption length and absolute quantum efficiency are two important parameters. TDAE with its high vapour pressure (55 Torr at 20^{o}C), large quantum efficiency, and broad spectrum of sensitivity has proved to be an ideal gas for the detection of ultraviolet photons.[129] Another interest in TDAE arises from its ferromagnetic properties when it is doped into fullerene crystals, i.e. TDAE-C_{60}. In 1991, Allemand et al.[130] for the first time realized that TDAE-C_{60} is a ferromagnetic material with a Curie transition temperature of 16 K. Later, Tanaka et al.[131], reported three magnetic phases for TDAE-C_{60} with Curie transition temperature of 25, 16, and 10 K.

TDAE is also making an impact on the emerging field of multiply-charged anions. One of the challenges in the research area of multiply-charged anions (MCA) is the production of multiply-charged anions in the gas-phase. The development of the electrospray ionization source has revolutionized the process of producing MCAs. However for some species such as fullerenes, generating doubly charged anions still remains a difficult task. Interestingly, applying TDAE as a strong electron donor to fullerene solution before spraying the solution into electrospray ionization source

generally assists in the production of doubly-charged anions of fullerenes. In this context, Hampe et al.[132] produced doubly charged of C_n^{2-} where n= 74 and 78…124 upon adding 2 mol of TDAE to the fullerene solution. The $C_{60}F_{34}^{2-}$ and $C_{60}F_{46}^{2-}$ ion signals were also greatly enhanced using TDAE as an electron donor.[133]

Historically, in 1950, Pruett et al.[134] were the first to synthesize tetrakis(dimethylamino)ethylene ($C_{10}H_{24}N_4$, TDAE). In these studies, they also observed the emission of green chemiluminescence when this organic compound was in contact with air. TDAE is a pale green liquid, which forms a white solid upon contact with oxygen. This observation was an unexpected behavior for such ethylene type derivatives. Later this was explained by noting that since TDAE is an exceptionally electron rich alkene it could be oxidized very easily. This property of TDAE can be effectively used in the detection of oxygen. In addition to the synthesis method used by Pruett et al.[134] a few other alternate methods have been successful in the preparation of TDAE.[135,136]

The reactivity of an organic compound with at least one carbon-carbon double bond is strongly influenced by the substituents attached to the carbons. If the substituents withdraw the electrons from the carbon-carbon double bond, then the organic compound is an electron acceptor. However, if the substituents attached to the carbon atoms are electron-donating substituents, this compound can be an electron donor. TDAE is an example of a strong electron donor in many reactions. In TDAE, the two central ethylenic carbon atoms are attached to four amino groups. Wiberg[137] also attributed the readiness of TDAE to give up electrons to the presence of the four amino groups. In this review, the amino groups were determined to stabilize the positive ions of TDAE by partially

transferring their free electron pairs to the central carbon atoms (C=C). The chemical properties of TDAE have been discussed extensively in Wiberg's review article.

The first gas-phase IP of TDAE was reported in 1971 by Nakato et al.[120] They obtained an adiabatic IP of $\leq 5.36 \pm 0.02$ eV and a vertical IP of 6.11 ± 0.02 eV for TDAE using a photoionization method. The ionization potentials were estimated by measuring the photoelectron current as a function of photon energy. The accurate measurement of the adiabatic ionization potential was difficult since the onset of ionization was rather gradual. In addition the sample was held at room temperature making possible "hot band" effects in the ionization threshold. A photoionization experiment performed by Cetinkaya et al.[138] reported the vertical IP of TDAE to be 5.95 eV.

There are also a few theoretical studies of adiabatic and vertical ionization potentials of TDAE. A study by Martin et al.[139] reported values of 4.95eV and 5.62eV for the adiabatic and vertical IPs, respectively. Martin et al., employed the density functional theory and cc-pVDZ basis set to compute these values. Pederson and Laouini also reported two calculated values for vertical IP. They obtained the vertical IP of 5.88 eV including spin polarization effects and value of 5.80eV with spin unpolarized.[140] Pederson and Laouini also calculated the highest occupied molecular orbital (HOMO) of the TDAE in order to identify its donor electron. It turns out that the donor electron mostly is delocalized over the C═C bond and the neighboring four N atoms, i.e. interior part of the molecule. They also concluded that the TDAE molecule donors an electron without great changes in its molecular geometry.

Although there have been exclusive studies describing the properties of TDAE as that of an electron donor, its molecular confirmation is not very well known. Gas-phase

electron diffraction studies[141] show that TDAE is composed of four identical $N(CH_3)_2$ groups attached to the C=C double bond. The repulsion between the four amino groups in TDAE prevents a planar structure for TDAE, and makes its structure non-planar. A Raman spectrum showed[142] a very intense band in the C=C region (1630 cm^{-1}) whereas this mode exhibits no infrared absorption[143]. This mutual exclusion showed that the TDAE is symmetric about the C=C region, but it gives no information about the arrangement of the dimethylamino groups. A study by Wiberg[137] showed that since the energy barrier for rotation of the dimethylamino groups about the C-N bond is very small they can rapidly rotate about the C-N bond. Due to this rotation TDAE exists as super position of all interconnectible isomers. A study by Bock et al.[141] employing gas-phase electron refraction revealed some structural information on TDAE. They determined the two molecular halves $[N_2(CH_3)_2]$ on both sides of the C=C axis are twisted relative to each other by 28^o. The bond distances were reported to be C=C 1.36 Å, C-N 1.403 Å, and $N\text{-}CH_3$ 1.453 Å.

In the present work, the results of measurements on the adiabatic ionization potential of TDAE employing two different techniques, electron impact and photoionization methods will be reported. Mass spectra of the TDAE molecule also will be presented employing a linear time-of-flight mass spectrometer. We have determined the geometry of TDAE and its positive ion using Density Functional theory. In addition, measurements of TDAE's Raman vibrational frequencies will be compared with the results from many theoretical calculations.

Electron Impact Experiment

Nearly a century of research in mass spectrometry has demonstrated that time-of-flight mass spectrometry (TOFMS) is a powerful probe into the structure and composition of molecules. Historically, electron impact was first employed as a source of ionization. Although TOFMS can be also coupled with a number of sources such as electrospray ionization source (ESI) and matrix assisted laser desorption (MALDI) electron impact ionization (EI) continues to provide the most useful technique in investigating structural information for atoms and molecules such as electron affinities, ionization potentials, bond dissociation energies, etc. In this work, a linear time-of-flight mass spectrometer was employed to record the mass spectra and ionization potential of TDAE. A schematic drawing of the linear TOFMS used in this study is shown in Figure 7.1. The linear time of flight was constructed in our laboratory as partial fulfillment of the Master of Science degree by Wesley D. Robertson.[144] In this apparatus, electron impact ionization is used as the source of ionization. The electrons are generated by one or both of the two electron guns, a low-resolution standard electron gun or high-resolution trochoidal electron monochromator. In the standard electron gun, electrons are produced by thermionic emission from a 5 mil. tungsten wire, heated by passing an electrical current (~ 4 amps) through the filament. This gun can generate low-and high-energy electron beams and can produce a large amount of ion signal due to its large electron beam current, ~10^{-5}amps. Because the energy of the emitted electrons has a Maxwell-Boltzmann distribution, the energy resolution of the standard electron gun is usually poor (~ 0.5 eV). A main contributor to the energy spread is due to the voltage drop across the filament. In the TOFMS, this gun is mostly used in order to produce significant ion

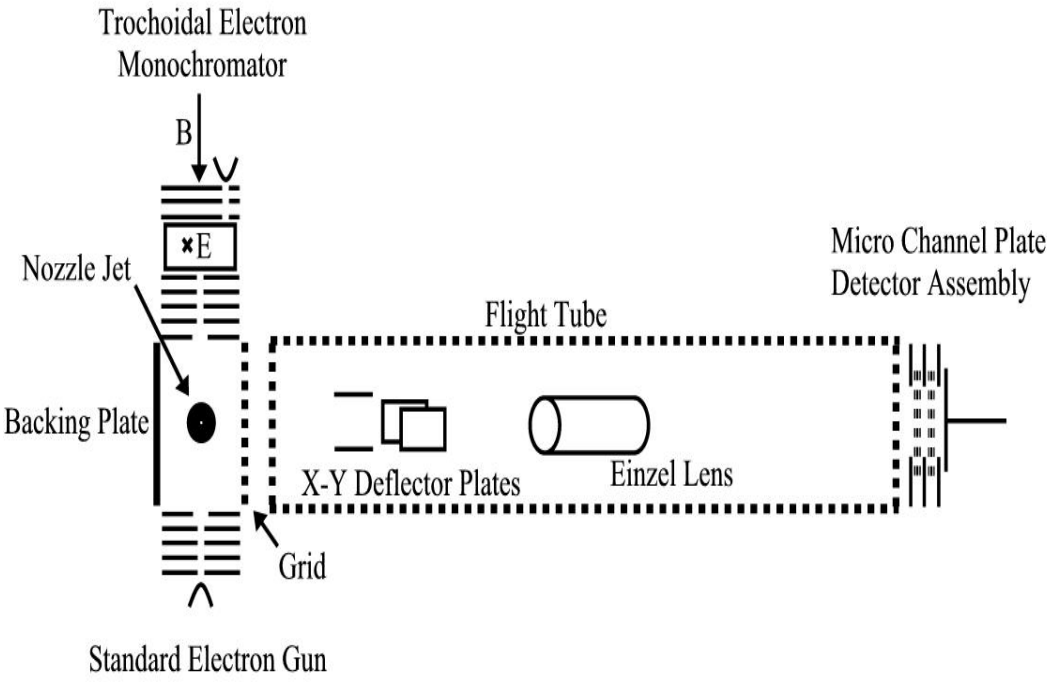

Figure7.1 A schematic diagram of the linear electron impact time-of-flight mass spectrometer. The low-resolution standard electron gun and high-resolution trochoidal electron monochromator are located on opposite sides of the ionization region. In the drift region, a set of x-y deflectors and a cylindrical Einzel lens are used to focus the ions beam.[144]

signal in order to record the weaker intensity peaks. However, in many electron impact studies, a narrowly-defined energy distribution is desirable. In this apparatus, a trochoidal electron monochromator (TEM)[145] is used to generate high-resolution electron beams. In the TEM, crossed magnetic and electric field ($\vec{E}\times\vec{B}$) are used to move electrons in a spatial path perpendicular to the electric and magnetic field so that a narrow energy distribution can be selected. A typical TEM produces a tunable monoenergetic electron beam with intensities on the order of nanoamperes and an electron energy resolution of 0.1 to 0.02 eV. The resolution is determined by the electron energy in the $\vec{E}\times\vec{B}$ region as the defining aperture dimensions.

In our TOFMS, molecules are introduced into the interaction region via a seeded nozzle jet that provides a rotationally, vibrationally, and translationally cooled molecular beam. This molecular beam is crossed perpendicularly with the beam of energy-selected electrons in the interaction region. The electrons are produced by one of the electron guns discussed above depending on the required energy resolution and intensity of the electron beam in the study. The molecules that do not interact with the electron beam are pumped out of the chamber. A 550 liter per second turbomolecular pump (Varian 550) is located directly below the nozzle jet in order to help keep the pressure of the entire chamber below 10^{-6} Torr during operation. The base pressure of the TOFMS is ~ 10^{-9} Torr. As shown in Figure 7.1, in the drift region, a set of x-y deflectors and a cylindrical Einzel lens are used to focus the ion beam. In this equipment, so-called Wiley-McLaren space-focusing is used to increase the time-of-flight mass resolution of the ion beam. Wiley and McLaren[146] observed that ion beams with the same m/q ratio would arrive at the detector

with a spread in times due to the fact ions are created at different positions in the ion source. As a result of their different positions, two identical ions would fall through different potentials and gain different velocities. Consequently, the time-of-arrival of the same mass-to-charge ions to the detector would spread resulting in peak broadening in the TOFMS. Wiley and McLaren attempted to correct for this time spread in order to improve the mass resolution. According to their derived equation[146], adding an extra grid between the grounded grid (backing plate) and the voltage applied to the flight tube as shown in Figure 7.1 can be employed to improve the mass resolution. Ions initially created further from the detector will receive more energy from the field and therefore will "catch up" with ions created closer to the detector. While adjusting the grid voltage and/or flight tube voltage manually, the peak width becomes narrower (higher mass resolution, $m/\Delta m$ increases).

The detector used with this TOFMS is an assembly of two micro-channel plates coupled together. When ions hit the front surface of the first channel-plate, it produces a shower of electrons that are accelerated into the second channel-plate and these electrons are further amplified by the second channel-plate. After passage through two channel-plates, enough electrons are produced that it is possible to detect a voltage pulse. A Hewlett-Packard digital oscilloscope (Infinium 500MHz) is used to view the time-of-flight spectrum. Grams™ software is used to convert the time scale to the mass scale spectrum using known mass peaks for the calibration. In order to record a mass signal versus electron energy, a mass peak is selected and averaged by using a Stanford Research Systems box integrator (SR 250). A Labview™ computer program is also used to collect the data from the Boxcar Integrator in order to plot the intensity of a chosen

peak versus electron energy. In the Labview program, the user can set the initial and final electron energies, increment size between the energies, and the time between iterations. The program first sets the initial electron energy and reads the area under the selected peak. Then the Lab view program waits a specific time (iteration time) and increases the electron energy by the selected increment size. This process continues until the program reaches the final selected electron energy. At the end of the run, the data can be saved to a text file. The text file can then be opened by the Excel workbook and a graph of the intensity of the selected peak versus the electron energy can be plotted. This procedure is used to determine the ionization potential of a sample molecule or the appearance potential of fragment ions.

Mass resolution of the TOFMS in our study is $\frac{m}{\Delta m} \equiv \frac{t}{2\Delta t} \approx 750$ (mass of a peak divided by its width) which is sufficient for the purpose of this study.

Mass spectra of the TDAE ions were obtained using the standard electron gun (10^{-5} amps) in order to produce sufficient ion signals. The trochoidal electron monochromator (10^{-9} amps) was used to record the ionization potential (IP) of the parent ion. The resolution of the TEM was set to approximately 0.1 eV. Argon gas (IP= 15.75 eV) was used to calibrate the electron energy scale.

Photoionization Experiment

Photoionization results were carried out in the laboratory of Dr. Dong-Sheng Yang at the University of Kentucky. The experimental setup has been described in a previous publication.[147] It consists of two vacuum chambers. The first chamber contains a

supersonic molecular beam source, and the second chamber houses a homemade, two-field, time-of-flight spectrometer. TDAE was vaporized at room temperature. The vapor of the compound was seeded in ultra high purity He or Ar gas (Scott-Gross) at 50 psi. The mixture of the inert gas and organic vapor was then supersonically expanded to the vacuum through a general valve (series 9) or a homemade piezoelectric valve[148] operated in a 10 Hz pulsed mode. Mass spectra were obtained by photoionization time-of-flight mass spectrometry, and photoionization efficiency spectra were obtained by recording the mass-selected ion signal as a function of the laser wavelength. Ionization was carried out by a frequency- doubled dye laser (Lumonics HD-500), pumped by the second (532 nm) or third (355 nm) harmonic output of a Nd:YAG laser (Quanta-Ray GCR-3). The ion signal was detected by a dual micro-channel-plate detector (Galileo), amplified by a preamplifier (Stanford Research System SR445), averaged by a gated integrator (Stanford Research System SR250), and recorded in a laboratory computer.

Raman Experiment

The Raman spectrum was recorded with a Dilor XY-800 confocal micro-Raman spectrometer. Laser excitation was obtained using a 100mW Lexel, Inc, 3500 argon ion laser (514.5Å). Due to the air sensitivity of TDAE, the sample was placed in a sealed glass tube. The data were recorded at room temperature (20°C). The laser light was focused on the sealed sample through a 80 × objective of the microscope.

Computational Methods

Geometry optimizations of neutral and positively charged TDAE ($C_{10}H_{24}N_4$) were carried out employing Density Functional Theory (B3LYP) and two basis sets; 6-311++G**, and 6-311+G(d,p).

Vibrational frequencies of TDAE and its singly charged positive ion were also computed for several reasons. First to confirm that the optimized geometry is a stable structure, i.e. a stable structure should have no negative/imaginary frequencies. Second, to obtain the zero-point energy in order to calculate the adiabatic ionization potential of TDAE. Further, the calculated vibrational frequencies will be compared to the experimental Raman spectrum.

Computational Results

Computed molecular structures and bond lengths of neutral TDAE and singly charged positive ion of TDAE are presented in Figures 7.2 and 7.3. The TDAE structure was found to be a non-planar structure with D_2 symmetry. As shown in Figure 7.2, the distances between C=C, C-N, and N-CH_3 were found to be 1.37 Å, 1.41Å, and 1.45Å, respectively, for the neutral TDAE. The distances found from the calculation are in a good agreement with the data presented from gas-phase electron diffraction.[141] For the singly charged TDAE, distances between C=C, C-N, and N-CH_3 are 1.43 Å, 1.37Å, and 1.46Å. These numbers indicate that the structure of the charged TDAE changes slightly from its neutral geometry. The C=C bond increases slightly upon ionization whereas the C-N bond decreases. The N-CH_3 bond remains fairly unchanged. One will also note that aside from the bond length change, the geometry appears to be unaltered upon ionization.

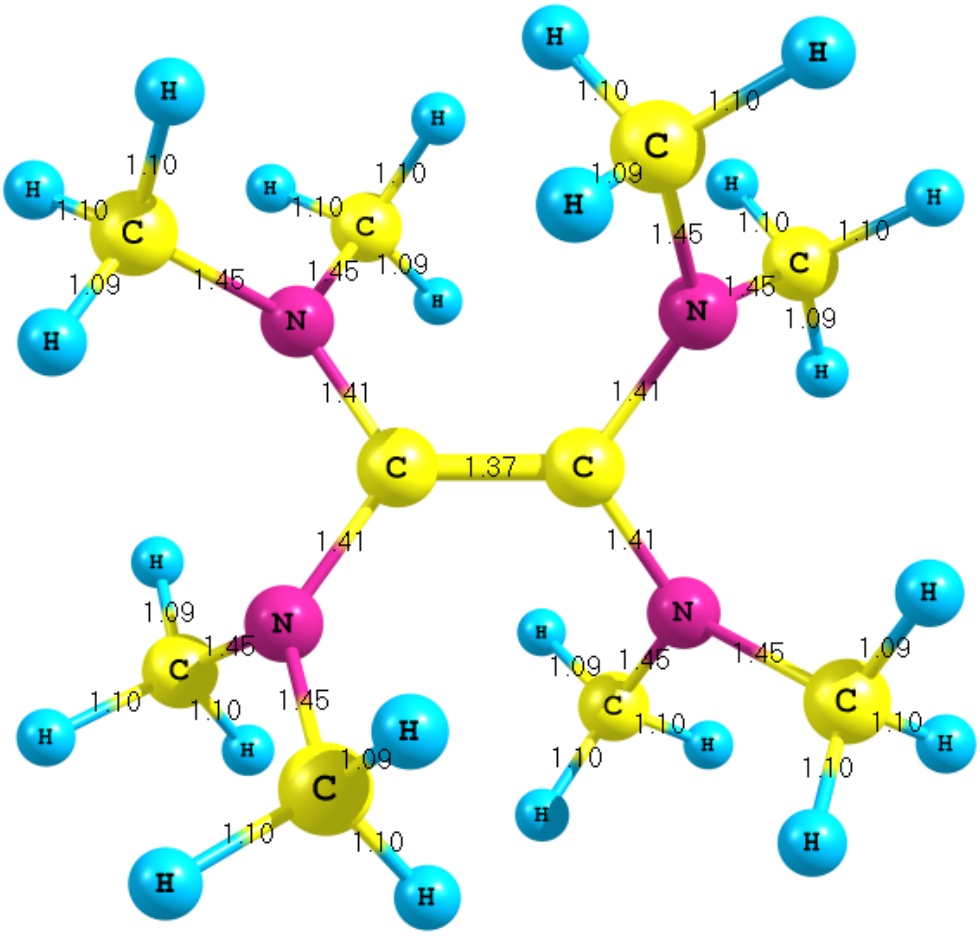

Figure 7. 2 The computed D_2 symmetry structure and bond lengths of neutral TDAE. All bond lengths are in angstroms.

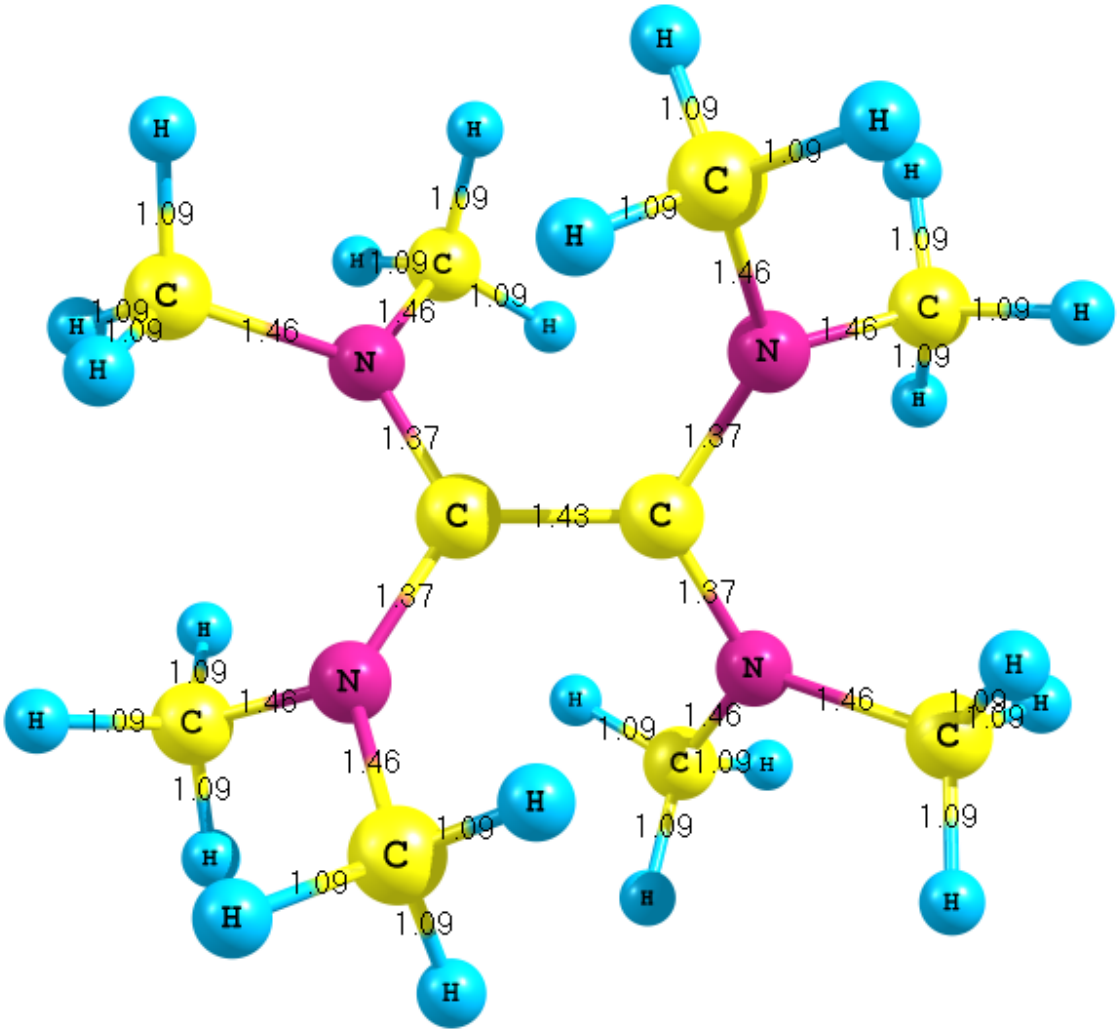

Figure 7. 3 The computed structure and bond lengths of singly charged positive ion of TDAE. All bond lengths are in angstroms.

Calculated and experimental vertical and adiabatic ionization potentials of TDAE are shown in Tables 7.1 and 7.2, respectively. Calculation of the adiabatic and (vertical) ionization potential using B3LYP method and 6-311++G**, and 6-311+G(d,p) basis sets gave adiabatic IPs of 5.15 eV (5.83 eV) and 5.16 eV (5.72 eV), respectively. The difference between the adiabatic and vertical ionization potential is on the order of ~ 0.6 eV which is another indication of some structural change of TDAE upon ionization.

Computed vibrational frequencies and their Raman and IR intensities are listed in Table 7.3 for the neutral, and in Table 7.4 for the singly charged positive ion of TDAE. Since for both basis sets the calculated frequencies are in a close agreement, only the results from one basis set (6-311++G**) are presented. The values of calculated frequencies are usually higher than the observed frequencies. Depending upon the method used for the computation, an empirical scaling factor is used to match up the computed frequencies with observed frequencies. In our calculation, the frequencies are scaled by 0.98 for comparison with the experimental frequencies.[149]

According to the calculation, there is a very intense vibrational feature in the neutral TDAE that is attributed to the symmetric stretching mode of the central C_1= C_2 (1622 cm^{-1}). This mode is Raman active and shows almost no IR activity. The 1622 cm^{-1} mode is also very well separated from the other modes, making it easy to be found experimentally. Calculation of the vibrational frequencies of the positive ion shows that C=C mode shifts to 1544 cm^{-1} upon ionization of TDAE. This is a further evidence of a weakening C=C bond and increasing the bond length as stated above.

Table 7.1 Computed values for adiabatic (IP_a), and vertical (IP_v) ionization potentials of TDAE. All values are in eV.

Computational Method	IP_a (eV)	IP_v (eV)	Reference
B3LYP/6-311++G**	5.15	5.83	This work
B3LYP/6-311+G(d,p)	5.16	5.72	This work
B3LYP/4-21G	4.65	5.28	139
B3LYP/cc-pVDZ	4.95	5.62	139
Density functional (spin unpolarized)	----------	5.80	140
Density functional (spin polarized)	----------	5.88	140

Table 7.2 Experimental values for adiabatic (IP_a), and vertical (IP_v) ionization potentials of TDAE. All values are in eV.

Experimental Method	IP_a (eV)	IP_v (eV)	Reference
Electron impact	5.3 ± 0.2 eV	----------	This work
Photoionization	5.20 ± 0.05	----------	This work
Photoionization	$\leq 5.36 \pm 0.02$	6.11	120
Photoionization	----------	5.95	138

Table 7.3 Computed scaled vibrational frequencies (multiply by 0.98) and Raman (IR) intensities for TDAE using B3LYP/6-311++G**. Frequencies are in cm^{-1}. Raman activities are in $Å^4$/amu. IR activities are in km/mol. The intense C=C stretch mode is highlighted.

Mode ν_n	Frequency	Raman (IR) Activity	Mode ν_n	Frequency	Raman (IR) Activity	Mode ν_n	Frequency	Raman (IR) Activity
1	65.8	1.0 (2.3)	37	1032.6	0.8 (199.6)	73	1456.2	5.7 (2.2)
2	66.4	0.6 (0.0)	38	1047.5	4.3 (2.6)	74	1462.1	0.6 (15.0)
3	76.7	0.3 (0.0)	39	1047.8	7.0 (8.0)	75	1465.8	5.7 (5.0)
4	80.8	0.1(0.6)	40	1050.2	4.8 (5.0)	76	1467.6	0.9 (19.2)
5	102.0	3.3 (0.6)	41	1050.4	2.7 (10.1)	77	1467.8	4.4 (0.9)
6	125.1	0.4 (2.5)	42	1081.6	0.6 (191.4)	78	1476.9	2.5 (13.1)
7	126.2	2.4 (0.1)	43	1091.3	0.6 (0.4)	79	1477.5	2.8 (10.3)
8	131.3	1.2 (1.3)	44	1093.7	0.8 (23.9)	80	1485.3	20.2 (0.6)
9	162.1	0.1 (3.2)	45	1095.3	1.2 (1.9)	81	1487.8	0.0 (27.3)
10	174.9	0.8 (1.1)	46	1097.3	6.6 (6.1)	82	1495.9	8.3 (28.8)
11	177.0	1.8 (0.1)	47	1119.2	9.7 (0.0)	83	1498.0	34.3 (6.2)
12	185.8	0.9 (0.6)	48	1134.5	0.2 (9.8)	84	1622.0	347.5 (1.5)
13	188.4	1.5 (0.5)	49	1136.3	10.2 (3.0)	85	2849.7	210.8 (102.5)
14	204.9	1.5 (0.0)	50	1138.9	0.6 (17.6)	86	2851.1	279.0 (167.0)
15	217.9	0.1 (2.2)	51	1142.1	2.8 (3.2)	87	2872.4	133.2 (107.2)
16	230.9	0.3 (2.5)	52	1213.3	0.9 (11.5)	88	2873.8	180.5 (120.8)
17	237.0	0.7 (0.0)	53	1219.3	3.0 (0.0)	89	2879.1	5.2 (281.4)
18	243.7	1.0 (1.7)	54	1226.7	8.5 (46.4)	90	2880.0	491.7 (5.1)
19	261.2	3.9 (3.0)	55	1235.0	0.2 (60.8)	91	2907.8	6.4 (185.3)
20	296.9	0.7 (9.6)	56	1288.5	1.3 (0.5)	92	2909.1	284.3 (1.2)
21	313.2	7.8 (0.0)	57	1315.4	1.3 (109.5)	93	2954.8	17.7 (110.9)
22	323.9	4.7 (2.1)	58	1330.6	0.5 (184.1)	94	2955.0	204.3 (6.7)
23	337.9	0.8 (13.8)	59	1340.0	14.9 (18.9)	95	2964.0	36.2 (102.1)
24	354.7	0.6 (1.6)	60	1407.1	6.3 (0.2)	96	2964.2	291.4 (18.6)
25	358.2	0.5 (0.7)	61	1408.1	9.0 (1.0)	97	2968.6	96.0 (66.2)
26	411.8	4.3 (0.6)	62	1410.4	7.3 (1.0)	98	2968.8	262.4 (50.2)
27	419.4	1.5 (1.5)	63	1411.7	5.5 (2.2)	99	2978.8	40.2 (100.6)
28	512.3	1.7 (3.3)	64	1430.6	0.4 (1.0)	100	2979.1	228.8 (4.1)
29	535.0	1.3 (1.0)	65	1431.2	19.6 (6.6)	101	3037.0	43.1 (26.7)
30	594.7	5.5 (6.1)	66	1435.6	4.0 (8.9)	102	3037.3	39.3 (15.0)
31	630.9	2.5 (13.4)	67	1437.2	7.3 (5.6)	103	3053.3	51.4 (5.4)
32	703.4	2.2 (0.9)	68	1445.7	15.4 (0.3)	104	3053.4	24.9 (27.7)
33	840.5	1.8 (4.3)	69	1446.7	18.9 (14.0)	105	3055.3	17.6 (12.3)
34	863.5	9.6 (14.0)	70	1448.1	2.8 (2.6)	106	3055.3	77.3 (27.8)
35	915.8	4.8 (3.0)	71	1448.6	9.7 (0.0)	107	3062.5	21.1 (2.0)
36	981.5	25.6 (4.3)	72	1454.0	1.3 (11.9)	108	3062.8	23.8 (26.7)

Table 7.4 Computed scaled vibrational frequencies (multiply by 0.98), and Raman (IR) intensities for singly charged positive ion of TDAE using B3LYP/6-311++G**. Frequencies are in cm^{-1}. Raman activities are in $Å^4$/amu. IR activities are in km/mol. The C=C stretch mode is highlighted.

Mode ν_n	Frequency	Raman (IR) Activity	Mode ν_n	Frequency	Raman (IR) Activity	Mode ν_n	Frequency	Raman (IR) Activity
1	64.9	1.2 (0.0)	37	1044.6	0.0 (17.5)	73	1460.2	6.1 (39.7)
2	74.5	0.7 (0.9)	38	1046.7	0.1 (2.2)	74	1462.5	0.9 (29.9)
3	87.9	0.0 (0.8)	39	1047.3	1.2 (12.2)	75	1467.8	42.3 (6.2)
4	117.5	0.2 (1.4)	40	1047.9	1.6 (0.0)	76	1474.9	0.4 (6.5)
5	123.7	0.3 (2.7)	41	1056.1	3.9 (141.8)	77	1475.6	0.0 (16.2)
6	133.5	4.6 (0.0)	42	1094.8	0.0 (12.6)	78	1480.8	59.5 (0.0)
7	142.9	1.7 (2.0)	43	1097.1	0.1 (0.6)	79	1482.3	5.7 (35.4)
8	146.2	0.3 (5.1)	44	1097.1	3.5 (0.0)	80	1486.4	121.8 (0.0)
9	152.5	1.9 (0.0)	45	1098.2	0.2 (0.2)	81	1505.6	3.5 (48.0)
10	172.8	1.8 (0.6)	46	1123.5	0.3 (73.5)	82	1525.1	0.1 (251.9)
11	180.6	1.3 (0.0)	47	1126.8	1.6 (1.3)	83	1535.3	5.1 (49.8)
12	184.0	0.1 (0.4)	48	1133.6	2.2 (0.0)	84	1544.4	59.1 (0.0)
13	187.8	0.2 (0.1)	49	1135.1	0.1 (2.1)	85	2957.7	15.4 (15.4)
14	190.8	0.2 (0.1)	50	1142.7	0.3 (57.5)	86	2957.7	13.9 (12.9)
15	198.8	2.8 (0.0)	51	1155.3	0.2 (2.6)	87	2958.4	60.6 (11.2)
16	219.1	1.0 (0.0)	52	1204.5	17.0 (0.0)	88	2958.7	87.7 (0.0)
17	245.6	0.1 (0.6)	53	1204.9	0.0 (11.7)	89	2960.9	74.6 (13.6)
18	247.6	0.1 (1.1)	54	1219.2	3.3 (31.3)	90	2961.5	64.4 (134.6)
19	262.4	2.2 (4.5)	55	1246.2	0.9 (67.5)	91	2962.4	0.1 (108.3)
20	284.3	0.0 (7.4)	56	1296.3	18.1 (0.0)	92	2964.8	1618.6 (0.0)
21	301.1	0.6 (0.0)	57	1362.5	9.4 (148.5)	93	3003.9	23.9 (42.9)
22	324.1	15.9 (0.0)	58	1396.3	3.7 (31.6)	94	3004.3	117.9 (38.9)
23	335.7	0.4 (1.5)	59	1403.1	0.0 (119.6)	95	3006.4	311.2 (0.0)
24	342.2	0.8 (4.9)	60	1418.0	1.5 (10.8)	96	3006.4	186.6 (30.2)
25	353.2	1.7 (0.4)	61	1419.1	8.4 (0.7)	97	3009.7	16.0 (6.5)
26	407.3	5.7 (0.0)	62	1419.9	9.5 (0.0)	98	3010.3	75.7 (1.9)
27	416.6	1.4 (0.4)	63	1420.9	2.8 (35.6)	99	3010.5	122.8 (0.0)
28	502.4	0.0 (3.6)	64	1441.4	15.8 (0.0)	100	3011.0	4.3 (4.6)
29	538.8	1.2 (1.7)	65	1441.9	1.6 (6.4)	101	3079.8	42.8 (0.0)
30	570.3	7.9 (1.6)	66	1447.1	2.6 (4.2)	102	3079.9	19.5 (0.1)
31	591.6	21.2 (0.0)	67	1450.6	36.8 (0.0)	103	3081.3	37.3 (6.2)
32	665.3	0.8 (1.9)	68	1453.4	22.7 (9.4)	104	3081.4	23.0 (14.0)
33	841.6	0.5 (6.7)	69	1454.4	2.5 (0.5)	105	3083.0	72.6 (8.5)
34	858.3	10.9 (40.5)	70	1457.5	0.6 (14.4)	106	3083.2	5.2 (14.7)
35	902.3	1.9 (11.9)	71	1459.3	10.5 (0.0)	107	3083.2	0.4 (6.0)
36	987.0	15.5 (0.0)	72	1459.9	17.7 (15.7)	108	3083.4	26.4 (0.0)

Results and Discussion

TDAE mass spectra obtained with the linear time of flight mass spectrometer are presented in Figures 7.4-7.6. The spectra are recorded at three different electron energies, 20, 40, and 70 eV. The parent peak (200 amu), along with parent-CH_3 (185 amu) , parent- $(CH_4)_2$ (168 amu), parent- $N(CH_3)CH_2$ (157 amu), parent- $N(CH_3)_2H_6$ (150 amu), parent-$N_2(CH_3)_2H_7$ (135 amu), parent-$N_2(CH_3)_3H_4$ (123 amu) , parent-$N_2(CH_3)_3CH_2$(113 amu), parent/2(100 amu), $N_2(CH_3)_4$ (88 amu), $C_3H_9N_2$(73 amu), C_3H_8N(58 amu), $NH(CH_3)_2$ (45 amu) , etc. were observed in the mass spectrum. The mass 100 amu could be attributed to the doubly charged ion of TDAE ($TDAE^{2+}$), however, the mass resolution of the accompanying isotopes in this apparatus does not allow us to verify this possibility. Yatsuhashi et al, have reported evidence for the existence of doubly charged TDAE previously.[150] Fragment ions were observed to be more dominant than that of the parent ion for electron energies above ~ 40eV.

It needs to be mentioned that in order to obtain these sets of data, extreme care was taken in order to prevent any reaction of TDAE with oxygen since, as stated before, TDAE is extremely reactive to oxygen. However, in the reproduction of data (Figure 7.7), we observed a mass peak at 116 amu, which was not present in the first set of data. We contribute this peak to the reaction of TDAE with oxygen. Oxidation of TDAE results in dissociation of the central C=C bond to give excited species, which subsequently fluorescence with a bright green color. In this regard, 116 amu, can be assigned to the $C_5H_{12}N_2O^+$ ion as a result of a reaction of TDAE with oxygen.

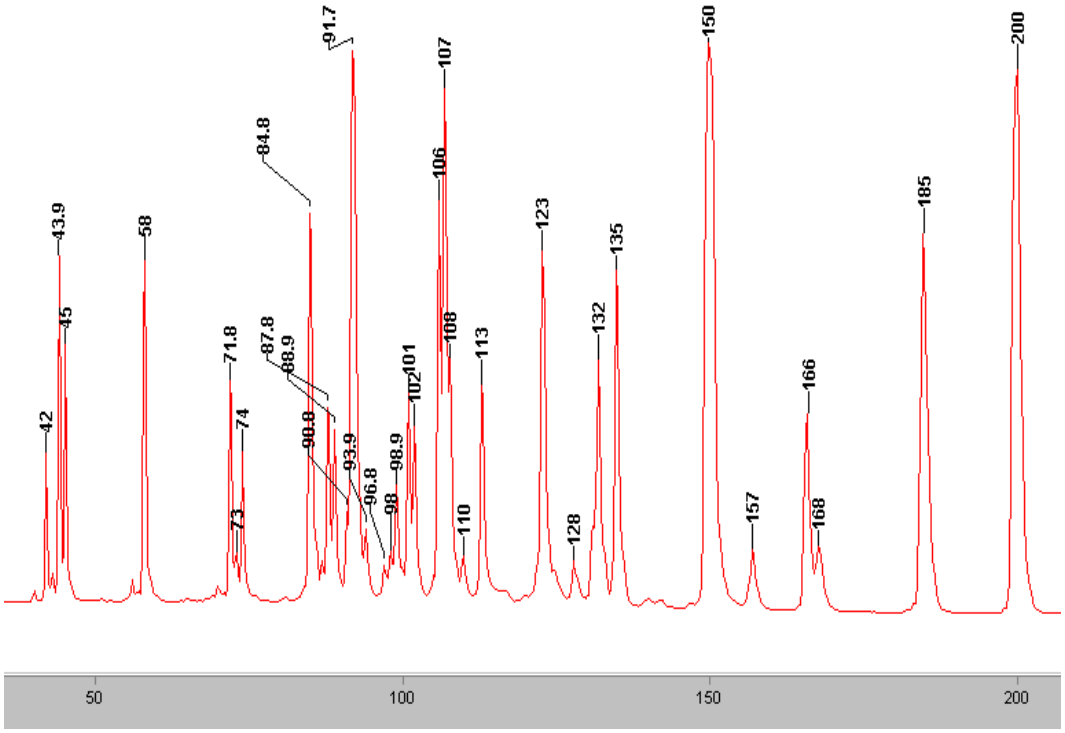

Figure 7.4 Mass spectrum of TDAE employing TOFMS with electron energy of 20 eV.

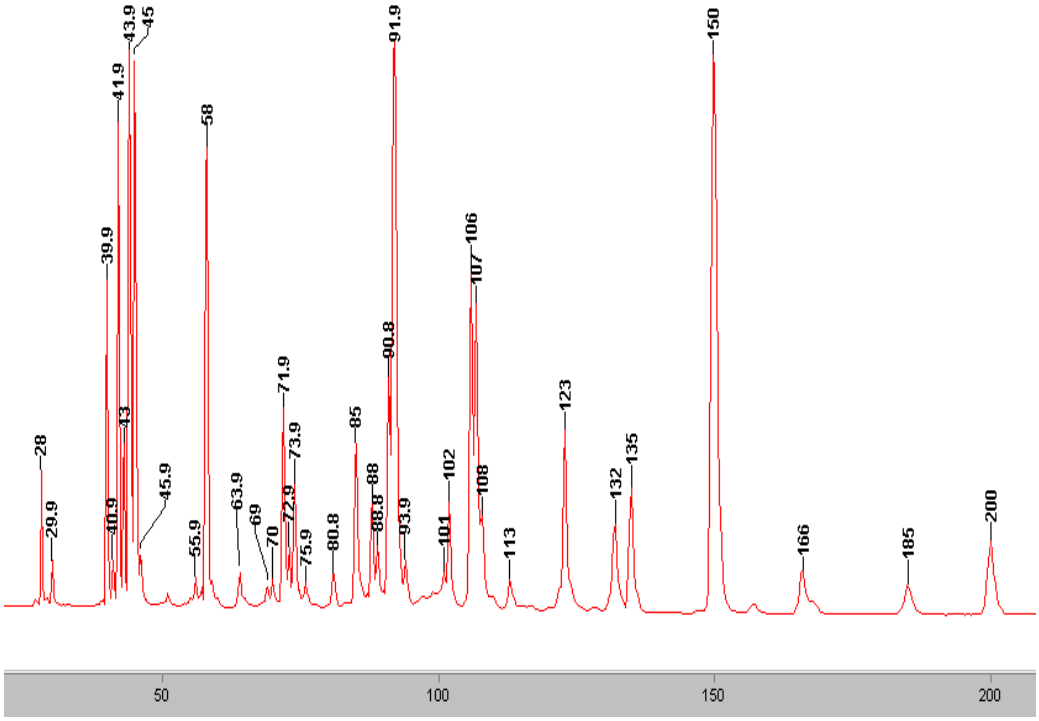

Figure 7.5 Mass spectrum of TDAE employing TOFMS with electron energy of 40 eV.

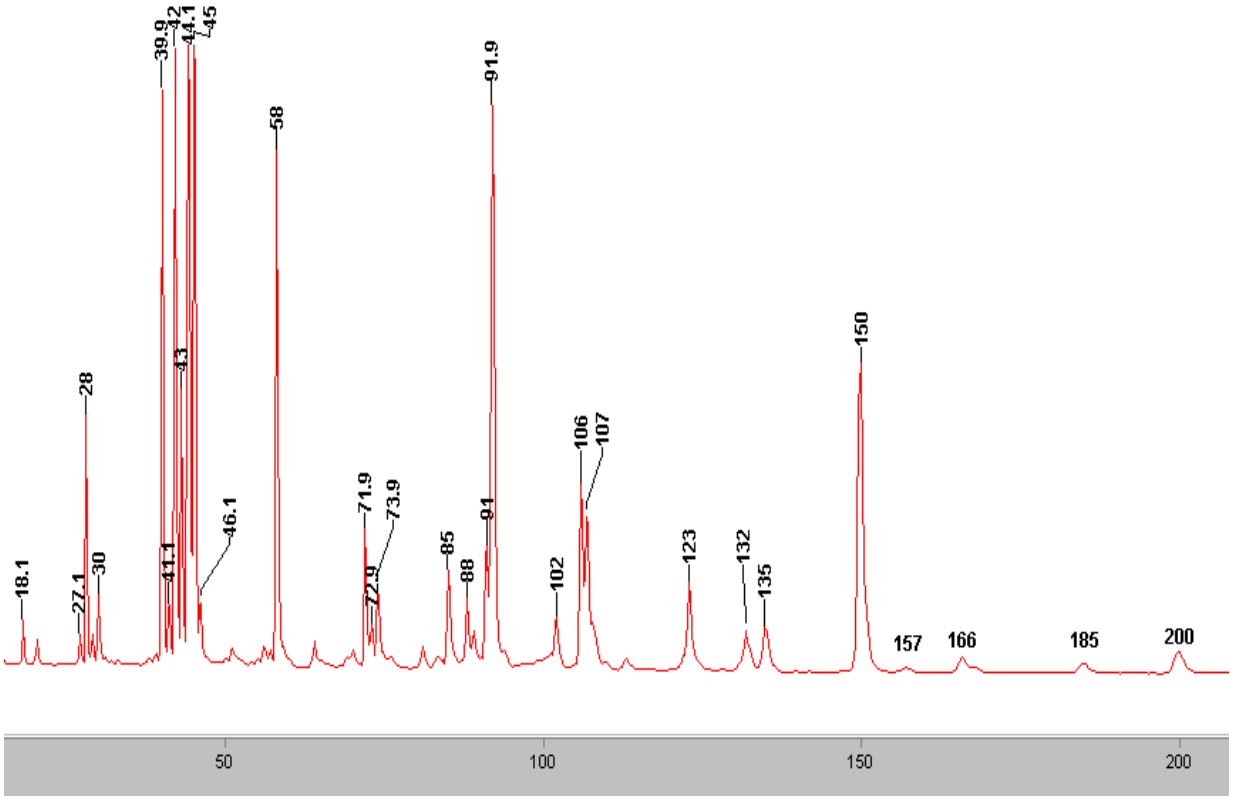

Figure 7.6 Mass spectrum of TDAE employing TOFMS with electron energy of 70 eV.

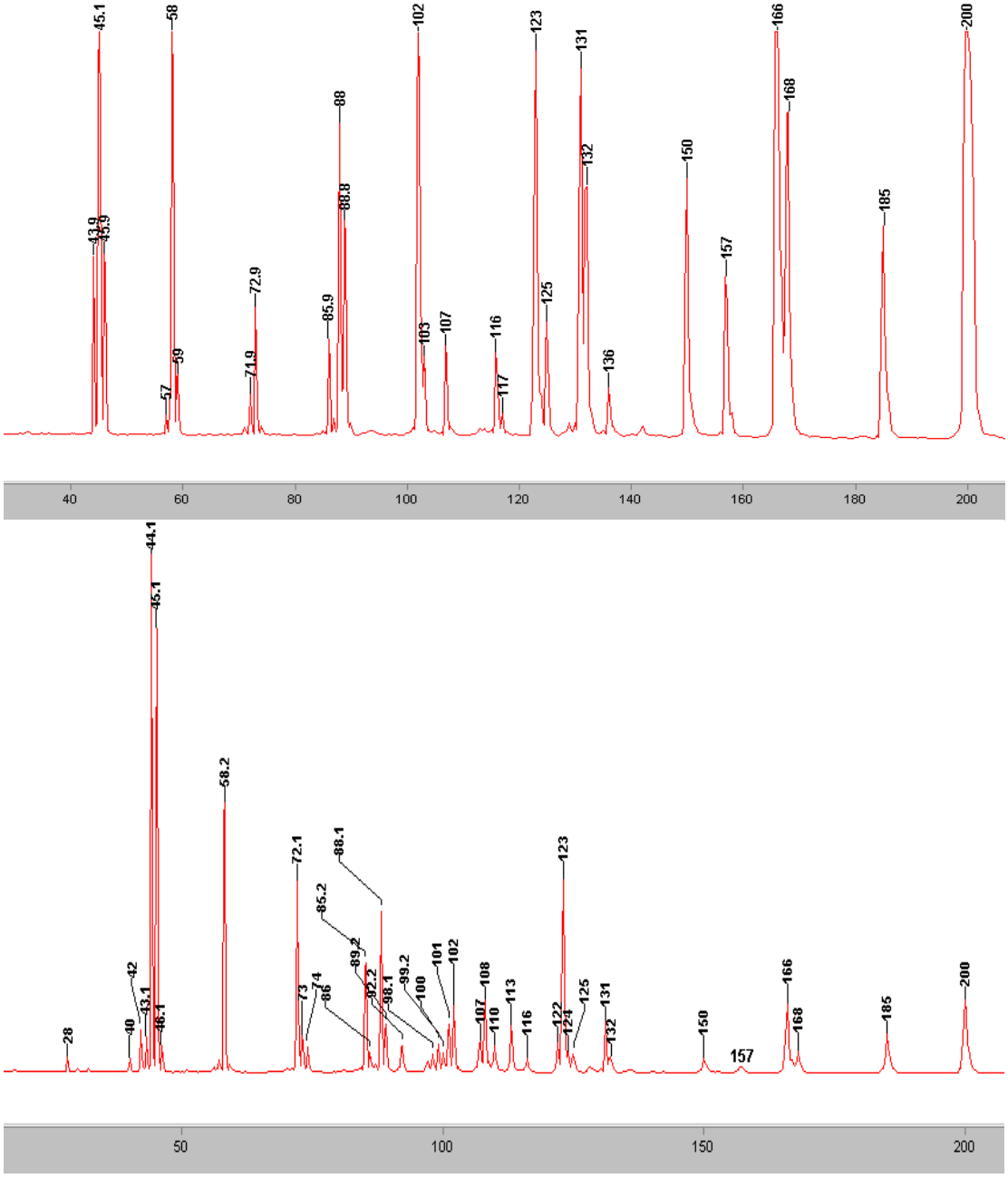

Figure 7.7 Mass spectra of TDAE employing TOFMS with electron energy of 20 eV (top) and 40 eV (bottom).

Figure 7.8 illustrates the intensity of the parent ion ($C_{10}H_{24}N_4^+$) as a function of electron energy. The argon ion intensity as a function of electron energy, which was used to calibrate the electron energy is also shown. As it can be seen from the Figure 7.8, the parent ion onset is at 5.3 eV and peaks at ~20eV. The cross section steadily decreases above ~ 20 eV. The energy threshold for the formation of the parent ion was found to be 5.3 ± 0.2 eV. This value is in close agreement with an earlier low-resolution photoionization result, ≤ 5.36 ±0.02[120] and the laser ionization result in this thesis. Figure 7.9 shows the photoionization efficiency spectrum of TDAE. The parent ion signal begins at ~ 5.20 (5) eV, slowly rises to 5.30 (5) eV, and then continues to rise more sharply. These values were corrected by adding 0.014 eV (110 cm^{-1}) to the laser energy used for photoionization. This small correction is due to the ionization-threshold shift induced by the DC field (320 V cm^{-1}) used to extract the ions in the time-of-flight mass spectrometer. This correction number is obtained experimentally by comparison of a known spectrum with and without the field.[147]

The slowly rising ion signal in Figure 7.9 between 5.20 and 5.30 eV may arise from photoionization of vibrationally excited neutral molecules or poor Franck-Condon factors due to a large geometry difference between the neutral and ionized states. To investigate the origin of the ion signal in this energy region, we measured photoionization efficiency spectra by replacing He with Ar as the carrier gas. If these ions originate from ionization of the excited molecules, their relative intensities should decrease with Ar pressure. This is because the Ar supersonic beam has a higher cooling efficiency than He, resulting in

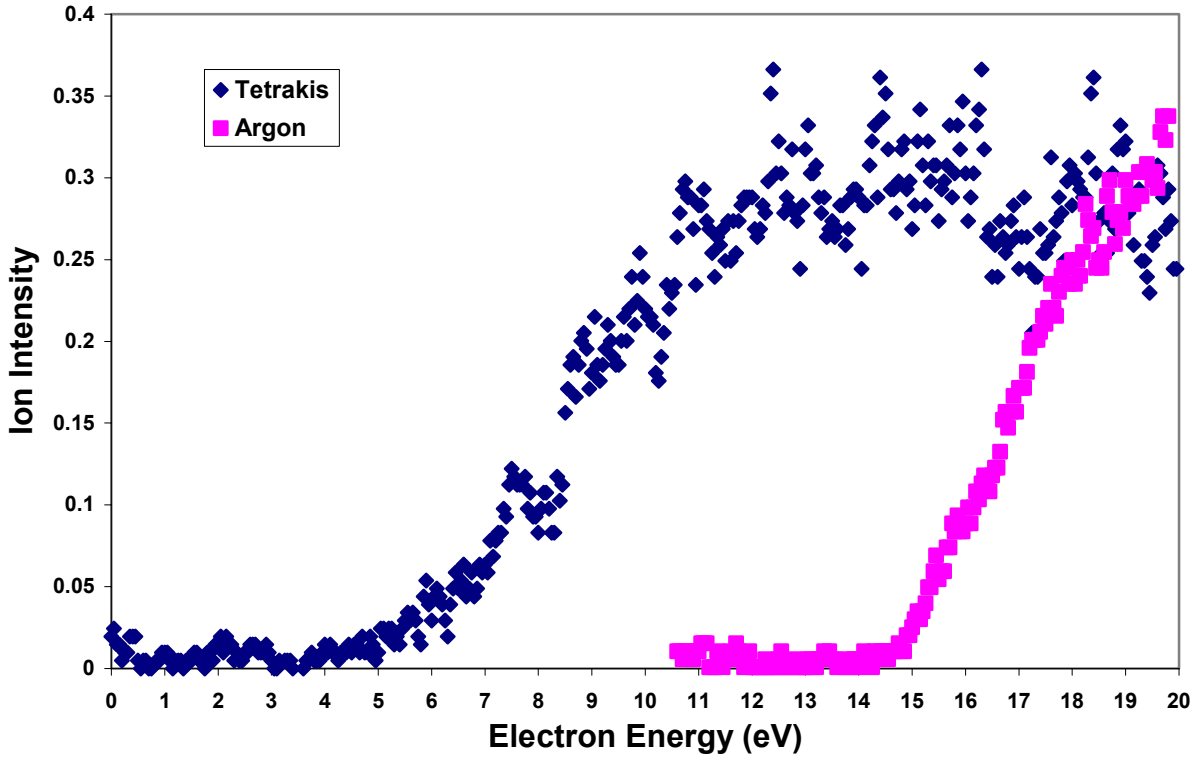

Figure 7. 8 Ionization potential of parent ion of TDAE (200 amu) compared with Ar gas.

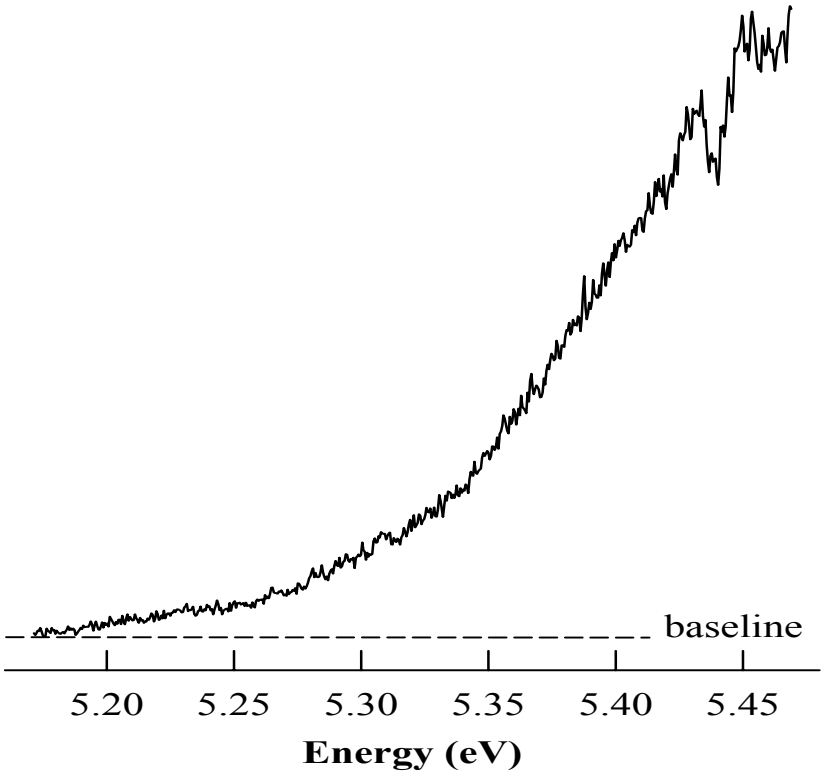

Figure 7.9 Photoionization efficiency spectrum of TDAE seeded in helium carrier gas.

lower internal temperatures of the neutral molecules and thus smaller populations in the excited levels.[151] However, the photoionization spectra of TDAE seeded in Ar and He show very similar profiles, suggesting that the slowly rising ion signal is unlikely to be due to vibrational hot-band effects. Moreover, our density functional theory calculations predict significant geometry differences between the ground electronic states of the neutral and ionized molecules, which should result in a small Franck-Condon factor for the transition between the electronic-vibrational ground state levels of the neutral and ionic states. Based on this experimental and computational evidence, we believe that the first ionization onset at 5.20 (5) eV corresponds to the IP of TDAE.

Figure 7.10 shows a comparison between the calculated and observed Raman vibrational frequencies of TDAE. As it can be seen, the strongest Raman shift in the experimental spectrum is 1632 cm^{-1}. From the calculation, this mode was attributed to the C=C stretch mode. This stretch mode is also in close agreement by the previously reported data (1630 cm^{-1}).[142] There is also good agreement between most of the experimental and computed frequencies demonstrating the presented D_2 symmetry for TDAE is a reasonable structural symmetry. However, the calculated intensities do not correspond exactly to the experimental values, which is not unusual. The difficulty in predicting the Raman intensities is due to the fact that the Raman intensity is the differentiated frequency-dependent polarizibility with respect to nuclear displacements and such a calculation demands a very high computational method with the inclusion of sufficient basis sets in the wave function describing the molecule.

The intense C=C Raman mode has no accompanying IR activity (from the calculation) and confirms that TDAE has a centro-symmetric symmetry structure. This is

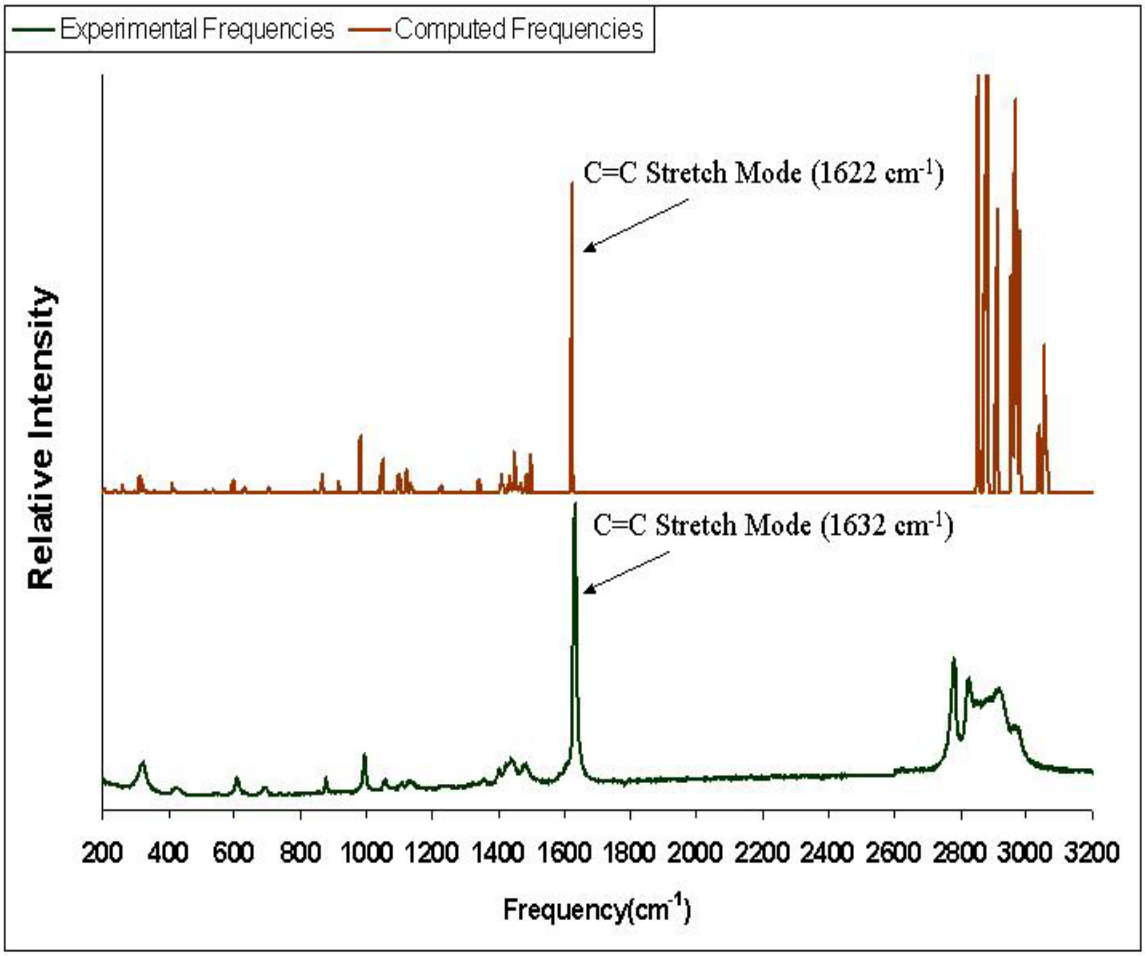

Figure 7.10 Comparison between calculated (top) and experimental (bottom) Raman vibrational frequencies of TDAE using Ar laser. The data were recorded at room temperature (20°C).

known as the mutual exclusion principle. As discussed in the computation section, this mode is expected to shift to 1544 cm^{-1} upon ionization of TDAE.

In summary, we were able to revisit the adiabatic ionization potential of TDAE and experimentally confirmed that TDAE has a very low ionization potential of ~ of 5.2 eV, in reasonable agreement with the pervious photoionization studies.[120] Raman vibrational frequency measurements, as well as calculations, provided further structural information for TDAE.

CHAPTER VIII

Conclusions

This dissertation successfully employed an electrospray ionization source to produce gas-phase multiply-charged anions (MCA). The role of the repulsive Coulomb barrier (RCB) in determining the properties of gaseous MCAs was analyzed. In this work, the collision-induced dissociation (CID) technique was employed to study the stability of MCAs toward electron detachment and ionic fragmentation.

In the collision-induced dissociation experiment of salt clusters, i.e., $Na_7Cl_9^{2-}$, the role of the repulsive Coulomb barrier in stabilization of an unstable MCA was confirmed. Although calculations were presented showing that the salt dianions were unstable toward ionic fragmentation, these dianions appeared to be stable in the CID experiment. Metastability of these dianions was attributed in part to the existence of the RCB. This result was direct experimental proof of the repulsive Coulomb barrier toward ionic fragmentation.

Following the observation of the RCB in the salt dianions, more experiments were performed to estimate the heights of inner and outer RCB of groups of MCAs. The main objective was to relate the heights of the RCB to the electronic properties of the dianions. In this regard two groups of dianions, dicarboxylate and disulfonic dianions, were chosen as a result of their different electronic properties. The CID experiment provided some interesting results regarding the stability of these dianions. Disulfonic dianions appeared to be stable and their dissociation pathway was through loss of SO_3^-. The outer and inner RCBs of disulfonic dianions toward ionic fragmentation were determined. The results of the CID experiment for the dicarboxylate dianions were very interesting. These dianions

were believed to decay through loss of neutral CO_2. Therefore there is no repulsive Coulomb barrier for this decay. In this study, the dissociation pathways of dicarboxylate and disulfonic dianions toward ionic fragmentation were computed. The computed heights of RCBs for disulfonic dianions were roughly in agreement with the results obtained from the CID experiment.

We demonstrated that the CID technique, along with the theoretical approaches, is an excellent tool to investigate the stability of MCAs toward ionic fragmentation. The stability of MCAs toward electron detachment has been very well investigated primarily employing photoelectron spectroscopy. The CID technique will enable us studying the stability of MCAs toward ionic fragmentation. An ideal experiment would be to employ these two methods, photoelectron spectroscopy and CID methods concurrently on MCAs. Photodetachment experiment will provide information on the electronic stability of the MCAs, whereas the CID experiment will yield information regarding the thermodynamic stability of the MCAs.

Multiply-charged anion research is a relatively new field of research. There are still many questions regarding the properties of MCAs; however there have been significant advances in this area in the past few years. This progress is mainly attributed to the development of the electrospray ionization source (ESI). Future development in the field of multiply-charged anions research looks very promising since there is a powerful tool, ESI, to produce the gas-phase MCAs and as well as many techniques such as photoionization and the CID method, to study the produced MCAs.

REFERENCES

[1] H. S. W. Massey, *Negative ions* (Cambridge University Press, UK, 1976).

[2] B. M. Smirnov, *Negative ions*. (McGraw-Hill, New York, 1982).

[3] D. R. Bates, Adv. At. Mol. Opt. Phys. **27**, 1 (1991).

[4] T. Andersen, H. K. Haugen, and H. Hotop, J. Phys. Chem. Ref. Data **28**, 1511 (1999).

[5] J. C. Rienstra-Kiracofe, G. S. Tschumper, H. F. Schaefer, S. Nandi, and G. B. Ellison, Chem. Rev. **102**, 231 (2002).

[6] G. J. Schulz, Rev. Mod. Phys. **45**, 423 (1973).

[7] R. N. Compton, L. G. Christophorou, G. S. Hurst, and P. W. Reinhardt, J. Chem. Phys. **45**, 4634 (1966).

[8] G. Z. Whitten, and B. S. Rabinovitch, J. Chem. Phys. **38**, 2466 (1963).

[9] M K. Scheller, and L. S. Cederbaum, J. Phys. B, **25**, 2257 (1992).

[10] A. I. Boldyrev, and J. Simons, J. Phys. Chem. **98**, 2298 (1994).

[11] W. K. Stuckey, and R. W. Kiser, Nature. **211**, 963 (1966).

[12] J. H. Fremlin, Nature. **211**, 1453 (1966).

[13] R. W. Kiser, Top. Curr. Chem. **83**, 89 (1979).

[14] M. Anbar, and R. Schnitzer, Science, **191**, 463 (1976).

[15] R. Schnitzer, and M. Anbar, J. Chem. Phys. **64**, 2466 (1976).

[16] B. Jane Stapleton, and J. H. Bowie, Aust. J. Chem. **30**, 417 (1977).

[17] R. C. Dougherty, J. Chem. Phys. **50**, 1896 (1969).

[18] J. H. Bowie, and B. J. Stapleton, J. Am. Chem. Soc. **98**, 6480(1976).

[19] A. P. Bruins, T. R. Covey, and J. D. Henion, Anal. Chem. **59**, 2642 (1987).

[20] W. P. M. Maas, and N. M. M. Nibbering, Int. J. Mass Spectrom. Ion Processes **88**, 257 (1989).

[21] K. Leiter, W. Ritter, A. Stamatovic, and T. D. Märk, Int. J. of Mass Spectrom. and Ion Processes **68**, 341(1986).

[22] S. N. Schauer, P. Williams, and R. N. Compton, Phys. Rev. Lett. **65**, 625 (1990).

[23] P. A. Limbach, L. Schweikhard, K. A. Cowen, M. T. McDermott, and A. G. Marshall, J. Am. Chem. Soc. **113**, 6795 (1991).

[24] R. L. Hettich, R. N. Compton, and R. H. Ritchie, Phys. Rev. Lett. **67**, 1242 (1991).

[25] R. N. Compton, A. A. Tuinman, C. E. Klots, M. R. Pederson, and D. C. Patton, Phys. Rev. Lett. **78**, 4367 (1997).

[26] Tuinman, and R. N. Compton, Phys. Rev. A **65**, 052724 (2002).

[27] S. Yu. Ovchinnikov, J. Macek, A. A. Tuinman, J. D. Steill, R. N. Compton, P. Hvelplund, A. I. S. Holm, S. B. Nielsen, and M. B. Nielsen, Phys. Rev. A **73**, 064704 (2006).

[28] T. Blades, and P. J. Kebarle, J. Am. Chem. Soc. **116**, 10761(1994).

[29] M. K. Scheller, R. N. Compton, and L. S. Cederbaum, Science **270**, 1160 (1995).

[30] A. I. Boldyrev, M. Gutowski, and J. Simons, Acc. Chem. Res. **29**, 497 (1996).

[31] L. S. Wang, and X. B. Wang, J. Phys. Chem. A **104**, 1978 (2000).

[32] A. Dreuw, and L.S. Cederbaum, Chem. Rev. **102**, 181 (2002).

[33] M K. Scheller, and L. S. Cederbaum, J. Chem. Phys. **99**, 441 (1993).

[34] X. B. Wang, and L. S. Wang, Phys. Rev. Lett. **83**, 3402 (1999).

[35] T. Sommerfeld, and M. S. Child, J. Chem. Phys. **110**,5670 (1999)

[36] H. G. Weikert, and L. S. Cederbaum, J. Chem. Phys. **99**, 8867 (1993).

[37] R. Middleton, and J. Klein, Phys. Rev. Lett. **60**, 3515 (1999).

[38] C. Jin, R. L. Hettich, R. N. Compton, A. A. Tuinman, A. Derecskeikovac, D. S. Marynick, and B. I. Dunlap, Phys. Rev. Lett. **73**, 2821 (1994).

[39] C. Yannouleas, and U. Landman, Chem. Phys. Lett. **210**, 437 (1993).

[40] R. L. Martin, and J. P. Ritchie, J. Phys. Rev. B **48**, 4845 (1993).

[41] J. D. Jackson, *Classical electrodynamics* (John Wiley & Sons, New York, 1963).

[42] S. M. Bachrach, M. Hare, and S. R. Kass, J. Am. Chem. Soc. **120**, 12646 (1998).

[43] K. W. M. Siu, G. J. Gardner, and S. S. Berman, Org. Mass Spectrom. **24**, 931 (1989).

[44] X. B. Wang, C. F. Ding, and L. S. Wang, Phys. Rev. Lett. **81**, 3351 (1998).

[45] X. B. Wang, and L. S. Wang, Nature, **400**, 245 (1999).

[46] S. Tomita, J. U. Andersen, H. Cederquist, B. Concina, O. Echt, J. S. Forster, K. Hansen, B. A. Huber, P. Hvelplund, J. Jensen, B. Liu, B. Manil, L. Maunoury, S. Brøndsted Nielsen, J. Rangama, H. T. Schmidt, and H. Zettergren, J. Chem. Phys. **124**, 024310 (2006).

[47] O. T. Ehrler, J. M. Weber, F. Furche, and M. M. Kappes, Phys. Rev. Lett. **91**, 113006 (2003).

[48] J. M. Weber, I. N. Ioffe, K. M. Berndt, D. Loffler, J. Friedrich, O. T. Ehrler, A.S. Danell, J. H. Parks, and M.M. Kappes, J. Am. Chem. Soc. **126**, 8585 (2004).

[49] O. T. Ehrler, F. Furche, J. M. Weber, and M. M. Kappes, J. Chem. Phys. **122**, 94321 (2005).

[50] P. Weis, O. Hampe, S. Gilb, and M. M. Kappes, Chem. Phys. Lett. **321**, 425 (2000).

[51] J. Friedrich, S. Gilb, O. T. Ehrler, A. Behrendt, and M.M. Kappes, J. Chem. Phys. **117**, 2635 (2002).

[52] X. B. Wang, and L. S. Wang, J. Chem. Phys. **111**, 4497 (1999).

[53] W. E. Boxford, J. K. Pearce, and C. E. H. Dessent, Chem. Phys. Lett. **399**, 465 (2004).

[54] W. E. Boxford, and C. E. H. Dessent, Phys. Chem. Chem. Phys. **8**, 5151 (2006).

[55] W. E. Boxford, R. M. Burke, and E. H. Dessent, Phys. Scr. **76**, C56 (2007).

[56] N. Mirsaleh Kohan, S. Ard, A. A. Tuinman, R. N. Compton, P. Weis, and M. M. Kappes, Chem. Phys. **329**, 239 (2006).

[57] M. Yamashita, and J. B. Fenn, J. Phys. Chem., **88**, 4451 (1994); J. B. Fenn, M. Mann, C. K. Meng, S. F. Wong, and C.M. Whitehouse, Science, **64**, 246 (1985).

[58] S. Gaskell, J. Mass Spectrometry, **32**, 677 (1997).

[59] M. Yamashita, and J. B. Fenn, J. Phys. Chem. **88**, 4671 (1984).

[60] M. G. Ikonomou, A. T. Blades and P. Kebarle, J. Am. Soc. Mass Spectrom. **2**, 497 (1991).

[61] D. P. H. Smith, IEEE Trans. Ind. Appl. **1A-22**, 527 (1986).

[62] F. M. Wampler III, A. T. Blades, and P. Kebarle, J. Am. Soc. Mass Spectrom. **4**, 289 (1993).

[63] K. Levsen. *Fundamental Aspects of Organic Mass Spectrometry* (Verlag Chemie, New York, 1978).

[64] K. M. Ervin, S. K. Loh, N. Aristov, P. B. Armentrout, J. Phys. Chem. **87**, 3593 (1983).

[65] N. Aristove, P. B. Armentrout, J. Am. Chem. Soc. **108**, 1806 (1986).

[66] T. S. Beyer and D.F. Swinehart, Comm. Assoc. Comput. Machines **16**, 379 (1973).

[67] P. B. Armentrout Advances in Gas Phase Ion Chemistry, Volume1. JAI Press: New York, 83 (1992).

[68] P. J. Chantry, J Chem. Phys. **55**, 2746 (1971).

[69] S.K. Loh, D. A. Hales, L. Lian, and P.B. Armentrout, J. Chem. Phys. **90**, 5466 (1989).

[70] M. T. Rodgers, K. M. Ervin, and P. B. Armentrout. J. Chem. Phys.**106**, 4499 (1997).

[71] A. Mandelbaum, and A. Etinger, Org. Mass. Spectrom. **28**, 487 (1993).

[72] G. Khairallah, and J. B. Peel, Chem. Phys. Lett. **268**, 218 (1997).

[73] A. T. Blades, and P. Kebarle, J. Am. Chem. Soc. **116**, 10761 (1994).

[74] C. P. G. Butcher, B. F. G. Johnson, J. S. Mclndoe, X. Yang, X. B. Wang, and L. S. Wang, J. Chem. Phys. **116**, 6560 (2002)

[75] A. A. Tuinman and R. N. Compton. J. Phys. Chem. A **102**, 9791 (1998).

[76] X. Yang, X. B. Wang, and L. S. Wang, Int. J. Mass Spectrom. **228**, 797 (2003).

[77] K. W. Oum, M. J. Lakin, D. O. Dehaan, and T. Brauers, Science, **279**, 74 (1998).

[78] D. Rosenfeld, R. Lahav, A. Khain, and M. Pinsky, Science, **297**, 1667 (2002).

[79] G. C. Bruce, Science **303**, 1146 (2004).

[80] M. K. Scheller, and L. S. Cederbaum, J. Chem. Phys. **100**, 8934 (1994).

[81] J. Friedrich, P. Weis, J. Kaller, R. L. Whetten, and M. M. Kappes. Eur. Phys. J. D, **9**, 269 (1999).

[82] F. R. Bichowsky, and L. C. Copeland, Phys. Rev. A **31**, 1113 (1928).

[83] L. C. Copeland, Phys. Rev. **36**, 1221 (1930).

[84] R. N. Compton and J. N. Bardsley, in *Electron-Molecule Collisions* (I. Shimamura and K. Takayanagi, Eds.), Plenum Press, pp. 275 (1984).

[85] D. P. Stevenson, J. Chem. Phys. **10**, 291 (1942).

[86] R. L. C. Wu, and T. O. Tiernan, Planet. Space Sci. **29**, 735 (1981).

[87] T. F. Magnera, D. E. David, and J. Michl, J. Am. Chem. Soc.**111**, 4100 (1989).

[88] S. T. Graul, and R. R. Squires, J. Am. Chem. Soc. **112**, 2517 (1990)

[89] R. H. Schultz, and P. B. Armentrout, Int. J. Mass Spectrom. Ion Process **107**, 29 (1991).

[90] D. A. Prinslow, and P. B. Armentrout, J. Chem. Phys. **94**, 3563 (1991).

[91] E. R. Fisher, B. L. Kickel and P. B. Armentrout, J. Chem. Phys. **97**, 4859 (1992).

[92] J. S. Klassen, S. G. Anderson, A. T. Blades and P. Kebarle, J. Phys. Chem.**100**, 14218 (1996).

[93] K. E. Nizzi, C. A. Pommerening, and L. S. Sunderlin, J. Phys. Chem. **102**, 7674 (1998).

[94] J. M. Bailey, C. Hao, B. J. Johnson, and L. S. Sunderlin, Int. J. Mass Spectrom. **241**, 133 (2005).

[95] F. A. Akin, J. Ree, K. M. Ervin, and H. K. Shin, J. Chem. Phys.**123**, 064308 (2005).

[96] L. S. Sunderlin and R. R. Squires, J. Am. Chem. Soc. **115**, 337 (1993).

[97] N.F. Dalleska, K. Honma, L. S. Sunderlin, and P. B. Armentrout, J. Am. Chem. Soc. **116**, 3519 (1994).

[98] M. B. More, E. D. Glendening, D. Ray, D. Feller, and P. B. Armentrout, J. Phys. Chem. **100**, 1605 (1996).

[99] A. Grushow, and K. M. Ervin, J. Am. Chem. Soc. **117**, 11612 (1995).

[100] V. A. Spaspv, T. Lee, and K. M. Ervin, J. Chem. Phys. **112**, 1713 (2000).

[101] C. Hao, J. D. Kaspar, C. E. Check, K. C. Lobring, T. M. Gilbert, and L. S. Sunderlin. J. Phys. Chem. A **109**, 2026 (2005).

[102] M. L. Vestal, and G. H. Mauclaire, J. Chem. Phys. **67**, 3758 (1977).

[103] L. S. Sunderlin, D. Wang, and R. P. Squires, J. Am. Chem. Soc. **115**. 12060 (1993).

[104] F. A. Khan, D. A. Steele, and P. B. Armentrout, J. Phys. Chem. **99**, 7819 (1995).

[105] G. L. Gutsev, R. J. Bartlett, A. I. Boldyrev and J. Simons, J. Chem. Phys. **107**, 3867 (1997).

[106] A. N. Alexandrova, A. I. Boldyrev, Y. J Fu, X Yang, X. B. Wang, and L. S. Wang, J. Chem. Phys. **121**, 5709 (2004).

[107] Gaussian 03, Revision C.02, M. J. Frisch, G. W. Trucks, H. B. Schlegel, G. E. Scuseria, M. A. Robb, J. R. Cheeseman, J. A. Montgomery, Jr., T. Vreven, K. N. Kudin, J. C. Burant, J. M. Millam, S. S. Iyengar, J. Tomasi, V. Barone, B. Mennucci, M. Cossi, G. Scalmani, N. Rega, G. A. Petersson, H. Nakatsuji, M. Hada, M. Ehara, K. Toyota, R. Fukuda, J. Hasegawa, M. Ishida, T. Nakajima, Y. Honda, O. Kitao, H. Nakai, M. Klene, X. Li, J. E. Knox, H. P. Hratchian, J. B. Cross, V. Bakken, C. Adamo, J. Jaramillo, R. Gomperts, R. E. Stratmann, O. Yazyev, A. J. Austin, R. Cammi, C. Pomelli, J. W. Ochterski, P. Y. Ayala, K. Morokuma, G. A. Voth, P. Salvador, J. J. Dannenberg, V. G. Zakrzewski, S. Dapprich, A. D. Daniels, M. C. Strain, O. Farkas, D. K. Malick, A. D. Rabuck, K. Raghavachari, J. B. Foresman, J. V. Ortiz, Q. Cui, A. G. Baboul, S. Clifford, J. Cioslowski, B. B. Stefanov, G. Liu, A. Liashenko, P. Piskorz, I. Komaromi, R. L. Martin, D. J. Fox, T. Keith, M. A. Al-Laham, C. Y. Peng, A. Nanayakkara, M.

Challacombe, P. M. W. Gill, B. Johnson, W. Chen, M. W. Wong, C. Gonzalez, and J. A. Pople, Gaussian, Inc., Wallingford CT, 2004.

[108] A. D. Walsh, J. Chem. Soc. , 2260 (1953).

[109] J. D. D. Martin, J.W**.** Hepburn, J. Chem. Phys**. 109**, 8139 (1998) ; R. Trainham, G.D. Fletcher, D.J. Larson, J. Phys. B **20**, L777 (1987); U. Berzinsh, M. Gustafsson, D. Hanstorp, A. Klinkmuller, U. Ljungblad, A.M. Martenssonpendrill, Phys. Rev. A **51**, 231 (1995).

[110] J. Guan-Zhi, and E. R. Davidson, J. Phy. Chem. **96**, 3683 (1992).

[111] P. Skurski, J. Simons, X. B. Wang, and L.S. Wang, J. Am. Chem. Soc. **122**, 4499 (2000).

[112] P. Schwerdtfeger, A. Hammerl, and R. Wesendrup, Int. J. Mass Spectrom. **228,** 341 (2003).

[113] C. D. Cooper, R. N. Compton. Chem. Phys. Lett. **14,** 29 (1972).

[114] E. Merzbacher, *Quantum Mechanics* (Wiley, New York, 1961).

[115] K. W. M. Siu, G. J. Gardner, and S.S. Berman, Org. Mass Spectrom. **24**, 931 (1989).

[116] S. M. Bacharch, M. Hare, and S. R. Kass, J. Am. Chem. Soc. **120**, 12646 (1998).

[117] R. N. Compton, P. W. Reinhardt, P. W. Cooper, and C. D. Cooper, J. Chem. Phys. **63,** 3821 (1975).

[118] P. G. Wenthold, R. R. Squires, and W. C. Lineberger, J. Am. Chem. Soc. **120**, 5279 (1998).

[119] S. P. Møller, Nucl. Instrum. Meth. Phys. Research A **394**, 281 (1997).

[120] Y. Nakato, M. Ozaki, A. Egawa, and H. Tsubomura, Chem. Phys. Lett. **9,** 615 (1971).

[121] M. Larousi, Int. J. Infrared Millim. Waves **16**, 2069 (1995).

[122] M. Larousi, Int. J. Infrared Millim. Waves **17**, 2215 (1996).

[123] J. Vidmar, IEEE Trans. Plasma Sci. **18**, 733 (1990).

[124] J. R. Woodworth, T. A. Green, C. A. Frost, J. Appl. Phys. **57**, 1648 (1985).

[125] Y. S. Zhang, and J. E. Scharer, J. Appl. Phys. **73**, 4779 (1993).

[126] K. L. Kelly, J. E. Scharer, E.S. Paller, and G. Ding, J. Appl. Phys. **92**, 698 (2002).

[127] J. Seguinot, T. Ypsilantis, Nucl. Instrum. Mth. **142**, 377 (1977).

[128] J. Seguinot, T. Ypsilantis, Nucl. Instrum. Mth. Phys. Res. A **343**, 1 (1994).

[129] D. F. Anderson, IEEE Trans. Nucl. Sci. **28**, 842 (1981).

[130] P. M. Alemand, K. C. Khemani, A. Koch, F. Wudl, K. Holczer, S. Donovan, G. Grüner, and J. D. Thompson, Science **253**, 302 (1991).

[131] K. Tanaka, A. A. Zakhidov, K. Yoshizawa, K. Okahara, T. Yamabe, and K. Yukushi, Phys. Rev. B **47**, 7554 (1993).

[132] O. Hampe, M. Neumaier, M. N. Blom and M. m. Kappes, Chem. Phys. Lett. **354**, 303 (2002).

[133] I. N. Ioffe, S. M. Avdoshenko, O. V. Boltalina, L. N. Sidorov, K. Berndt, J. M. Weber, Int, J. Mass Spectrom. **243**, 223 (2005).

[134] R. L. Pruett, J. T. Barr, K. E. Rapp, C. T. Bahner, J. D. Gibson, and R. H. Lafferty, J. Am. Chem. Soc. **72**, 3646 (1950).

[135] H. Weingarten, and W. E. White, J. Am. Chem. Soc. **88**, 850 (1966).

[136] H. Brederick, F. Effenberger, and T. Brendle. Angew. Chem. **78**, 147 (1966).

[137] N. Wiberg, Angew. Chem. Internal. Edit. **7**, 766 (1968).

[138] B. Centinkaya, G. H. King, S. S. Krishnamurthy, M. F. Lappert, and J. B. Pedlev, Chem. Commun. 1370 (1971).

[139] J. M. L. Martin, A. Warshawsky, A. Breskin, and R. Chechik, Chem. Phys. Lett. **279**, 389 (1997).

[140] M. R. Pederson, and N. Laouini, J. Cluster Sci. **10**, 557 (1999).

[141] H. Bock, H. Borrmann, Z. Havlas, H. Oberhammer, K. Ruppert, and A. Simon, Angew. Chem. Int. Ed. Engl. **30**, 1678 (1991).

[142] N. Wiberg, D. R. Downing, and D. D. Coffman, J. Amer. Chem. Soc. **87**, 2054 (1965).

[143] N. Wiberg, and J. W. Buchler, Z. Naturforsch. **19b**, 5 (1964).

[144] W. D. Robertson, N. I. Hammer, J. E. Bartmess, R. N. Compton, K. Diri, and K. D. Jordan, J. Chem. Phys. **122**, 204319 (2005).

[145] W. E. Barr, and W. A. Perkins, Rev. Sci. Instrum. **37**, 1354 (1966).

[146] W. C. Wiley, and I. H. McLaren, Rev. Sci. Instr. **26**, 1150 (1955).

[147] G. K. Rothschopf, J. S. Perkins, S. Li, and D. –S. Yang, J. Phys. Chem. A, **104**, 8178 (2000).

[148] D. Proch, and T. Trickl, Rev. Sci. Instrum*.* **60***,* 713 (1989).

[149] M. P. Andersson, and P. Uvdal, J. Phys. Chem. A **109**, 2937 (2005).

[150] T. Yatsuhashi, T. Obayashi, M. Tanaka, M. Murakami, and N. Nakashima, J. Phys. Chem. A **110**, 7763 (2006).

[151] J. F. Fuller, S. Li, B. R. Sohnlein, G. K. Rothschopf, and D. –S. Yang, Chem. Phys. Lett. **366**, 141 (2002).

APPENDICES

Appendix A: Optimized and Energy Minimized Z-Matrices for Dianions of Interest in Chapter VI

1,2-disulfonate dianion
B3LYP/6-311++G**

C
C,1,R2
C,1,R3,2,A3
H,1,R4,2,A4,3,D4,0
C,2,R5,1,A5,3,D5,0
C,3,R6,1,A6,2,D6,0
H,2,R7,1,A7,5,D7,0
S,3,R8,1,A8,6,D8,0
C,5,R9,2,A9,1,D9,0
H,5,R10,2,A10,9,D10,0
S,6,R11,3,A11,1,D11,0
O,8,R12,3,A12,1,D12,0
O,8,R13,3,A13,12,D13,0
O,8,R14,3,A14,12,D14,0
H,9,R15,5,A15,2,D15,0
O,11,R16,6,A16,3,D16,0
O,11,R17,6,A17,16,D17,0
O,11,R18,6,A18,16,D18,0

Variables:

R2=1.39047688
R3=1.40335891
R4=1.08277885
R5=1.39243111
R6=1.4113744
R7=1.08767776
R8=1.87552813
R9=1.39046594
R10=1.08767332
R11=1.8756248
R12=1.48480791
R13=1.50040577
R14=1.47398764
R15=1.08279101
R16=1.47395642
R17=1.48480732
R18=1.50041316
A3=122.36127577
A4=120.81622023
A5=119.18699022
A6=118.45151872
A7=119.90783008
A8=112.1467441
A9=119.18532661
A10=120.90503
A11=129.34056692
A12=104.27500741
A13=102.54543008
A14=107.73592504
A15=120.81711293
A16=107.74275659
A17=104.26928383
A18=102.53730878
D4=-179.43409881
D5=0.07326331
D6=-0.26223818
D7=179.80216921
D8=177.20861051
D9=0.02573065
D10=-179.80087636
D11=-176.30686837
D12=-97.61973691
D13=116.90646468
D14=-123.98297061
D15=-179.36069231
D16=-44.72678523
D17=123.98143668
D18=-119.1155442

2,6-naphthalenedisulfonic dianion
B3LYP/6-311++G**

C
C,1,R2
C,1,R3,2,A3
H,1,R4,2,A4,3,180.,0
C,2,R5,1,A5,3,0.,0
C,3,R6,1,A6,2,0.,0
C,3,R7,1,A7,2,180.,0
H,2,R8,1,A8,3,180.,0
C,5,R9,2,A9,1,0.,0
C,6,R10,3,A10,1,180.,0
C,7,R11,3,A11,1,180.,0
S,5,R12,2,A12,1,180.,0

H,7,R13,3,A13,1,0.,0
C,10,R14,6,A14,3,0.,0
H,9,R15,5,A15,2,180.,0
H,10,R16,6,A16,3,180.,0
S,11,R17,7,A17,3,180.,0
O,12,R18,5,A18,2,180.,0
O,12,R19,5,A19,2,D19,0
O,12,R19,5,A19,2,-D19,0
H,14,R21,10,A21,6,180.,0
O,17,R22,11,A22,7,0.,0
O,17,R23,11,A23,7,D23,0
O,17,R23,11,A23,7,-D23,0

Variables:

R2=1.37386092
R3=1.42256228
R4=1.08647931
R5=1.41679957
R6=1.4296998
R7=1.42195292
R8=1.08366861
R9=1.37324324
R10=1.42256228
R11=1.3732425
R12=1.82804436
R13=1.08448664
R14=1.37386092
R15=1.08448569
R16=1.08647931
R17=1.82799944
R18=1.48778388
R19=1.48926685
R21=1.08366861
R22=1.48778388
R23=1.48926685
A3=121.28650492
A4=120.22496747
A5=120.28805362
A6=118.21036191
A7=122.5350979
A8=120.92519826
A9=120.03659805
A10=118.21036191
A11=120.92396952
A12=118.91896257
A13=120.24282239
A14=121.28650492
A15=118.83321943
A16=118.48852761
A17=121.04446913
A18=105.07149601
A19=104.50370705
A21=120.92519826
A22=105.07149447
A23=104.50370783
D19=-59.61166892
D23=120.38833074

Terephthalic dianion

B3LYP/6-311++G**

C
C,1,R2
O,1,R3,2,A3
O,1,R3,2,A3,3,180.,0
C,2,R5,1,A5,3,0.,0
C,2,R5,1,A5,3,180.,0
C,5,R7,2,A7,1,180.,0
C,6,R7,2,A7,1,180.,0
H,5,R9,2,A9,1,0.,0
H,6,R9,2,A9,1,0.,0
C,7,R11,5,A11,2,0.,0
H,7,R12,5,A12,2,180.,0
H,8,R12,6,A12,2,180.,0
C,11,R14,7,121.34927459,5,180.,0
O,14,R15,11,A15,7,180.,0
O,14,R15,11,A15,7,0.,0

Variables:

R2=1.55
R3=1.2596601
R5=1.40111959
R7=1.39669
R9=1.08545022

R11=1.40112011
R12=1.08545074
R14=1.54951
R15=1.2596601
A3=116.23897421
A5=121.34923966
A7=121.34923966
A9=117.44165953
A11=121.34927459
A12=121.20914595
A15=116.23897421

2,6-naphthalenedicarboxylate dianion
B3LYP/6-311++G**

C
C,1,R2
C,1,R3,2,A3
H,1,R4,2,A4,3,180.,0
C,2,R5,1,A5,3,0.,0
C,3,R6,1,A6,2,0.,0
C,3,R7,1,A7,2,180.,0
H,2,R8,1,A8,3,180.,0
C,5,R9,2,A9,1,0.,0
C,6,R10,3,A10,1,180.,0
C,7,R11,3,A11,1,180.,0
C,5,R12,2,A12,1,180.,0
H,7,R13,3,A13,1,0.,0
C,10,R14,6,A14,3,0.,0
C,11,R15,7,A15,3,180.,0
O,12,R16,5,A16,2,0.,0
O,12,R17,5,A17,2,180.,0
H,9,R18,5,A18,2,180.,0
H,10,R19,6,A19,3,180.,0
O,15,R20,11,A20,7,0.,0
O,15,R21,11,A21,7,180.,0
H,14,R22,10,A22,6,180.,0

Variables:

R2=1.37620475
R3=1.42318231
R4=1.08794403
R5=1.42100045
R6=1.43243655
R7=1.42132712
R8=1.08434514
R9=1.37986804
R10=1.42318163
R11=1.37986804
R12=1.55095541
R13=1.08574266
R14=1.37620448
R15=1.54999999
R16=1.25833983
R17=1.25607913
R18=1.08574266
R19=1.087945
R20=1.25607933
R21=1.25834037
R22=1.08434447
A3=121.32946243
A4=120.39034078
A5=121.39625014
A6=117.73479836
A7=123.01858918
A8=121.60447441
A9=118.14958604
A10=117.73476885
A11=122.14329057
A12=120.34750158
A13=120.0422986
A14=121.32953199
A15=121.50289409
A16=115.58994502
A17=116.14564791
A18=117.81441084
A19=118.28018054
A20=116.14571092
A21=115.59002561
A22=121.60455337

4-sulfobenzoic dianion
B3LYP/6-311++G**

C
C,1,R2
C,1,R3,2,A3

H,1,R4,2,A4,3,D4,0
C,2,R5,1,A5,3,D5,0
C,3,R6,1,A6,2,D6,0
C,3,R7,1,A7,6,D7,0
H,2,R8,1,A8,5,D8,0
C,5,R9,2,A9,1,D9,0
O,7,R10,3,A10,1,D10,0
O,7,R11,3,A11,10,D11,0
S,5,R12,2,A12,9,D12,0
H,6,R13,3,A13,1,D13,0
O,12,R14,5,A14,2,D14,0
O,12,R15,5,A15,14,D15,0
O,12,R16,5,A16,14,D16,0
H,9,R17,5,A17,2,D17,0

Variables:

R2=1.39605745
R3=1.40009828
R4=1.08476639
R5=1.39558737
R6=1.40017041
R7=1.55000062
R8=1.08447736
R9=1.39565745
R10=1.257966
R11=1.25796737
R12=1.82853743
R13=1.08476526
R14=1.49249884
R15=1.49168509
R16=1.49169606
R17=1.08448748
A3=121.41836138
A4=121.0696212
A5=120.13884789
A6=117.65375773
A7=121.17296275
A8=121.05774745
A9=119.23085171
A10=115.99768578
A11=115.99710423
A12=120.36850573
A13=117.51042649
A14=105.39162555
A15=105.21943452
A16=105.2194894
A17=118.80541713
D4=-179.74417658
D5=0.18226121
D6=-0.24427494
D7=-179.45550084
D8=178.86203299
D9=-0.10993443
D10=-0.28166161
D11=179.97576071
D12=-177.37710116
D13=-179.50668171
D14=88.96813884
D15=-119.78274678
D16=119.77391359
D17=178.99406424

Appendix B: Sample Gaussian Input File for Calculation of Dissociation Pathway of Dianion toward Ionic Fragmentation

Input file to calculate the dissociation pathway of terephtahlic dianion toward ionic fragmentation, $C_6H_4(CO_2)_2^{2-}$ by stepwise (0.5 a.u) increasing the distance between CO_2^- ion and $C_6H_4(CO_2)^-$ ion.

#B3LYP/6-311++G** Opt=modredundant

Dissociation pathway of terephtahlic dianion toward ionic fragmentation

-2 1
C
C,1,R2
O,1,R3,2,A3
O,1,R3,2,A3,3,180.,0
C,2,R5,1,A5,3,0.,0
C,2,R5,1,A5,3,180.,0
C,5,R7,2,A7,1,180.,0
C,6,R7,2,A7,1,180.,0
H,5,R9,2,A9,1,0.,0
H,6,R9,2,A9,1,0.,0
C,7,R11,5,A11,2,0.,0
H,7,R12,5,A12,2,180.,0
H,8,R12,6,A12,2,180.,0
C,11,R14,7,121.34927459,5,180.,0
O,14,R15,11,A15,7,180.,0
O,14,R15,11,A15,7,0.,0
Variables:

R2=1.55
R3=1.2596601
R5=1.40111959
R7=1.39669
R9=1.08545022
R11=1.40112011
R12=1.08545074
R14=1.54951
R15=1.2596601
A3=116.23897421
A5=121.34923966
A7=121.34923966
A9=117.44165953
A11=121.34927459
A12=121.20914595
A15=116.23897421

B 1 2 1.5500 S 50 0.5000

VITA

Nasrin Mirsaleh Kohan was born in Tehran, Iran on September 21, 1975. She attended public schools in Tehran and graduated from 15 Khordad High School. She received an Honors Bachelor of Science in Physics degree from the University of Tehran. She completed her Masters degree in Computational Physics at Bowling Green State University. Nasrin attended graduate school at the University of Tennessee where she worked under the direction of Dr. Robert N. Compton in the area of Chemical Physics. The doctoral degree was received August 2008.